(2)

AFWL-TR-
79-72

ENERGETICS AND RADIATIVE PROPERTIES OF EXCIMER LASERS

H. H. Michels
R. H. Hobbs

United Technologies Research Center
Silver Lane
East Hartford, CT 06108

January 1981

Final Report

Approved for public release; distribution unlimited.

AIR FORCE WEAPONS LABORATORY
Air Force Systems Command
Kirtland Air Force Base, NM 87117

AFWL-TR-79-72

This final report was prepared by the United Technologies Research Center, East Hartford, Connecticut, under Contract F29601-78-C-0031, Job Order 34320801 with the Air Force Weapons Laboratory, Kirtland Air Force Base, New Mexico. Captain Lawrence A. Wright (NTY) was the Laboratory Project Officer-in-Charge.

When US Government drawings, specifications, or other data are used for any purpose other than a definitely related Government procurement operation, the Government thereby incurs no responsibility nor any obligation whatsoever, and the fact that the Government may have formulated, furnished, or in any way supplied the said drawings, specifications, or other data, is not to be regarded by implication or otherwise, as in any manner licensing the holder or any other person or corporation, or conveying any rights or permission to manufacture, use, or sell any patented invention that may in any way be related thereto.

This report has been authored by a contractor of the United States Government. Accordingly, the United States Government retains a nonexclusive, royalty-free license to publish or reproduce the material contained herein, or allow others to do so, for the United States Government purposes.

This report has been reviewed by the Public Affairs Office and is releasable to the National Technical Information Service (NTIS). At NTIS, it will be available to the general public, including foreign nations.

This technical report has been reviewed and is approved for publication.

Lawrence A. Wright

LAWRENCE A. WRIGHT
Captain, USAF
Project Officer

Norman F. Roderick

NORMAN F. RODERICK
Lt Colonel, USAF
Chief, Advanced Concepts Branch

FOR THE DIRECTOR

Thomas W. Ciambrone

THOMAS W. CIAMBRONE
Colonel, USAF
Applied Physics Division

DO NOT RETURN THIS COPY. RETAIN OR DESTROY.

UNCLASSIFIED

SECURITY CLASSIFICATION OF THIS PAGE *(When Date Entered)*

REPORT DOCUMENTATION PAGE	READ INSTRUCTIONS BEFORE COMPLETING FORM
1. REPORT NUMBER: AFWL-TR-79-72	2. GOVT ACCESSION NO.: AD-A115 168
	3. RECIPIENT'S CATALOG NUMBER:
4. TITLE *(and Subtitle)*: ENERGETICS AND RADIATIVE PROPERTIES OF EXCIMER LASERS	5. TYPE OF REPORT & PERIOD COVERED: Final Report
	6. PERFORMING ORG. REPORT NUMBER: 924270
7. AUTHOR(s): H. H. Michels R. H. Hobbs	8. CONTRACT OR GRANT NUMBER(s): F29601-78-C-0031
9. PERFORMING ORGANIZATION NAME AND ADDRESS: United Technologies Research Center Silver Lane East Hartford, CT 06108	10. PROGRAM ELEMENT, PROJECT, TASK AREA & WORK UNIT NUMBERS: 62301E/34320801
11. CONTROLLING OFFICE NAME AND ADDRESS: Air Force Weapons Laboratory (NTY) Kirtland Air Force Base, NM 87117	12. REPORT DATE: January 1981
	13. NUMBER OF PAGES: 168
14. MONITORING AGENCY NAME & ADDRESS *(if different from Controlling Office)*:	15. SECURITY CLASS. *(of this report)*: Unclassified
	15a. DECLASSIFICATION/DOWNGRADING SCHEDULE:

16. DISTRIBUTION STATEMENT *(of this Report)*

Approved for public release; distribution unlimited.

17. DISTRIBUTION STATEMENT *(of the abstract entered in Block 20, if different from Report)*

18. SUPPLEMENTARY NOTES

This research was sponsored by the Defense Advance Research Projects Agency (ARPA) under ARPA Order Number 3432.

19. KEY WORDS *(Continue on reverse side if necessary and identify by block number)*

ArF	Ar_2^+	Ar_3^+	Excimer Molecules
Ar_2F	Kr_2^+	Electronic Structure	Noble Gas Dimer Ions
Ne_2^+	Xe_2^+		Noble Gas Trimer Ions

20. ABSTRACT *(Continue on reverse side if necessary and identify by block number)*

This research program was concerned with a theoretical study of the energetics of the noble gas halides and noble gas dimer and trimer molecular ions. The electronic structure, potential energy curves, and radiative transition probabilities of excimer systems such as ArF and Ar_2F have been examined using quantum mechanical methods.

A systematic study of the electronic structure in the noble gas dimer ion sequence, Ne_2^+, Ar_2^+, Kr_2^+ and Xe_2^+, was carried out. This study included

DD FORM 1 JAN 73 1473

UNCLASSIFIED

SECURITY CLASSIFICATION OF THIS PAGE *(When Date Entered)*

20. ABSTRACT (Continued)

detailed calculations of the pertinent potential energy curves and an analysis of the calculated spectroscopic properties of the bound states of these ions.

Finally, calculations were carried out on the electronic structure and photoabsorption characteristics of the noble gas trimer ion Ar_3^+. This study included detailed calculations of the potential energy surfaces for Ar_3^+, an analysis of the spectroscopic properties of the ground state of this ion and prediction of the strong absorption bands.

SUMMARY

The electronic structure, potential energy curves, and radiative transition probabilities of excimer systems have been examined using quantum mechanical methods. These molecules are characterized by repulsive or weakly bound ground state potential curves and by bound, strongly ionic, or Rydberg, excited states. They constitute a very interesting class of molecules which offer the possibility for high power, high efficiency UV laser operation. Calculations have been carried out using the density functional SCF-X_α method, modified extensively to correct for well known errors arising from approximations to the potential and exchange terms. A limited number of ab initio calculations were also carried out for comparison purposes. For the ArF system we find that the lowest excited ionic state has symmetry $^2\Sigma^+_{1/2}$, and that the dominant laser transition observed at 1933 Å should be assigned to B $^2\Sigma^+_{1/2} \rightarrow X\ ^2\Sigma^+_{1/2}$. The C $^2\Pi_{3/2} \rightarrow X\ ^2\Sigma^+_{1/2}$ transition is calculated to be two orders of magnitude smaller in emission intensity than the dominant transition, thus ruling out this assignment for the observed laser line in ArF. Preliminary calculations carried out for Ar_2F indicate that the bound upper ionic state has $^2B_2$ symmetry and that the most probable ground state also has $^2B_2$ symmetry. This polyatomic system is predicted to exhibit a broadband emission spectrum with a relatively long radiative lifetime.

In addition to calculations performed on noble gas halide excimer molecules, a systematic study of the electronic structure and chemical binding in the dimer ion sequence, Ne_2^+, Ar_2^+, Kr_2^+, and Xe_2^+, has been carried out using density functional methods. For comparison, ab initio configuration interaction calculations were also performed for the Ar_2^+ ion. These studies include detailed calculations of the pertinent potential energy curves and an analysis of the calculated spectroscopic properties of the bound states of these ions. A regular progression is found in the spectroscopic properties for the ground A $^2\Sigma^+_{1/2u}$ state which leads to some remarkably simple conclusions concerning the nature of the binding and the size of these dimer ions. For the heavier systems, Kr_2^+ and Xe_2^+, spin-orbit coupling becomes important, resulting in a strong mixture of the Λ-S coupled Σ and Π states. This mixing affects the strength of the binding in the ground state. A comparison with other ab initio studies and analsyis of the asymptotic behavior at large internuclear separations is given.

As a final study under this research program, calculations were carried out on the electronic structure and photoabsorption characteristics of the noble gas trimer ion Ar_3^+. This study included detailed density functional calculations of the potential energy surfaces for Ar_3^+, an analysis of the spectroscopic properties of the ground state of this ion and predicition of the strong absorption bands. Studies in D_{3h}, C_{2v}, and $D_{\infty h}$ symmetries were carried out. The lowest state of Ar_3^+ corresponds to the degenerate $^2E'$ symmetry with an indicated dissociation energy of $\sim$0.17 eV relative to

$Ar_2^+ (A^2\Sigma_u^+)$ + Ar (1_{So}). This trimer ion exhibits a very small Jahn-Teller distortion which does not significantly alter our conclusions concerning the ground state stability or absorption characteristics. A strong and very broad photoabsorption band (λ=496-670 nm) is predicted for the $^2E' \rightarrow {}^2A_1'$ transition of this trimer ion. This suggests that such species may be very important in the analysis of loss mechanisms in visible excimer lasers, operating under high pressure conditions with mixtures containing the noble gases.

PREFACE

The author wishes to acknowledge the helpful advice and encouragement of Captain Lawrence A. Wright (DYP) who was the Project Officer of the Contract. Very useful discussions with Dr. G. A. Peterson (UTRC) are also acknowledged.

Dr. Frank E. Harris (University of Utah) contributed to the technical program of this Contract as a Consultant to the United Technologies Research Center.

All aspects of the research work reported herein were aided by the skilled help of Judith B. Addison (UTRC) who carried out much of the computer program development and assisted in the analysis of the calculated data and in the preparation of this final report.

TABLE OF CONTENTS

		Page
I.	INTRODUCTION	7
II.	CURRENT STATUS OF QUANTUM MECHANICAL METHODS FOR DIATOMIC SYSTEMS	12
III.	METHOD OF APPROACH	17
	1. Quantum Mechanical Calculations	17
	a. Levels of Approximation	17
	b. Spin and Symmetry	18
	c. Method of Ab Initio Calculation	18
	d. Molecular Integrals	22
	e. Configuration Selection	22
	f. Density Functional Approach-X_α Method	23
	g. Computational Aspects of the X_α Method	29
IV.	DISCUSSION OF RESULTS	33
	REFERENCES	39
	APPENDICES	45
	A. The Electronic Structure of ArF and Ar_2F	45
	B. The Electronic Structure of Excimer	59
	C. Electronic Structure of the Noble Gas Dimer Ions	95
	D. Electronic Structure of the Noble Gas Dimer Ions. I. Potential Energy Curves and Spectroscopic Constants	117
	E. Electronic Structure of the Noble Gas Dimer Ions. II. Absorption Spectrum for the $A\ ^2\Sigma_g^+ \rightarrow D\ ^2\Sigma_g^+$	163
	F. Electronic Structure of the Noble Gas Dimer Ions. III. Absorption Spectrum for the $A\ ^2\Sigma_u^+ \rightarrow B\ ^2\Pi_g$ System	164
	G. Electronic Structure and Photoabsorption of the Hg_2^+ Dimer Ion	165
	H. Electronic Structure and Photoabsorption Properties of Noble Gas Trimer Ions	166
	I. Electronic Structure of Noble Gas Dimer and Trimer Ions	167
	J. Visible Photoabsorption by Noble Gas Trimer Ions	168
DISTRIBUTION		169

SECTION I

INTRODUCTION

The noble gas monohalides constitute an interesting and important class of molecules for laser applications. These molecules are characterized by a repulsive or very weakly bound ground state potential curve and bound, strongly ionic, excited states. The character of the electronic structure of these excited states is similar to that of the ground state alkali halide salts.

Emission spectra from several noble gas halides have been obtained in low pressure discharge flow experiments and were first reported by Velazco and Setser (ref. 1) and by Golde and Thrush (ref. 2). More recently emission spectra for several systems which have exhibited lasing have been reported by Brau and Ewing (ref. 3). These spectra are consistent with a model whereby the lasing transition is between a strongly bound upper electronic state and a nearly flat repulsive ground state. A group theoretical analysis of the possible electronic configurations for these states does not lead to a unique assignment since both the upper and lower levels could be of $^2\Sigma^+$ or $^2\Pi$ symmetry. Even a detailed experimental spectroscopic study of XeCl (ref. 4) failed to uniquely assign the symmetries of the lasing transition.

Theoretical approaches to this problem have consisted of analogies with alkali halide systems (ref. 5), predictions based on an electron-gas model (ref. 6) and ab initio calculations for the KrF system (ref. 7). Unfortunately, the theoretical methods utilized to date have been unable to

positively define the electronic states involved in the noble gas halide laser systems. The ab initio methods would appear to be applicable only to the lighter systems such as ArF and KrF owing to greatly increased computational complexity for larger numbers of electrons. In addition, past experience indicates that the ab initio calculations would not be of uniform quality in going from a simple system such as ArF to a heavier system such as XeCl. The electron-gas model calculations suffer from the lack of self-consistency in the molecular potential. Recent density functional calculations performed in this Center indicate self-consistency in the potential is crucial to determining optimum electronic wavefunctions for these systems. Thus a theoretical study of the electronic structure of the noble gas halide systems, capable of uniformly describing XeBr as well as ArF, and relevant to the understanding and interpretation of current experimental programs in noble gas halide laser systems seems desirable at the present time.

The primary information to be obtained from a theoretical study of noble gas halide systems is the electronic structure, energetics and lifetimes of the low-lying excited states which are involved in the chemical reaction mechanisms leading to population of the excited laser levels. Knowledge of the partition of energy between the products of a chemical reaction is fundamental to the understanding of the dynamics of the process, and to the design of chemical lasers. Atom-atom and atom-molecule reactions that yield electronically excited molecules are of particular scientific and military interest. From the point of view of the theoretical chemist, an understanding of the dynamics of the simplest of these reactions is a prerequisite for understanding more complicated gas phase reactions. From the

viewpoint of the engineer interested in the design of chemical lasers, studies of these reactions yield kinetics information and scaling parameters that enable one to design devices with the potential of having very high specific power. A great deal of work in these two areas of science and engineering has been stimulated by the recent development of a number of highly sophisticated techniques for measuring the nonequilibrium distribution of the vibrational and rotational states of the products of a chemical reaction. Over the past decade, many atom-molecule reactions yielding vibrationally excited hydrogen halides have been studied by infrared chemiluminescent techniques. These studies have furnished a great deal of information on how the exothermicity of a chemical reaction may be distributed among the energy levels (vibration, rotation, and translation) of the products (refs. 8-12). More recently, it has been possible to use laser technology and molecular beam techniques to measure the internal energy distribution of reactions yielding vibrationally excited hydrogen halides (refs. 13-15).

A knowledge of at least limited regions of potential energy surfaces is of importance in analyzing the electronic, vibrational and rotational relaxation rates in chemical laser systems. These relative relaxation rates govern both the feasibility of lasing and the power that is potentially available. Such relaxation rates are governed by long-range forces between atomic and molecular fragments and thus knowledge of the dissociation behavior represented by the potential energy surfaces for the laser system can be used in calculations of the kinetic behavior. A recent example is the use of such potential energy data in analyzing deactivation in CO_2 (00°1) through collisions with H_2 (ref. 16).

The discussion above has indicated the way in which knowledge of potential energy surfaces can be useful in analyzing the behavior of an existing chemical laser system. More recently it has become apparent that detailed knowledge of such surfaces can be utilized in a predictive fashion. Michels and Broida (ref. 17) have recently outlined a mechanism for the chemiluminescence in the visible region of the BaO system. This suggestion was based on the combined knowledge of the results of calculations on the potential energy curves for BaO and measured lifetime data for excited electronic states of this system. A similar parallel study of AlO has also been reported by Michels (ref. 18) and Johnson, et al. (ref. 19).

The initial impetus for these studies came from a practical problem in aeronomy. The release of certain chemical species into the upper atmosphere results in luminous clouds that display the resonance electronic-vibrational-rotation spectrum of the released species. Such spectra are seen in rocket releases of chemicals for upper atmospheric studies and upon reentry into the atmosphere of artificial satellites and missiles. Of particular interest in this connection is the observed spectra of certain metallic oxides and halides. From band intensity distribution of the spectra, and knowledge of the f-values for electronic and vibrational transitions, the local optical conditions of the atmosphere can be determined.

Because of inherent difficulties in the experimental determination of transition probabilities for certain metal oxide and halide systems and because of recent progress in the ab initio calculation of electronic wavefunctions for diatomic systems, theoretical programs for calculating band absorption and emission coefficients were undertaken at UTRC (Contracts

F29601-71-C-0119 and F44620-73-C-0077). These programs based on current quantum mechanical techniques and capabilities developed at UTRC were directed toward determining the vibrational and electronic transition probabilities and integrated absorption coefficients for the metal oxide band systems SiO, AlO, TiO, FeO, BaO and UO. Additional studies of halide systems have included LiCl, LiF, NaF, HCl and HF. Progress on the studies of certain of these systems has been reported (refs. 16-21). These studies formed a very sound basis for more extensive analysis of metal oxides and metal halides as candidate laser systems. To the best of our knowledge, no other laboratory in the country has such an extensive catalogue of theoretical calculations of the electronic structure of diatomic oxides and halides or our computational experience with these types of molecules. In addition, UTRC has fully developed sophisticated computer programs for studying both diatomic and polyatomic molecules. These programs have been extensively used at UTRC and at the Air Force computational laboratories at AFWL, Kirtland Air Force Base and AFGL, Hanscom Field.

The research program presented herein was devoted to a theoretical study of the energetics of noble gas halides, the prediction of the radiative lifetimes of electronically excited species, and studies of photon energy loss paths such as photoabsorption or ionization of the upper excited electronic states. The goal of this research program was to develop sufficient information to enable one to determine promising candidates for UV laser systems and to develop an information base of kinetic data useful for analyzing loss process in excimer lasers.

SECTION II

CURRENT STATUS OF QUANTUM MECHANICAL METHODS FOR DIATOMIC SYSTEMS

The application of quantum mechanical methods to the prediction of electronic structure has yielded much detailed information about atomic and molecular properties (ref. 22). Particularly in the past few years, the availability of high-speed computers with large storage capacities has made it possible to examine both atomic and molecular systems using an *ab initio* approach, wherein no empirical parameters are employed (ref. 23). *Ab initio* calculations for diatomic molecules employ a Hamiltonian based on the nonrelativistic electrostatic interaction of the nuclei and electrons, and a wavefunction formed by antisymmetrizing a suitable many-electron function of spatial and spin coordinates. For most applications it is also necessary that the wavefunction represent a particular spin eigenstate and that it have appropriated geometrical symmetry. Nearly all the calculations performed to date are based on the use of one-electron orbitals and are of two types: Hartree-Fock or configuration interaction (ref. 24).

Hartree-Fock calculations are based on a single assignment of electrons to spatial orbitals, following which the spatial orbitals are optimized, usually subject to certain restrictions. Almost all Hartree-Fock calculations have been subject to the assumption that the diatomic spatial orbitals are all doubly occupied, as nearly as possible, and are all of definite geometrical symmetry. These restrictions define the *conventional*, or *restricted*, Hartree-Fock (RHF)

method (refs. 25 and 26). RHF calculations can be made with relatively large Slater-type orbital (STO) basis sets for diatomic molecules with first or second-row atoms, and the results are convergent in the sense that they are insensitive to basis enlargement. The RHF model is adequate to give a qualitatively correct description of the electron interaction in many systems, and in favorable cases can yield equilibrium interatomic separations and force constants. However, the double-occupancy restriction makes the RHF method inappropriate in a number of circumstances of practical interest. In particular, it cannot provide potential curves for molecules dissociating into odd-electron atoms (e.g., NO at large internuclear separation), or into atoms having less electron pairing than the original molecule [e.g., $O_2\ ^3\Sigma_g^- \rightarrow O(^3P)$]; it cannot handle excited states having unpaired electrons (e.g., the $^3\Sigma$ states of O_2 responsible for the Schumann-Runge bands); and, in general, it gives misleading results for molecules in which the extent of electron correlation changes with internuclear separation.

Configuration-interaction (CI) methods have the capability of avoiding the limitations of the RHF calculations. If configurations not restricted to doubly-occupied orbitals are included, a CI can, in principle, converge to an exact wavefunction for the customary Hamiltonian. However, many CI calculations have in fact been based on a restriction to doubly-occupied orbitals and therefore retain many of the disadvantages of the RHF method (ref. 24). The use of general CI formulations involves three considerations, all of which have been satisfactorily investigated: the choice of basis orbitals, the

choice of configurations (sets of orbital assignments), and the specific calculations needed to make wavefunctions describing pure spin states (ref. 27). The first consideration is the art associated with quantum mechanical electronic electronic structure calculations. Many methods (iterative NSO, perturbation selection, first order CI, etc.) have been advocated for the optimum choice of configurations. There are no firm rules at present and the optimum choice is a strong function of the insight of the particular research investigator. The last consideration, proper spin and symmetry projection, has proved difficult to implement, but computer programs have been developed for linear projection algebra at this Center, and the CI method has been found of demonstrable value in handling excited states and dissociation processes which cannot be treated with RHF techniques.

Either of the above described methods for ab initio calculations reduces in practice to a series of steps, the most important of which are the evaluation of molecular integrals, the construction of matrix elements of the Hamiltonian, and the optimization of molecular orbitals (RHF) or configuration coefficients (CI). For diatomic molecules, these steps are all comparable in their computing time, so that a point has been reached where there is no longer any one bottleneck determining computation speed. In short, the integral evaluation involves the use of ellipsoidal coordinates and the introduction of the Neumann expansion for the interelectronic repulsion potential (ref. 28); the matrix element construction depends upon an analysis of the algebra of spin eigenfunctions (ref. 29); and the orbital or configuration

optimization can be carried out by eigenvalue techniques (refs. 30 and 31). All the steps have by now become relatively standard, and can be performed efficiently on a computer having 32,000 to 65,000 words of core storage, a cycle time in the microsecond range, and several hundred thousand words of peripheral storage.

Both the RHF and CI methods yield electronic wavefunctions and energies as a function of the internuclear separation, the RHF method for one state, and the CI method for all states considered. The electronic energies can be regarded as potential curves, from which may be deduced equilibrium internuclear separations, dissociation energies, and constants describing vibrational and rotational motion (including anharmonic and rotation-vibration effects). It is also possible to solve the Schrodinger equation for the motion of the nuclei subject to the potential curves, to obtain vibrational wavefunctions for use in transition probability calculations. The electronic wavefunctions themselves can be used to estimate dipole moments of individual electronic states, transition moments between different electronic states, and other properties. While all of the calculations described in this paragraph have been carried out on some systems, the unavailability of good electronic wavefunctions and potential curves has limited actual studies of most of these properties to a very small number of molecules.

It is not always possible or practical to perform an ab initio or mathematically rigorous calculation of the electronic structure of a diatomic molecule containing a large number of electrons and it is sometimes useful to

resort to approximations based on certain physical insights. One such approximation is the density functional method (ref. 32) as applied to molecules. In one implementation of this approach, namely the X_α model, the one-electron Schrodinger equation is set up within an approximation to the true potential which is spherically symmetric within spheres surrounding the several nuclei, constant in the region between adjacent spheres and spherically symmetric outside an outer sphere which encloses the entire collection of nuclei. The resulting equations are solved by a multiple-scattering method, equivalent to the KKR method (ref. 33) often used for crystals. From the resulting charge densities, one can compute a total energy, using a statistical approximation for the exchange correlations. This approximation is defined apart from a multiplicative factor, α, hence the name X_α method.

The X_α method has been very successful in predicting excitation energies in molecules and molecular ions but has met with only limited success in calculation of total energies. The basic deficiency appeared to lie in the muffin-tin approximation to the true potential rather than in the statistical treatment of the correlation energy. However, recent studies at this Center have shown that when certain variational constraints are applied to the X_α wavefunctions, significant improvements in the calculated total energies can be obtained. At this time the method appears to have utility for constructing regions of potential energy surfaces.

SECTION III

METHOD OF APPROACH

1. QUANTUM MECHANICAL CALCULATIONS

Central to the proposed studies are the actual quantum-mechanical calculations which must be carried out for the molecular species. For added clarity, various aspects of these calculations are discussed in individual subsections.

a. Levels of Approximation

Much evidence on diatomic and polyatomic systems indicates the near adequacy of a minimum Slater-type-orbital (STO) basis for constructing molecular wavefunctions (refs. 34 and 35). This means inner-shell and valence-shell STO's of quantum numbers appropriate to the atoms (1s, 2s, 2p for C, N, O; 1s for H). The main deficiency of the minimum basis set is in its inability to describe polarization of π orbitals in atoms adjacent to H atoms, and successful calculations usually result if one (or a set) of p orbitals is supplied for each H atom. Values of the screening parameters ζ for each orbital can either be set from atomic studies or optimized in the molecule; the later approach is indicated for studies of maximum precision. When high chemical accuracy is required, as for the detailed studies of the ground state of a system, a more extended basis should be used. Double-Zeta plus polarization functions or optimized MO's usually are required.

The chosen basis sets give good results only when used in a maximally flexible manner. This implies the construction of CI wavefunctions with all

kinds of possible orbital occupancies, so that the correlation of electrons into overall states can adjust to an optimum form at each geometrical conformation and for each state. Except when well-defined pairings exist for as many electrons as possible, a single-configuration study (even of Hartree-Fock quality) will be inadequate.

b. Spin and Symmetry

Proper electronic states for systems composed of light atoms should possess definite eigenvalues of the spin operator S^2 as well as an appropriate geometrical symmetry. The geometrical symmetry can be controlled by the assignment of orbitals to each configuration, but the spin state must be obtained by a constructive or projective technique. Formulas have been developed (ref. 36) for projective construction of spin states from orthogonal orbitals, and programs implementing these formulas have for several years been in routine use at UTRC.

One of the least widely appreciated aspects of the spin-projection problem is that the same set of occupied spatial orbitals can sometimes be coupled to give more than one overall state of given S quantum number. It is necessary to include in calculations all such spin couplings, as the optimum coupling will continuously change with changes in the molecular conformation. This is especially important in describing degenerate or near-degenerate excited electronic states.

c. Method of Ab Initio Calculation

A spin-free nonrelativistic Hamiltonian will be employed in the Born-Oppenheimer approximation. For a molecule containing n electrons and m

nuclei, the approximation leads to an electronic Hamiltonian depending parametrically on the nuclear positions:

$$\mathcal{H} = -\frac{1}{2}\sum_{i=1}^{n}\nabla_i^2 - \sum_{i=1}^{n}\sum_{\mu=1}^{m}\frac{Z_\mu}{|\vec{r}_i - \vec{R}_\mu|} + \sum_{1\le\mu<\nu}^{m}\frac{Z_\mu Z_\nu}{|\vec{R}_\mu - \vec{R}_\nu|} + \sum_{1\le i<j}^{n}\frac{1}{|\vec{r}_i - \vec{r}_j|} \qquad (1)$$

where Z_μ and $\bar{R}_\mu$ are the charge and position of nucleus μ, $\bar{r}_i$ is the position of electron i, and ∇_i^2 is the Laplacian operator for electron i. The Hamiltonian H is in atomic units (energy in Hartrees, length in Bohrs).

Electronic wavefunctions ψ, depending parametrically on the nuclear positions are made to be optimum approximations to solutions of the Schrödinger equation

$$\mathcal{H}(R)\Psi(R) = E(R)\Psi(R) \qquad (2)$$

by involving the variational principle

$$\delta W(R) = \delta\,\frac{\int \Psi^*(R)\mathcal{H}(R)\Psi(R)\,d\tau}{\int \Psi^*(R)\Psi(R)\,d\tau} \qquad (3)$$

The integrations in equation (3) are over all electronic coordiates and the stationary values of W are approximations to the energies of states described by the corresponding ψ. States of different symmetries are studied by restricting to the appropriate form, and excited states of any symmetry can be handled by simultaneously determining the ψ for the excited state and all lower-lying states of the same symmetry.

The specific form for Ψ may be written

$$\Psi(R) = \sum_{\mu} c_{\mu} \Psi_{\mu}(R) \tag{4}$$

where each ψ_{μ} is referred to as a configuration, and has the general structure

$$\Psi_{\mu}(R) = \mathcal{A} \mathcal{O}_S \prod_{i=1}^{n} \Psi_{\mu i}(\underset{\sim}{r}_i, R)\, \theta_M \tag{5}$$

where each $\psi_{\mu i}$ is a spatial orbital, $\mathcal{A}$ is the antisymmetrizing operator, $\mathcal{O}_S$ is the spin-projection operator for spin quantum number S, and θ_M is a product of α and β one-electron spin functions of magnetic quantum number M. No requirement is imposed as to the double occupancy of the spatial orbital, so equations (4) and (5) can describe a completely general wavefunction.

In Hartree-Fock calculations Ψ is restricted to a single ψ_{μ} which is assumed to consist as nearly as possible of doubly-occupied orbitals. The orbitals $\psi_{\mu i}$ are then selected to be the linear combinations of basis orbitals best satisfying equation (3). Writing

$$\Psi_{\mu i} = \sum_{\nu} a_{\nu i} \chi_{\nu} \tag{6}$$

the $a_{\nu i}$ are determined by solving the matrix Hartree-Fock equations

$$\sum_{\nu} F_{\lambda \nu} a_{\nu i} = \epsilon_i \sum_{\nu} S_{\lambda \nu} a_{\nu i} \quad \text{(each } \lambda\text{)} \tag{7}$$

where ϵ_i is the <u>orbital energy</u> of $\psi_{\mu i}$.

The Fock operator $F_{\lambda \nu}$ has been thoroughly discussed in the literature (ref. 37) and depends upon one- and two-electron molecular integrals and upon

the $a_{\nu i}$. This makes equation (7) nonlinear and it is therefore solved iteratively. UTRC has developed programs for solving equation (7) for both closed- and open-shell systems, using basis sets consisting of Slater-type atomic orbitals. Examples of their use are in the literature (ref. 38).

In configuration interaction calculations, the sumation in equation (4) has more than one term, and the c_μ are determined by imposing equation (3), to obtain the secular equation

$$\sum_\nu (H_{\mu\nu} - wS_{\mu\nu})\, c_\nu = 0 \qquad (\text{each } \mu) \tag{8}$$

where

$$H_{\mu\nu} = \int \Psi_\mu^*(R)\, \mathcal{H}(R)\, \Psi_\nu(R)\, d\tau$$

$$S_{\mu\nu} = \int \Psi_\mu^*(R)\, \Psi_\nu(R)\, d\tau \tag{9}$$

Equation (7) is solved by matrix diagonalization using either a modified Givens method (ref. 30) or a method due to Shavitt (ref. 31).

The matrix elements $H_{\mu\nu}$ and $S_{\mu\nu}$ may be reduced by appropriate operator algebra to the forms

$$H_{\mu\nu} = \sum_P \epsilon_P \left\langle \theta_M \middle| \mathcal{O}_S P \middle| \theta_M \right\rangle \left\langle \prod_{i=1}^{n} \Psi_{\mu i}(\underset{\sim}{r}_i, R) \middle| \mathcal{H}(R) P \middle| \prod_{i=1}^{n} \Psi_{\nu i}(\underset{\sim}{r}_i, R) \right\rangle \tag{10}$$

$$S_{\mu\nu} = \sum_P \epsilon_P \left\langle \theta_M \middle| \mathcal{O}_S P \middle| \theta_M \right\rangle \left\langle \prod_{i=1}^{n} \Psi_{\mu i}(\underset{\sim}{r}_i, R) \middle| P \middle| \prod_{i=1}^{n} \Psi_{\nu i}(\underset{\sim}{r}_i, R) \right\rangle \tag{11}$$

where P is a permutation and ϵ_p its parity. The sum is over all permutations. $\langle \theta_M | \mathcal{O}_S^P | \theta_M \rangle$ is a "Sanibel coefficient" and the remaining factors are

spatial integrals which can be factored into one- and two-electron integrals. If the $\psi_{\mu i}$ are orthonormal, equations (10) and (11) become more tractable and the $H_{\mu\nu}$ and $S_{\mu\nu}$ may be evaluated by explicit methods given in the literature (ref. 36). Computer programs have been developed for carrying out this procedure, and they have been used for problems containing up to 40 total electrons, 10 unpaired electrons, and several thousand configurations.

The CI studies described above can be carried out for any orthonormal set of $\psi_{\mu i}$ for which the molecular integrals can be calculated. Programs developed by URTC make specific provision for the choice of the $\psi_{\mu i}$ as Slater-type atomic orbitals, as symmetry molecular orbitals, as Hartree-Fock orbitals, or as more arbitrary combinations of atomic orbitals.

d. Molecular Integrals

The one- and two-electron integrals needed for the above described method of calculation are evaluated for STO's by methods developed by the present investigators (ref. 39). All needed computer programs have been developed and fully tested at UTRC.

e. Configuration Selection

Using a minimum basis plus polarization set of one-electron functions, a typical system can have of the order of 10^4 configurations in a full CI (that resulting from all possible orbital occupancies). It is therefore essential to identify and use the configurations describing the significant part of the wavefunction. There are several ways to accomplish this objective. First, one may screen atomic-orbital occupancies to eliminate those with excessive formal charge. Alternatively, in a molecular-orbital framework

one may eliminate configurations with excessive numbers of antibonding orbitals. A third possibility is to carry out an initial screening of configurations, rejecting those whose diagonal energies and interaction matrix elements do not satisfy significance criteria. Programs to sort configurations on all the above criteria are available at UTRC.

Other, potentially more elegant methods of configuration choice involve formal approaches based on natural-orbital (ref. 40) or multiconfiguration SCF (ref. 41) concepts. To implement the natural-orbital approach, an initial limited-CI wave-function is transformed to natural-orbital form, and the resulting natural orbitals are used to form a new CI. The hoped-for result is a concentration of the bulk of the CI wavefunction into a smaller number of significant terms. The multiconfiguration SCF approach is more cumbersome, but in principle more effective. It yields the optimum orbital choice for a pre-selected set of configurations. This approach works well when a small number of dominant configurations can be readily identified.

f. Density Functional Approach - X_α Model

The X_α model (ref. 42) for the electronic structure of atoms, molecules, clusters and solids is a local potential model obtained by making a simple approximation to the exchange-correlation energy. If we assume a non-relativistic Hamiltonian with only electrostatic interactions, it can be shown that the total energy E of a system can be written exactly (ref. 43) (in atomic units) as

$$E = \sum_i n_i \langle u_i \left| -\tfrac{1}{2}\nabla_i^2 + \sum_\mu \frac{z_\mu}{r_{1\mu}} \right| u_i \rangle + \tfrac{1}{2} \sum_{\mu \neq \nu} \frac{z_\mu z_\nu}{r_{\mu\nu}}$$

$$+ \tfrac{1}{2} \sum_{ij} n_i n_j \langle u_i u_j \left| \frac{1}{r_{12}} \right| u_i u_j \rangle + E_{xc} \qquad (12)$$

This expression is exact provided the u_i are natural orbitals and n_i are their occupation numbers (i.e., eigenfunctions and eigenvalues of the first order density matrix). The first term in equation (12) represents the kinetic and electron-nuclear energies. The second term is the nuclear repulsion energy. The sums (μ,ν) are over all the nuclear charges in the system. The third term is the electron-electron repulsion term, which represents the classical electrostatic energy of the charge density ρ interacting with itself, where

$$\rho(1) = \sum_i n_i u_i^*(1)\, u_i(1) \qquad (13)$$

The last term E_{xc} represents the exchange correlation energy and can be expressed formally as

$$E_{xc} = \tfrac{1}{2} \int \rho(1)\, d\vec{r}_1 \int \frac{\rho_{xc}(1,2)}{r_{12}}\, d\vec{r}_2 \,, \qquad (14)$$

where $\rho_{xc}(1,2)$ represents the exchange-correlation hole around an electron at position 1. In the exact expression, ρ_{xc} is dependent on the second-order density matrix. In the Hartree-Fock approximation E_{xc} is the exchange energy, ρ_{xc} represents the Fermi hole due to the exclusion principle and depends only on the first-order density matrix. In the X_α method, we make a simpler assumption about ρ_{xc}. If we assume that the exchange-correlation

hole is centered on the electron and is spherically symmetric, it can be shown that the exchange-correlation potential

$$u_{xc} = \int \frac{\rho_{xc}(1,2)}{r_{12}} \, d\vec{r}_2 \tag{15}$$

is inversely proportional to the range of the hole, r_s, where r_s is defined by

$$\frac{4\pi}{3} r_s^3 \rho(1) = 1 \tag{16}$$

Therefore, in the X_α model, the potential U_{xc} is proportional to $p^{1/3}(\vec{r})$. We define a scaling parameter α such that

$$U_{x_\alpha}(1) = -\frac{9\alpha}{2} (3\rho(1)/8\pi)^{1/3} \tag{17}$$

The expression in equation (17) is defined so that $\alpha = 2/3$ for the case of a free electron gas in the Hartree-Fock model (ref. 44) and $\alpha = 1$ for the potential origially suggested by Slater (ref. 45). A convenient way to choose this parameter for molecular and solid state applications is to optimize the solutions to the X_α equations in the atomic limit. Schwarz (ref. 46) has done this for atoms from Z = 1 to Z = 41 and found values between 2/3 and 1.

In the "spin polarized" version of the X_α theory, it is assumed (as in the spin-unrestricted Hartree-Fock model) that electrons interact only with a potential determined by the charge density of the same spin. In this case the contribution to the total energy is summed over the two spins, $s = \pm 1/2$.

$$E_{xc} = \frac{1}{2} \sum_s \int \rho_s(1)\, U_{x\alpha,s}(1)\, d\vec{r}_1 \qquad (18)$$

where the potential is spin-dependent

$$U_{x_{\alpha,s}}(1) = -\frac{9\alpha}{2} (3\rho_s(1)/4\pi)^{1/3} \qquad (19)$$

and ρ_s is the charge density corresponding to electrons of spin s. The spin-polarized X_α model is useful for describing atoms and molecules with open-shell configurations and crystals which are ferromagnetic or anti-ferromagnetic.

Once one has made the X_α approximation to the total energy functional E in equation (12), then the rest of the theory follows from the application of variational principle. The orbitals μ_i are determined by demanding that E be stationary with respect to variations in μ_i. This leads to the set of one-electron X_α equations

$$\left[-\frac{1}{2} \nabla_1^2 + \sum_\mu \frac{z_\mu}{r_{1\mu}} + \int \frac{\rho(2)}{r_{12}} d\vec{r}_2 + \frac{2}{3} U_{x\alpha} \right] u_i = \epsilon_i u_i \qquad (20)$$

where ϵ_i is the one-electron eigenvalue associated with μ_i. Since $\rho(\vec{r})$ is defined in terms of the orbitals μ_i, the equation (20) must be solved iteratively, until self-consistency is achieved. Empiricaly, if one takes as an initial guess that ρ is approximately a sum of superimposed atomic charge densities, then the convergence of this procedure is fairly rapid. The factor of 2/3 multiplying the potential is a result of the

nonlinear dependence of E_{xc} on ρ. This also has as a consequence that the X_α eigenvalues e_i do not satisfy Koopmans' theorem, i.e., they cannot be interpreted as ionization energies. However, it can be shown that the ϵ_i are partial derivatives of the total expression of equation (12) with respect to the occupation number,

$$\epsilon_i = \frac{\partial E}{\partial n_i} \tag{21}$$

If E were a linear function of n_i, then Koopmans' theorem would hold. However, because of the dominant Coulomb term, E is better approximated by a quadratic function in n_i. This leads to the "transition state" approximation which allows one to equate the difference in total energy between the state (n_i, n_j) and (n_i-1, n_j+1) to the difference in the one-electron energies $\epsilon_j - \epsilon_i$ calculated in the state $(n_i-1/2, n_j+1/2)$. The error in this approximation is proportional to third-order derivatives of E with respect to n_i and n_j, which are usually small (ref. 47). The main advantage of using the transition state rather than directly comparing the total energy values is computational convenience, especially if the total energies are large numbers and the difference is small.

The relationship of equation (21) also implies the existence of a "Fermi level" for the ground state. This can be seen by varying E with respect to n_i under the condition that the sum $\sum_i' n_i$ is a constant, i.e.,

$$\delta\left[E - \lambda \sum_i n_i\right] = 0 \tag{22}$$

implies $\frac{\partial E}{\partial n_i} = \lambda$, where λ is a Lagrangian multiplier. This implies that the

total energy is stationary when all the one-electron energies are equal. How-

e occupation numbers are also subject to the restriction $0 \leq n_i \leq 1$.

ds to the following conditions on the ground state occupation numbers;

$$\begin{aligned} \epsilon_i < \lambda \cdot) \cdot \; & n_i = 1 \\ \epsilon_i > \lambda \cdot) \cdot \; & n_i = 0 \\ \epsilon_i = \lambda \cdot) \cdot \; & 0 \leq n_i \leq 1 \end{aligned} \tag{23}$$

In other words, the ground state eigenvalues obey Fermi statistics with λ representing the Fermi energy. It should be noted that, in contrast to the Hartree-Fock theory, where all the n_i are either 0 or 1, the X_α model predicts, in some cases, fractional occupation numbers at the Fermi level. In particular, this will occur in a system (such as transition metal or actinide atom) which has more than one open shell.

The X_α model differs in other significant ways from the Hartree-Fock method. In fact, the simplification introduced in approximating the total energy expression introduces several distinct advantages over Hartree-Fock:

1. The primary advantage is purely computational. The one-electron potential in equation (20) is orbital-independent and local, i.e., it is the same for all electrons (except in the spin-polarized X_α theory) and is a multiplicative operator. On the other hand, the Hartree-Fock potential is non-local, or equivalently, there is a different local potential for each orbital. This involves a great deal more computational effort, especially for systems described by a large number of orbitals. It has been shown (ref. 48) that the X_α orbitals for the first and second row atoms are about as

accurate as a double-zeta basis set, and are probably better for larger atoms which involve electrons with $\ell \geq 2$.

2. The orbital-independent X_α potential leads to a better one-electron description of electronic excitations of a system. Both the unoccupied ($n_i = 0$) and occupied ($n_i = 1$) eigenfunctions are under the influence of the same potential resulting from the other N-1 electrons. The Hartree-Fock virtual orbitals see a potential characteristic of the N occupied orbitals, and therefore are not as suitable for describing the excited state. Actually, although the ground state virtual eigenvalues are usually a good description of the one-electron excitations, the virtual spectrum of the transition state potential where one-half an electron has been removed from the system give a much better first-order picture of these levels (ref. 49).

3. As has been shown by Slater (ref. 50), the X_α model rigorously satisfied both the virial and Hellman-Feynman theorems, independent of the value of the parameter α. This is convenient for calculating the force on a nucleus directly in terms of a three dimensional integral, rather than the six dimensional integrals in the expression for the total energy of equation (12).

g. Computational Aspects of the X_α Model

In application of the X_α model to finite molecular systems, there are two practical aspects of the calculations which must be considered. The first concerns the choice of the integration framework for describing the molecular wavefunctions and the second deals with the choice of the exchange parameter, α, in different regions of space.

In computations with heteronuclear molecules, there are several free parameters that must be chosen: the ratio of sphere radii for the atomic spheres of integration at a given internuclear separation, the degree of sphere overlap, and the value of the exchange parameter in the atomic spheres and the intersphere region.

It has been found that changing the ratio of the sphere radii for the two atoms in a heteronuclear diatomic molecule introduces changes in the total energy that can be large on a chemical scale, ($\sim$ 1 eV). A choice for sphere radii based on covalent bonding radii does not necessarily provide a good estimate for these calculations. The value of the exchange parameter, α, and the sphere radii and/or sphere overlap is normally fixed in X_α calculations for crystals where the geometry is fixed. However, to develop a potential curve, the molecular description needs to change substantially as the internuclear separation varies and the changing sphere radii include varying fractions of the total molecular charge (ref. 51). Studies made at UTRC have shown that at any given separation the total energy calculated from the X_α model is a minimum at the radii ratio where the spherically averaged potentials from the two atomic centers is equal at the sphere radius,

$$V_1(r_{s_1}) = V_2(r_{s_2}) \tag{24}$$

This relationship between the potential match at the sphere boundary and the minimum in the total energy appears to hold exactly for "neutral" atoms and holds well for ionic molecular constituents. In the case of two ionic species, the long range tail of the potential must go like +2/R from one ion

and -2/R (in Rydbergs) for the other ion and so at large internuclear separations, the 1/R character of the potential does not invalidate the potential match criterion for radii selection. This match for the atomic potentials is applied to the self-consistent potentials.

In molecules with significant charge sharing in the bonds, the radii of the atomic spheres is frequently increased in X_α calculations so that an overlap region appears in the vicinity of the bond (ref. 52). Studies made at UTRC show that the contribution to the total molecular energy from the exchange integral shows a minimum at the optimum sphere radius or sphere overlap. This provides a sensitive criterion for selecting these parameters.

The values of the exchange parameters in the spherical integration region around each atomic center are frequently set at the atomic values both for neutral and for ionic molecular constituents. However, for light atoms, the value of α which best reproduces Hartree-Fock results varies substantially with ionicity. In argon, the following table compares, for the neutral atom and the positive ion, the HF energy and the X_α energy calculated for several values of α.

TABLE 1. COMPARISON OF CALCULATED ATOMIC ENERGIES FOR ARGON

	α	X_α Energy	HF Energy
Ar^0	.72177	-526.8176	-526.8173
$Ar^{+1/2}$	.72177	-526.5857	--
	.72213	-526.6007	--
Ar^{+1}	.72177	-526.2447	--
	.72213	-526.2596	--
	.72249	-526.2745	-526.2743

The optimum value of α changes even more rapidly in the fluorine atom, going from 0.73732 for F^0 to 0.72991 for F^{-1}. Since the total energy depends linearly on α, this parameter must be chosen carefully.

The intersphere exchange coefficient, is chosen to be a weighted average of the atomic exchange parameters from the two constituents. At small internuclear separations, the optimum radius for an atomic sphere frequently places significant amounts of charge outside that atomic sphere - charge that is still strongly associated with its original center rather than being transferred to the other center or associated with the molecular binding region. To best account for these cases the weighting coefficients are chosen to reflect the origin of the charge in the intersphere (or outersphere region),

$$\alpha_{\text{intersphere}} = \frac{\alpha_{s_1}(Q_{s_1} - Q_1^{o}) + \alpha_{s_2}(Q_{s_2} - Q_2^{o})}{(Q_{s_1} - Q_1^{o}) + (Q_{s_2} - Q_2^{o})} \qquad (25)$$

where $(Q_{s_i} - Q_i^{o})$ is the charge lost from sphere i relative to its atomic value (or ionic value) Q_i^{o} and α_{s_i} is the atomic exchange parameter for sphere i. This value for $\alpha_{\text{intersphere}}$ is calculated dynamically - it is updated after each iteration in the self-consistent calculation.

While for heavy atoms, these changes in the exchange parameter would be small, the α's for small atoms vary rapidly with z (and with ionicity). The correct choice of the exchange parameters influences not only the total energy calculated for the molecule but also in some cases affects the distribution of charge between the atomic spheres and the intersphere region.

SECTION IV

DISCUSSION OF RESULTS

The theoretical research conducted under this program was concerned with a study of the energetics of the noble gas halides and noble gas dimer and trimer molecular ions. The emphasis of the study of the noble gas halides was on the definition of potential energy curves, prediction of the radiative lifetimes of electronically excited states, and studies of photon energy loss paths such as photoabsorption and photoionization of the upper excited electronic states. The major effort of the study of the noble gas dimer and trimer ions was the definition of the potential energy curves and predicition of the photoabsorption cross-section for these species.

For all of the noble gas halide systems there is an outer crossing of the upper ionic states arising from $R^+ + X^-$ (R = noble gas, X = halide) such that these upper molecular states, at their equilibrium internuclear separations, actually lie lower than any of the Rydberg molecular states.

The possible electronic transitions which correspond to laser activity in these systems therefore reduce to the following set:

$$A^2\Sigma^+ \rightarrow X^2\Sigma^+$$

$$B^2\Pi \rightarrow X^2\Sigma^+$$

$$A^2\Sigma^+ \rightarrow {}^2\Pi I$$

$$B^2\Pi \rightarrow {}^2\Pi I$$

Further, the $B^2\Pi$ state is split into ${}^2\Pi_{3/2}$ and ${}^2\Pi_{1/2}$ states owing to spin-orbit coupling effects in the noble gas positive ion. This splitting

is small (782 cm^{-1}) for Ne but is appreciable for Xe (10537 cm^{-1}).

As a result of these several possibilities, the definite assignment of the laser transitions becomes difficult. Brau and Ewing (refs. 3 and 53) have assigned the strong laser transitions in XeBr, XeCl, XeF and KrF to A $^2\Sigma^+_{1/2} \rightarrow$ X $^2\Sigma^+_{1/2}$ in accord with a simple ionic model for the potential curves. Ab initio calculations by Dunning and Hay (Ref. 7) for KrF also suggest the A $^2\Sigma^+_{1/2} \rightarrow$ X $^2\Sigma^+_{1/2}$ transition corresponds to the observed emission in KrF at 2480Å. Their potential curves, however, also indicate a B $^2\Pi_{3/2} \rightarrow$ $^2\Pi_{3/2}$ I transition at nearly the same calculated wavelength. Since this is also a strong parallel transition, a unique assignment does not appear to be possible on the basis of Dunning and Hay calculations. Further, their calculations indicate a near degeneracy of the upper ionic A $^2\Sigma^+_{1/2}$ and B $^2\Pi_{3/2}$ states which is difficult to understand in terms of simple charge density models for these excited states.

Clugston and Gordon (ref. 6) suggest that the dominant laser transition is B $^2\Pi_{3/2} \rightarrow$ X $^2\Sigma^+_{1/2}$, based on free-electron gas model calculations. Recent studies carried out at this Center, however, question the reliability of non-SCF model calculations for these systems. In addition, this assignment of a perpendicular transition to the laser emission goes against the experimental observations that such transitions should be weak compared to allowed transitions.

In order to shed some light on the above questions, both ab initio and density functional X_α calculations were carried out for the lower and

excited levels of ArF and Ar_2F. The ab initio calculations were carried out in a manner similar to that described previously (ref. 57). All nonlinear parameters of the molecular orbital basis functions were individually optimized for each separate electronic state. The results of these studies have been analyzed and published as technical papers. For completeness they are presented herein as Appendices A and B.

The theoretical principles underlying the electronic structure of the homonuclear noble gas molecular ions have been discussed by Mulliken (ref. 54) using Xe_2^+ as a prototype and, more recently, by Gilmore, Barr, and Dee (ref. 55) for the case of Kr_2^+. For these dimer ions, four electronic states ($A\ ^2\Sigma_u^+$, $B\ ^2\Pi_g$, $C\ ^2\Pi_u$, and $D\ ^2\Sigma_g^+$) arise from a ground state atom ($^1S_0$) and a ground state ion ($^2P_{1/2,3/2}$). The lowest state, usually labeled $A\ ^2\Sigma_u^+$, is bound for the four systems Ne_2^+, Ar_2^+, Kr_2^+, and Xe_2^+ and has been partially characterized experimentally through scattering experiments, although there has been much controversy concerning the dissociation energies of these ions. (ref. 54). For the heavier ions, Λ-S coupling is no longer strictly valid and the $B\ ^2\Pi_g$ and $C\ ^2\Pi_u$ states split into J-J coupled components with a resultant mixing of Σ and Π symmetries. This splitting is small for Ne_2^+ but six distinct J-J coupled molecular ion states arise for Xe_2^+.

With the exception of the recent calculations by Wadt,(ref. 56) no attempts at systematic studies of these ions have been reported. Accurate ab initio methods would appear to be practical only for the lighter ions with diminished accuracy for heavier systems such as Xe_2^+. Wadt reports

such a trend in his calculations (ref. 56) which indicate that his Gaussian basis is less flexible or less complete in the case of Xe_2^+ than for the corresponding study of Ar_2^+. Recent density functional calculations of noble gas halide molecules (ref. 57, ref. 58) have yielded reliable predictions of geometry and chemical binding, provided certain optimization criteria are followed. Such calculations, which should be of more uniform quality than ab initio studies, since numerical molecular orbitals not limited by basis set constraints are employed (ref. 59), constituted the principal effort in the present study. A limited number of ab initio calculations were carried out for Ar_2^+ for comparison purposes.

The results of our studies of the noble gas molecular ions have been prepared for publication as technical papers. For completeness our results are presented herein as Appendices C, D and J.

A brief summary of the most important results that were obtained for each of the molecular species that were examined is given below.

ArF

Our predicted emission spectra for ArF indicates that only the $B\ ^2\Sigma^+_{1/2} \rightarrow X\ ^2\Sigma^+_{1/2}$ transition exhibits a large transition moment. Our calculated radiative lifetime is 5 ns for this transition and our calculated peak emission intensity is at a wavelength of 196 nm, as compared with the experimental laser frequency of 193 nm.

Ar_2F

Calculations for Ar_2F indicate that the bound upper ionic state has $^2B_2$ symmetry with Ar-Ar and Ar-F bond lengths similar to those in the corresponding diatomic species. The terminating state of the emission from this

trimer species has $^2B_2$ symmetry while the ground state has $^2A_1$ symmetry. The $^2B_2^* \rightarrow {}^2B_2$ transition has a radiative lifetime of 200 ns with peak emission at 280 nm. The observed emission for Ar_2F is very broad (50 nm) and peaks at about 290 nm.

Ne_2^+

We find the A $^2\Sigma^+_{1/2u}$ ground state of Ne_2^+ to be bound by 1.31 eV with an equilibrium separation of 1.69 Å. Our calculated fundamental vibrational frequency is 597.0 cm^{-1}. Our predicted maximum photoabsorption cross-section at 300°K is 0.20 Å at a wavelength of 285 nm.

Ar_2^+

The A $^2\Sigma^+_{1/2u}$ ground state of Ar_2^+ is bound by 1.30 eV at an equilibrium separation of 2.43 Å. The fundamental vibrational frequency is calculated to be 297.9 cm^{-1}. We predict a maximum photoabsorption cross-section at 300°K of 0.48 Å at a wavelength of 300 nm.

Kr_2^+

The dissociation energy of the $A^2\Sigma^+_{1/2u}$ ground state of Kr_2^+ is 1.18 eV when spin-orbit effects are properly taken into account. Our calculated equilibrium separation is 2.75 Å and the fundamental frequency is found to be 176.7 cm^{-1}. We find a maximum photabsorption cross-section at 300°K of 0.57 Å at a wavelength of 320 nm.

Xe_2^+

The A $^2\Sigma^+_{1/2u}$ ground state of this ion is bound by 1.06 eV at an equilibrium separation of 3.18 Å. The calculated fundamental frequency

is 117.2 cm^{-1}. Our predicted photoabsorption spectrum at 300°K peaks at 340 nm at a value of 0.68 Å. We find a strong temperature dependence of the photoabsorption spectrum owing to the smallness of the vibrational spacing of the ground state.

Ar_3^+

An analysis of the electronic structure of Ar_3^+ was carried out in D_{3h}, C_{2v} and $D_{\infty h}$ symmetries. The lowest state of Ar corresponds to the degenerate $^2E'$ symmetry with an indicated dissociation energy of 0.17 eV relative to Ar_2^+ ($A\ ^2\Sigma_u^+$) + AR (^1S_o). This trimer ion exhibits a small Jahn-Teller distortion from D_{3h} symmetry. We find a wide, shallow well for the $^2E'$ ground state with an indicated R_e of 2.9 Å. The asymmetric stretch frequency is calculated to be 390 cm^{-1}.

A strong and very broad photoabsorption band (λ=500-670 nm) is predicted for the $^2E' \rightarrow {}^2A_1'$ transition of this trimer ion. This absorption exhibits a peak cross-section of 0.3 $Å^2$ at a wavelength of 580 nm. This suggests that such species may be very important in the analysis of loss mechanisms in visible excimer lasers.

REFERENCES

1. Velazco, J. E. and D. W. Setser: "Bound-Free emission Spectra of Diatomic Xenon Halides," Journal of Chemical Physics, Vol. 62, p. 1990, 1975.

2. Golde, M. F. and B. A. Thrush: "Vacuum Emission from Reactions of Metastable Inert Gas Atoms. Chemiluminescence of ArO and ArCl," Chemical Physics Letters, Vol. 29, p. 486, 1974.

3. Brau, C. A. and J. J. Ewing: "Emission of Spectra of XeBr, XeCl, XeF, and KrF," Journal of Chemical Physics, Vol. 63, p. 4640, 1975.

4. Tellinghuisen, J., G. C. Tisone, J. M. Hoffman, and A. K. Hayes: "Analysis of Spontaneous and Laser Emission from XeF," Journal of Chemical Physics, Vol. 64, p. 4976, 1976.

5. Ewing, J. J. and C. A. Brau: "Emission Spectrum of XeI in Electron-Beam-Excited Xe/I_2 Mixtures," Physical Review, Vol. A12, p. 129, 1975.

6. Clugston, M. J. and R. G. Gordon: "Electron-Gas Model for Open Shell-Closed Shell Interactions. I. Applications to the Emission Spectra of the Diatomic Noble-Gas Halides," Journal of Chemical Physics, Vol. 66, p. 239, 1977.

7. Dunning, T. H. Jr. and P. Jeffrey Hay: "The Electronic States of KrF," Applied Physics Letters, Vol. 28, p. 649, 1976.

8. Cashion, J. K. and J. C. Polanyi: "Infrared Chemiluminescence from the Gaseous Reaction Atomic H plus Cl_2," Journal of Chemical Physics, Vol. 29, p. 455, 1958.

9. Charters, P. E. and J. C. Polanyi: "Energy Distribution Among Reaction Products - Part I. The Reaction Atomic Hydrogen plus Molecular Chlorine," Faraday Society Discussions, Vol. 33, p. 107, 1962.

10. Anlauf, K. G., D. H. Maylotte, P. D. Pacey and J. C. Polanyi: "Vibrational Population-Inversion and Stimulated Emission from the Continuous-Mixing of Chemical Reagents," Physics Letters, Vol. 24A, p. 208, 1967.

11. Jonathan, N., C. M. Melliar-Smith and D. H. Slater: "Initial Vibrational Energy Distributions Determined by Infrared Chemiluminescence I. The Reaction of Fluorine Atoms with Hydrogen and Methane," Molecular Physics, Vol. 20, p. 93, 1971.

12. Jonathan, N., C. M. Melliar-Smith, S. Okuda, D. H. Slater and D. Timlin: "Initial Vibrational Energy Level Distributions Determined by Infrared Chemiluminescence II. The Reaction of Fluorine Atoms with Hydrogen Halides," Molecular Physics, Vol. 22, p. 561, 1971.

13. Parker, J. H. and G. C. Pimentel: "Vibrational Energy Distribution through Chemical Laser Studies I. Fluorine Atoms plus Hydrogen or Methane," Journal of Chemical Physics, Vol. 51, p. 91, 1969.

14. Schafer, T. P., P. E. Siska, J. M. Parson, F. P. Tully, Y. C. Wong and Y. T. Lee: "Crossed Molecular Beam Study of F + D_2," Journal of Chemical Physics, Vol. 53, p. 3385, 1970.

15. Shavitt, I., R. M. Stevens, F. L. Minn and M. Karplus: "Potential-Energy Surface for H_3," Journal of Chemical Physics, Vol. 48, p. 2700, 1968.

16. Kolker, H. J.: "The Deactivation of the Asymmetric Stretch Mode of Carbon Dioxide by Hydrogen," Chemical Physics Letters, Vol. 10, p. 498, 1971.

17. Michels, H. H. and H. P. Broida: "Analysis of the Electronic Structure, Radiative Transition Probabilities and Integrated IR Absorption Coefficients for AlO, FeO, BaO, UO and UO+." Technical Report ARPA-IVY OWL Meeting, AVCO Corporation, March 1972.

18. Michels, H. H.: "Ab Initio Calculation of the B $^2\Sigma^+$ - X $^2\Sigma^+$ Oscillator Strengths in AlO," Journal of Chemical Physics. Vol. 56, p. 665, 1972.

19. Johnson, S. E., G. Capella, and H. P. Broida: "Laser Excited Fluorescence and Radiative Lifetimes of AlO (B $^2\Sigma^+$ - X $^2\Sigma^+$)," Journal of Chemical Physics. Vol. 56, p. 663, 1972.

20. Michels, H. H.: Diatomic Oxide Vibrational Band Intensities. Final Report UARL Subcontract RL-98440-S. 1971.

21. Michels, H. H.: Theoretical Determination of Metal Oxide f-Numbers. Final Report AFWL Contract F29601-71-C-0119. February 1973.

22. Krauss, M.: Compendium of ab inito Calculations of Molecular Energies and Properties. NBS Technical Note 438. December 1967.

23. Allen, L. C.: Quantum Theory of Atoms, Molecules, and the Solid State. Edited by P. O. Lowdin, Academic Press, Inc. New York.

24. Wahl, A. C., P. J. Bertoncini, G. Das and T. L. Gilbert: "Recent Progress Beyond the Hartree-Fock Method for Diatomic Molecules. The Method of Optimized Valence Configurations," International Journal of Quantum Chemistry. Vol. IS, p. 123, 1967.

25. Roothan, C. C. J. and P. S. Bagus: "Atomic Self-Consistent Field Calculations by the Expansion Method," Methods in Computational Physics. Edited by B. Alder. Vol. 2, No. 47, 1963.

26. Roothan, C. C. J.: "New Developments in Molecular Orbital Theory," Reviews of Modern Physics, Vol. 23, No. 2, April 1951, p. 69.

27. Harris, F. E. and H. H. Michels: "Open-Shell Valence Configuration - Interaction Studies of Diatomic and Polyatomic Molecules," International Journal of Quantum Chemistry, Vol. IS, 1967, p. 329.

28. Harris, F. E.: "Molecular Orbital Studies of Diatomic Molecules. I. Method of Computation for Single Configurations of Heteronuclear Systems," Journal of Chemical Physics, Vol. 32, No. 1, January 1960, p. 3.

29. Harris, F. E.: "Open-Shell Orthogonal Molecular Orbital Theory," Journal of Chemical Physics, Vol. 46, No. 7, April 1967, p. 2769.

30. Givens, W.: Eigenvalue-Eigenvector Techniques. Oak Ridge Report Number ORNL 1574 (Physics).

31. Shavitt, I., C. F. Bender, A. Pipano, and R. P. Hosteny: "The Iterative Calculation of Several of the Lowest or Highest Eigenvalues and Corresponding Eigenvectors of Very Large Symmetric Matrices," Journal of Computational Physics, 11, 1973, p. 90.

32. Slater, J. C.: "Hellman-Feynman and Virial Theorems in the X_α Method," Journal of Chemical Physics, 57, 1972, p. 2389.

33. Slater, J. C.: "The Self-Consistent Field for Molecules and Solids," Quantum Theory of Molecules and Solids, Vol. 4, McGraw-Hill Book Co., New York, 1974.

34. Schaefer, F. E. and F. E. Harris: "Ab Initio Calculations of 62 Low-Lying States of the O_2 Molecule," Journal of Chemical Physics, Vol. 8, 1968, p. 4946.

35. Michels, H. H. and F. E. Harris: "Predissociation Effects in the A $^2\Sigma^+$ State of the OH Radical," Chemical Physics Letters, Vol. 3, 1969, p. 441.

36. Harris, F. E.: "Open-Shell Orthogonal Molecular Orbital Theory," Journal of Chemical Physics, Vo. 46, 1967, p. 2769.

37. Roothan, C. C. J. and P. S. Bagus: "Atomic Self-Consistent Field Calculations by the Expansion Method," Methods in Computational Physics, Vol. 2, edited by B. Alder, 1963, p. 47.

38. Harris, F. E. and H. H. Michels: "Open-Shell Valence Configuration-Interaction Studies of Diatomic and Polyatomic Molecules," International Journal of Quantum Chemistry, Vol. IS, 1967, p. 329.

39. Harris, F. E. and H. H. Michels: "The Evaluation of Molecular Integrals for Slater-Type Orbitals," Advances in Chemical Physics, Vol. 13, 1967, p. 205.

40. Davidson, E. R.: "Natural Expansions of Exact Wavefunctions, III. The Helium Atom Ground State," Journal of Chemical Physics, Vol. 39, p. 875, 1963.

41. Wahl, A. C., P. J. Bortoncini, G. Das and T. L. Gilbert: "Recent Progress Beyond the Hartree-Fock Method for Diatomic Molecules: The Method of Optimized Valence Configurations," International Journal of Quantum Chemistry, Vol. IS, 1967, p. 123.

42. For a recent review article on this method, see J. C. Slater, Advances in Quantum Chemistry, 6, 1, 1972.

43. Lowdin, P. O.: "Quantum Theory of Many-Particle Systems. I. Physical Interpretations by Means of Density Matrices, Natural Spin-Orbitals, and Convergence Problems in the Method of Configurational Interaction," Physical Review, Vol. 97, p. 1474, 1955.

44. Kohn, W. and L. Sham: "Self-Consistent Equations Including Exchange and Correlation Effects," Physical Review, Vol. 140A, p. 1133, 1965.

45. Slater, J. C.: "A Simplification of The Hartree-Fock Method," Physical Review, Vol. 81, p. 385, 1951.

46. Schwarz, K.: "Optimization of The Statistical Exchange Parameter For The Free Atoms H through Nb," Physical Review, Vol. B5, p. 2466, 1972.

47. Beebe, N. H. F.: "On the Transition State in the X_α Method," Chemical Physics Letters, Vol. 19, p. 290, 1973.

48. Schwarz, K. and J. W. D. Connolly: "Approximate Numerical Hartree-Fock Method for Molecular Calculations," Journal of Chemical Physics. Vol. 55, p. 4710, 1971.

49. Slater, J. C.: Advances in Quantum Chemistry, Vol. 6, Academic Press, New York, 1972.

50. Slater, J. C.: "Hellmann-Feynman and Virial Theorems in the X_α Method," Journal of Chemical Physics. Vol. 57, p. 2389, 1972.

51. Michels, H. H., R. H. Hobbs and J. C. Connolly: "Optimized SCF-X_α Procedures for Heterpolar Molecules," Journal of Chemical Physics (to be published).

52. Rosch, Notker and Keith H. Johnson: On the Use of Overlapping Spheres in The SCF-X_α Scattered-Wave Method," Chemical Physics Letters, Vol. 23, p. 149, 1973.

53. Brau, C. A. and J. J. Ewing: "354-nm Laser Action of XeF," Applied Physics Letters, Vol. 27, p. 435, 1975.

54. Mulliken, R. S.: "Potential Curves of Diatomic Rare-Gas Molecules and Their Ions, with Particular Reference to Xe_2", Journal of Chemical Physics, Vol. 52, p. 5170, 1970.

55. Gilmore, F. R., T. L. Barr and D. Dee: "Angular Momentum Coupling, Potential Curves and Radiative Selection Rules for Heavy Diatomic Molecules, with Particular Reference to Kr_2 and Kr_2^+," Journal of Quantum Spectroscopy and Radiation Transfer, Vol.15, p. 625, 1975.

56. Wadt, W. R.: "The Electronic States of Ar_2^+, Kr_2^+, Xe_2^+. I. Potential Curves With and Without Spin-Orbit Coupling", Journal of Chemical Physics, Vol. 68, p. 402, 1978.

57. Michels, H. H., R. H. Hobbs, and L. A. Wright: "The Electronic Structure of ArF and Ar_2F", Chemical Physics Letters, Vol. 48, p. 158, 1977.

58. Michels, H. H., R. H. Hobbs, L. A. Wright and J. W. D. Connolly: "Electronic Structure of Excimer Molecular Lasers", International Journal of Quantum Chemistry, Vol. 13, p. 169, 1978.

59. Connolly, J. W. D: Modern Theoretical Chemistry, Vol. VII, Plenum, New York, 1977.

APPENDIX A

THE ELECTRONIC STRUCTURE OF ArF AND Ar_2F*

L. A. Wright (DYP)
Kirtland Air Force Base, New Mexico 87117

Calculations have been performed on the electronic structure, potential energy curves and radiative transition probabilities of ArF and Ar_2F. Our predicted emission spectra for ArF indicates that only the $B\ ^2\Sigma^+_{1/2} \rightarrow X\ ^2\Sigma^+_{1/2}$ transition exhibits a large transition moment and hence a short ($\sim$ 5 nsec) radiative lifetime. Calculations for Ar_2F indicate that the bound upper ionic state has $^2B_2$ symmetry with Ar-Ar and Ar-F bond lengths similar to those in the corresponding diatomic species. The terminating state also has $^2B_2$ symmetry and this polyatomic system should exhibit a relatively long radiative lifetime ($\sim$ 200 nsec).

* Supported in part by AFOSR under Contract No. F44620-73-C-0077.

1. INTRODUCTION

The diatomic molecules formed from the noble gases, from the partially closed shell Group II B elements (Hg, Cd, Zn) or from the noble gas-halogen combinations constitute an interesting and important class of molecules for laser applications. These molecules are characterized by a repulsive or very weakly bound ground state potential curve and by bound electronically excited states. These excited diatomic molecules, known as excimers, radiate in a narrow visible or UV continuum band by making a transition to a repulsive lower state that dissociates to ground state neutral atoms. Laser behavior is controlled by competing kinetic processes for the formation and destruction of the excited molecular levels. The character of the electronic structure of the excited states in the noble gas halide systems is strongly ionic and is similar to that of the ground state alkali halide salts. The other molecules exhibit mainly Rydberg character in their excited electronic states.

Emission spectra for several noble gas halides have been obtained in low-pressure discharge flow experiments and were first reported by Velazco and Setser[1] and by Golde and Thrush.[2] More recently emission spectra and laser action in several noble gas halide systems have been reported.[3-14] The spectra are consistent with a model whereby the lasing transition is between a strongly bound upper electronic state and a nearly flat repulsive ground state. A group theoretical analysis of the possible electronic configurations for these states does not lead to a unique assignment since both the upper and lower levels could be of $^2\Sigma^+$ or $^2\Pi$ symmetry.

Theoretical studies of the noble gas halide molecules have consisted of

analogies with alkali halide systems,[3] predictions based on an electron-gas model[15] and ab initio calculations for the KrF system.[16] In some cases, the theoretical methods utilized to date have been unable to positively define the electronic states involved in the noble gas halide laser systems. Ab initio methods would appear to be practical only for the lighter systems such as ArF and KrF owing to greatly increased computational complexity for larger numbers of electrons. However, detailed ab initio CI calculations on systems as complex as XeCl are now in progress.[17] The electron-gas model calculations suffer from the lack of self-consistency in the molecular potential. Recent density functional calculations indicate that self-consistency in the potential is crucial for determining optimum electronic wavefunctions.[18] Such calculations, coupled with a limited number of ab initio calculations carried out for comparison purposes, constitute the principal effort in the present study of excimer systems.

2. ELECTRONIC STRUCTURE

For all of the noble gas halide systems there is an outer crossing of the upper ionic states arising from $R^+ + X^-$ (or R_2^+) (R = noble gas, X = halide) such that these upper molecular states, at their equilibrium internuclear separations, actually lie lower than any of the Rydberg molecular states.

The possible diatomic electronic transitions which correspond to laser activity in these systems therefore reduce to the following set:

$$\begin{array}{ll} B\ ^2\Sigma^+ \rightarrow X\ ^2\Sigma^+ & B\ ^2\Sigma^+ \rightarrow A\ ^2\Pi \\ C\ ^2\Pi \rightarrow X\ ^2\Sigma^+ & C\ ^2\Pi \rightarrow A\ ^2\Pi \end{array} \qquad (1)$$

Further, the $^2\Pi$ state is split into $^2\Pi_{3/2}$ and $^2\Pi_{1/2}$ states owing to spin-orbit

coupling effects in the noble gas positive ion. This splitting is small (782) cm^{-1}) for Ne but is appreciable for Xe (10537 cm^{-1}).

As a result of these several possibilities, a definite assignment of the laser transitions becomes difficult. Brau and Ewing[3,4] have assigned the strong laser transitions in XeBr, XeCl, XeF and KrF to B $^2\Sigma^+_{1/2} \rightarrow X\ ^2\Sigma^+_{1/2}$ in accord with a simple ionic model for the potential curves. Ab initio calculations by Dunning and Hay[16] for KrF also suggest the B $^2\Sigma^+_{1/2} \rightarrow X\ ^2\Sigma^+_{1/2}$ transition corresponds to the observed emission in KrF at 2480 Å. Their potential curves also indicate a C $^2\Pi_{3/2} \rightarrow X\ ^2\Sigma^+_{1/2}$ transition at nearly the same calculated wavelength. Further, their calculations indicate a near degeneracy of the upper ionic B $^2\Sigma^+_{1/2}$ and C $^2\Pi_{3/2}$ states which is difficult to understand in terms of simple charge density models for these excited states.

Clugston and Gordon[15] suggest that the dominant laser transition is C $^2\Pi_{3/2} \rightarrow X\ ^2\Sigma^+_{1/2}$, based on free electron gas model calculations. Recent studies, however, question the reliability of non-SCF model calculations for these systems. In addition, this assignment of a perpendicular transition to the laser emission goes against the experimental observations that such transitions should be weak compared to allowed parallel transitions.

3. CALCULATED RESULTS AND DISCUSSION

In order to shed some light on the above questions, both ab initio and density functional calculations were carried out for the lower and excited levels of ArF and Ar_2F. The ab initio calculations were carried out in a manner similar to that described previously.[19] All nonlinear parameters of the molecular orbital basis functions were individually optimized for each separate

electronic state. The resultant ab initio results are shown in Fig. 1 where we see that the B $^2\Sigma^+_{1/2}$ and C $^2\Pi_{3/2}$ systems are nondegenerate in ArF. The upper C $^2\Pi_{3/2}$ state is less strongly polarized and exhibits a somewhat flatter potential curve giving rise to an inner crossing of A $^2\Sigma^+_{1/2}$ and C $^2\Pi_{3/2}$ at about 1.8 Å.

These calculations indicate the following long-range behavior for the excited state potential curves:

$$B\ ^2\Sigma^+ : \quad V(R)\ (a.u.) = -\frac{1}{R} - \frac{1.16}{R^3} \qquad (2)$$

$$C\ ^2\Pi : \quad V(R)\ (a.u.) = -\frac{1}{R} + \frac{0.58}{R^3}$$

The R^{-3} term arises from the quadrupole contribution to the interaction potential at long range. This term vanishes for the alkali halide diatomic molecules M^+X^- since both positive and negative ions are in the ^1S state. However, for the noble gas halide systems, the noble gas ion is in a ^2P state with a non-vanishing quadrupole moment. Therefore, simple models of the ionic excited states of the noble gas halides, based on analogies with alkali halide systems, need to be modified to properly account for this long-range behavior. The calculated value for the coefficient, β, of the R^{-3} term has the correct theoretical form such as $\beta\ ^2\Sigma^+ = -2\beta\ ^2\Pi$. Although several system assignments are possible within the error of the potential curves, calculations based on the potentials shown in Fig. 1 clearly indicate that only the B $^2\Sigma^+_{1/2} \rightarrow$ X $^2\Sigma^+_{1/2}$ transition exhibits a large transition moment and hence a short ($\sim$5 nsec) radiative lifetime. Our calculated peak emission intensity is at a wavelength of 196 nm as compared with the experimental laser frequency of 193 nm.

Potential energy curves for ArF were also constructed using a density functional method. As described in Ref. 18, our program has been extensively developed beyond the standard techniques described in the literature. Modifications to minimize the muffin-tin potential error and to insure continuity in the molecular potential function have been incorporated into our code which result in more reliable total energies. The results for ArF (without including spin-orbit mixing) are shown in Fig. 2 which indicate quantitative agreement with our ab initio results. Again we see that the C $^2\Pi$ excited state is nondegenerate with the upper B $^2\Sigma^+$ state and that it is somewhat flatter in curvature. The origin of the somewhat steeper repulsion exhibited by all the calculated potentials using this density functional model is now understood as a manifestation of the exchange scaling parameter variation with the effective nuclear charge.

Regions of the potential energy surfaces for Ar_2F have been studied to examine the possible stability of this triatomic molecule in an excited electronic configuration. It has been suggested[20] that the long wavelength radiation seen at 2900 Å in e-beam excited argon-fluorine mixtures (4100 Å for krypton-fluorine mixtures) may be due to a triatomic molecule formed in an excited ionic state from $Ar_2^+ + F^-$, similar to the excited ionic state formed from $Ar^+ + F^-$. Such a molecule would radiate at longer wavelengths since Ar_2^+ is stable relative to $Ar^+ + Ar$.

The molecular correlation diagram for Ar_2F, given in Table I for C_{2v} symmetry, should represent the most stable geometry for both the excited ionic and ground state surfaces. The corresponding orbital designations are also

given for the linear molecule Ar-F-Ar. We have carried out preliminary calculations for the ground and first excited ionic states in $^2A_1$ and $^2B_2$ symmetries. Our calculated results are shown in Fig. 3.

We find a flat potential surface for Ar_2F in the lowest $^2A_1$ state for $R_2 > 2.8$ Å as shown in Fig. 3. This results from forward charge transfer from Ar to the F atom, thereby introducing some ionic character of the type Ar_2^{+x}-F^{-x} which will tend to cancel out neutral atom exchange and overlap effects. For heavier systems such as Xe_2F, some small long-range binding may be found for this lowest $^2A_1$ configuration. The lowest $^2B_2$ state exhibits a somewhat steeper repulsion. For Ar_2 - F separations shorter than 2.6 Å, both the $^2A_1$ and $^2B_2$ lower states exhibit a rapidly increasing repulsion ($\sim$ 5 eV/Å). This character leads to the observed broadband emission seen in these systems.

These initial studies indicate a stable Ar_2F molecule in the excited $^2B_2$ configuration as shown in Fig. 3. Such a molecule could dissociate symmetrically to Ar_2^+ ($^2\Sigma_u^+$) + F^-(^1S_o) or unsummetrically to Ar^+F^- ($^2\Sigma^+$) + Ar (^1S_o). The proper dissociation (or formation path) can be ascertained by more detailed calculations at larger internuclear separations. The excited $^2A_1$ configuration exhibits stability relative to Ar^+F^- + Ar, but not to Ar_2^+ + F^-. A symmetric dissociation leads to the unbound $^2\Sigma_g^+$ state of Ar_2^+ + F^- (^1S_o).

These limited calculations suggest that the upper radiating state of Ar_2F (and Kr_2F) is of $^2B_2$ symmetry with equilibrium bond lengths of $R_{Ar\text{-}Ar} < 2.6$ Å and $R_{Ar\text{-}F} < 2.5$ Å. Using a dissociation energy of 1.25 eV for X $^2\Sigma_u^+$ of Ar_2^+ and our calculated ground state $^2B_2$ repulsion energy, we predict an emission wavelength of $\sim$ 280 nm. The observed emission for Ar_2F is very broad ($\sim$ 50 nm) and

peaks at about 290 nm.

This $^2B_2^* \rightarrow {}^2B_2$ transition corresponds more closely to the C $^2\Pi \rightarrow$ A $^2\Pi$ transition in ArF than to the intense $^2\Sigma^+ \rightarrow {}^2\Sigma^+$ transition. Scaling our calculated transition intensities for C $^2\Pi \rightarrow$ A $^2\Pi$, we predict a radiative lifetime for the ionic $^2B_2^*$ state of $\sim$ 200 nsec. Further detailed studies are in progress to classify the state assignments and predict the radiation characteristics of all the triatomic noble gas halide excimer molecules.

TABLE I. MOLECULAR ORBITAL CORRELATION DIAGRAM FOR Ar_2F

Symmetry	Orbitals (Valence Shell Electrons)											
	Ar	Ar	F	Ar	Ar	Ar	Ar	Ar	Ar	F	F	F
Atomic	3s	3s	2s	$3p_z$	$3p_y$	$3p_x$	$3p_y$	$3p_x$	$3p_z$	$2p_x$	$2p_z$	$2p_y$
$D_{\infty h}$	$1\sigma_g$	$1\sigma_u$	$2\sigma_g$	$3\sigma_g$	$1\pi_u$	$1\pi_u$	$1\pi_g$	$1\pi_g$	$2\sigma_u$	$2\pi_u$	$3\sigma_u$	$2\pi_u$
C_{2v}	$1a_1$	$1b_2$	$2a_1$	$3a_1$	$4a_1$	$1b_1$	$2b_2$	$1a_2$	$3b_2$	$2b_1$	$4b_2$	$5a_1$

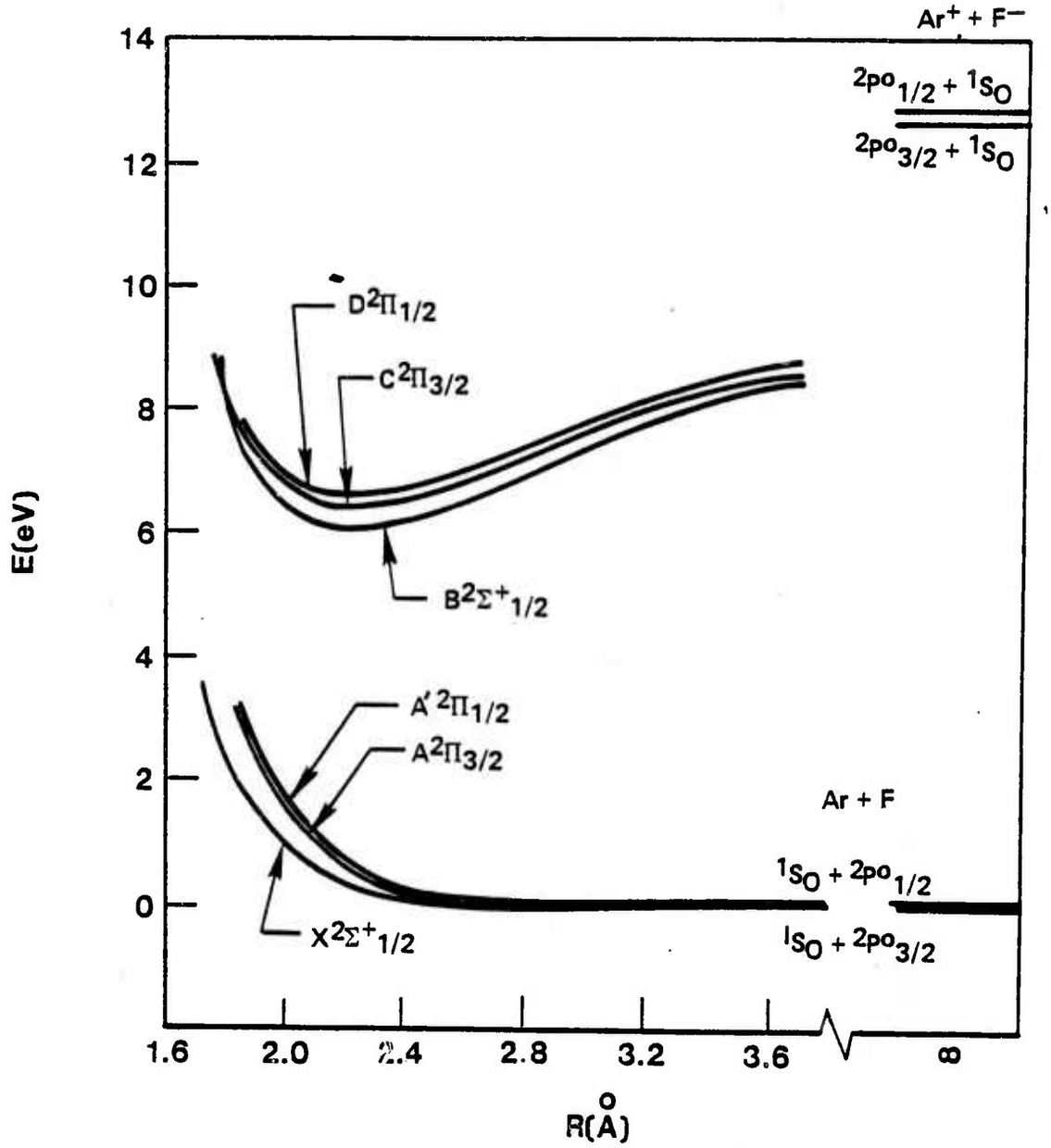

Figure 1 Potential Energy Curves for ArF
(Ab Initio Method)

77-04-40-3

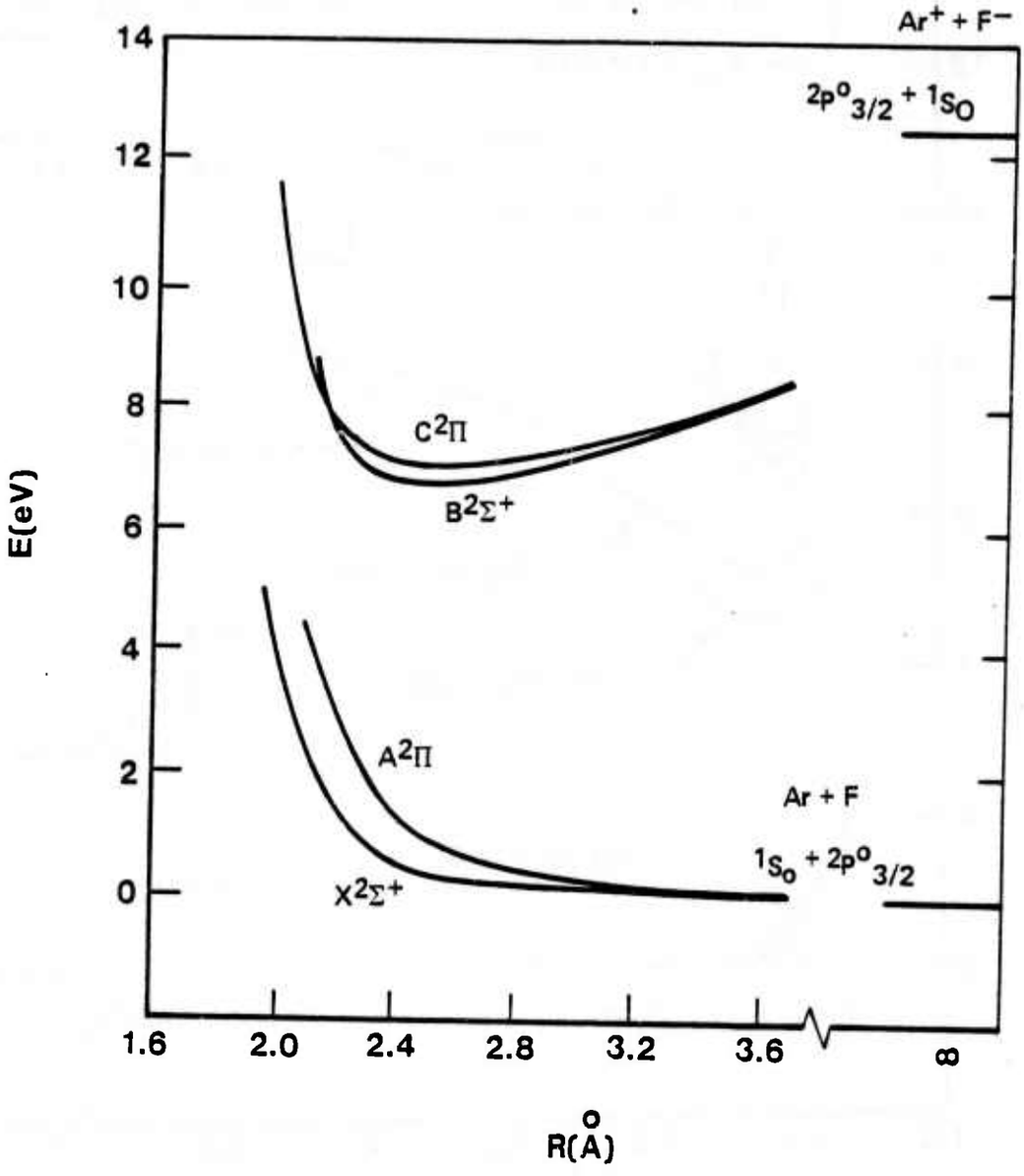

Figure 2 Potential Energy Curves for ArF (Density Functional Method)

77-04-40-2

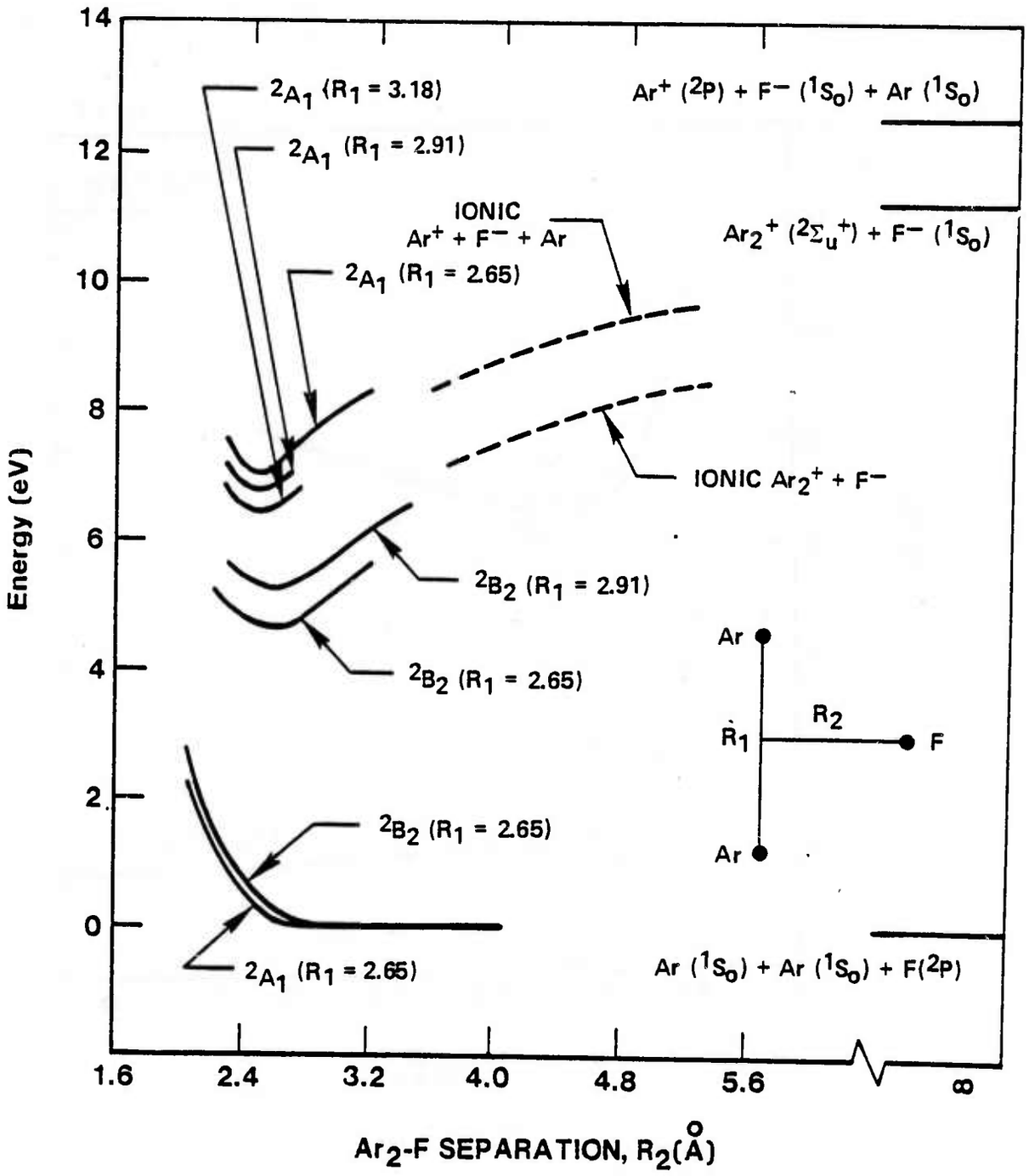

Figure 3 Potential Energy Curves for Ar_2F (Density Functional Method)

77-04-40-1

REFERENCES

1. J. E. Velazco and D. W. Setser, Journal of Chemical Physics, 62, 1990 (1975).
2. M. F. Golde and B. A. Thrush, Chemical Physics Letters, 29, 486 (1974).
3. C. A. Brau and J. J. Ewing, Journal of Chemical Physics, 63, 4640 (1975).
4. J. J. Ewing and C. A. Brau, Physical Review, 12, 129 (1975).
5. S. K. Searles and G. A. Hart, Applied Physics Letters, 27, 243 (1975).
6. J. J. Ewing and C. A. Brau, Applied Physics Letters, 27, 350 (1975).
7. C. A. Brau and J. J. Ewing, Applied Physics Letters, 27, 435 (1975).
8. E. R. Ault, R. S. Bradford, Jr., and M. L. Bhaumik, Applied Physics Letters, 27, 413 (1975).
9. M. L. Bhaumik, R. S. Bradford, Jr., and E. R. Ault, Applied Physics Letters, 28, 23 (1975).
10. G. C. Tisone, A. K. Hayes and J. M. Hoffman, Optical Communications, 15, 188 (1975).
11. J. Tellinghuisen, J. M. Hoffman, G. C. Tisone and A. K. Hayes, Journal of Chemical Physics, 65, 4473 (1976).
12. R. A. Gerber and E. L. Patterson, IEEE J. Quantum Electron. QE-11, 642 (1975).
13. M. F. Golde, Journal of Molecular Spectroscopy, 58, 261 (1975).
14. J. M. Hoffman, A. K. Hayes and G. C. Tisone, Applied Physics Letters, 28, 538 (1976).

15. M. J. Clugston and R. G. Gordon, Journal of Applied Physics (to be published).

16. T. H. Dunning, Jr. and P. J. Hay, Applied Physics Letters, 28, 649 (1976).

17. P. J. Hay and T. H. Dunning, Third Colloquium on Electronic Transition Lasers, Aspen, Colorado, September 7-10, 1976.

18. H. H. Michels, R. H. Hobbs and J. C. Connolly, Optimized SCF-X_α Procedures for Heterpolar Molecules, Journal of Chemical Physics (to be published).

19. F. E. Harris and H. H. Michels, Intern. J. Quant. Chem. IS, 329 (1967).

20. M. Krauss, private communication.

APPENDIX B

THE ELECTRONIC STRUCTURE OF EXCIMER MOLECULAR LASERS*

L. A. Wright (DYP)
Kirtland Air Force Base, New Mexico 87117

ABSTRACT

The electronic structure, potential energy curves and radiative transition probabilities of excimer systems have been examined using quantum mechanical methods. These molecules are characterized by repulsive or weakly bound ground state potential curves and by bound, strongly ionic, or Rydberg, excited states. They constitute a very interesting class of molecules which offer the possibility for high power, high efficiency UV laser operation. Calculations have been carried out using the density functional SCF-X_α method, modified extensively to correct for well-known errors arising from approximations to the potential and exchange terms. A limited number of ab initio calculations were also carried out for comparison purposes. For the ArF system we find that the lowest

*Supported in part by AFOSR under Contract No. F44620-73-C-0077.
**Permanent Address: Quantum Theory Project
University of Florida
Gainesville, Florida 32611

excited ionic state has symmetry $^2\Sigma^+_{1/2}$, and that the dominant laser transition observed at 1933 Å should be assigned to B $^2\Sigma^+_{1/2} \rightarrow$ X $^2\Sigma^+_{1/2}$. The C $^2\Pi_{3/2} \rightarrow$ X $^2\Sigma^+_{1/2}$ transition is calculated to be two orders of magnitude smaller in emission intensity than the dominant transition, thus ruling out this assignment for the observed laser line in ArF. Preliminary calculations carried out for Ar_2F indicate that the bound upper ionic state has $^2B_2$ symmetry and that the most probable ground state also has $^2B_2$ symmetry. This polyatomic system is predicted to exhibit a broadband emission spectra with a relatively long radiative lifetime.

ACKNOWLEDGMENT

The authors wish to thank Ms. J. B. Addison and acknowledge her valuable assistance in carrying out the computational analysis of this work. Use of the computational facilities at the Kirtland Air Force Base in Albuquerque is also acknowledged.

INTRODUCTION

The diatomic molecules formed from the noble gases, from the partially closed shell Group II B elements (Hg, Cd, Zn) or from the noble gas-halogen combinations constitute an interesting and important class of molecules for laser applications. These molecules are characterized by a repulsive or very weakly bound ground state potential curve and by bound electronically excited states. These excited diatomic molecules, known as excimers, radiate in a narrow visible or UV continuum band by making a transition to a repulsive lower state that dissociates to ground state neutral atoms. Laser behavior is controlled by competing kinetic processes for the formation and destruction of the excited molecular levels. The character of the electronic structure of the excited states in the noble gas halide systems is strongly ionic and is similar to that of the ground state alkali halide salts. The other molecules exhibit mainly Rydberg character in their excited electronic states.

The system Xe_2, shown in figure 1, is typical of the noble gas excimer lasers. Because the ground state potential is almost purely repulsive, the emission is a continuum which stretches from the atomic resonance line at 1470 Å to 2200 Å. This emission has been studied extensively (ref. 1) and has been widely used as a background source for VUV absorption spectroscopy. Houtermans (ref. 2) was the first to propose the use of bound-free transitions (in Hg_2) for a laser system, but it was not until 1970 that Basov (ref. 3) demonstrated gain

at 1750 Å by pumping liquid xenon with a high current beam of electrons. Since then many workers have reported laser action in the gaseous phase in xenon and krypton A (ref. 4).

Emission spectra for several noble gas halides have been obtained in low pressure discharge flow experiments and were first reported by Velazco and Setser (ref. 5) and by Golde and Thrush (ref. 6). More recently, emission spectra and laser action in several noble gas halide systems have been reported (refs. 7-18). The spectra are consistent with a model whereby the lasing transition is between a strongly bound upper electronic state and a nearly flat repulsive ground state. A group theoretical analysis of the possible electronic configurations for these states does not lead to a unique assignment since both the upper and lower levels could be of $^2\Sigma^+$ or $^2\Pi$ symmetry.

In addition to the noble gas molecules, systems such as Hg_2, HgCd, and HgTl have been proposed (refs. 2, 19-21) as a class of excimers which radiate in the visible region of the spectrum. For these systems, the partially filled shell of Hg ($5d^{10}$ $6s^2$) results in noble gas-like behavior and leads to potential curves analogous to those arising in Xe_2. For the HgTl system, a low-lying ionic state can occur, and the electronic structure is probably more like that of the noble gas halide molecules.

The theoretical principles governing the electronic structure of the homonuclear noble gas molecules have been discussed by Mulliken (ref. 22) using Xe_2 as a prototype and more recently by Barr, Dee, and Gilmore (ref. 23) for the case of Kr_2. In these molecules, the ground state is represented by a repulsive

potential curve connecting to ^1S_o states of the separated atoms. The excited states constitute a Rydberg series terminating on the molecular ion of symmetry $^2\Sigma^+_u$ or $1/2_u$, the latter being more appropriate for the heavier systems such as Xe_2 where L-S coupling is no longer strictly valid. These excited state potential curves can be located with good accuracy using quantum defect theory coupled with an accurate representation of the ground state of the molecular ion. the radiative decay time for an excited Xe_2 or Kr_2 molecule has been estimated to be so short (10 nsec), that fast pumping techniques are required to produce significant populations in their excited states.

Theoretical studies of the noble gas halide molecules have consisted of analogies with alkali halide systems (ref. 7), predictions based on an electron-gas model (ref. 24) and ab initio calculations for the KrF system (ref. 25). In some cases, the theoretical methods utilized to date have been unable to positively define the electronic states involved in the noble gas halide laser systems. Ab initio methods would appear to be practical only for the lighter systems such as ArF and KrF owing to greatly increased computational complexity for larger numbers of electrons. However, detailed ab initio CI calculations on systems as complex as XeCl are now in progress (ref. 26). The electron-gas model calculations suffer from the lack of self-consistency in the molecular potential. Recent density functional calculations indicate that self-consistency in the potential is crucial to determining optimum electronic wavefunctions (ref. 27). Such calculations, coupled with a limited number of ab initio calculations carried out for comparision purposes, constitute the principle effort in the present study of excimer systems.

METHOD OF APPROACH

Density Functional Approach - X_α Model

The X_α model (ref. 28) for the electronic structure of atoms, molecules, clusters and solids is a local potential model obtained by making a simple approximation to the exchange-correlation energy. If we assume a nonrelativistic Hamiltonian with only electrostatic interactions, it can be shown that the total energy E of a system can be written exactly (ref. 29) (in atomic units) as

$$E = \sum_i n_i \left\langle u_i \left| -\tfrac{1}{2}\nabla_i^2 + \sum_\mu \frac{z_\mu}{r_{i\mu}} \right| u_i \right\rangle + \tfrac{1}{2} \sum_{\mu \neq \nu} \frac{z_\mu z_\nu}{r_{\mu\nu}}$$

$$+ \tfrac{1}{2} \sum_{ij} n_i n_j \left\langle u_i u_j \left| \frac{1}{r_{12}} \right| u_i u_j \right\rangle + E_{xc} \qquad (1)$$

This expression is exact provided the u_i are natural orbitals and n_i are their occupation numbers (i.e., eigenfunctions and eigenvalues of the first order density matrix). The first term in equation (1) represents the kinetic and electron-nuclear energies. The second term is the nuclear repulsion energy. The sums (μ, ν) are over all the nuclear charges in the system. The third term is the electron-electron repulsion term, which represents the classical electrostatic energy of the charge density ρ interacting with itself, where

$$\rho(1) = \sum_i n_i u_i^*(1)\, u_i(1) \qquad (2)$$

The last term ρ_{xc} (1,2) represents the exchange-correlation energy and can be expressed formally as

$$E_{xc} = \frac{1}{2} \int \rho(1)\, d\vec{r}_1 \int \frac{\rho_{xc}(1,2)}{r_{12}}\, d\vec{r}_2 \,, \tag{3}$$

where ρ_{xc} (1,2) represents the exchange-correlation hole around an electron at position 1. In the exact expression, ρ_{xc} is dependent on the second-order density matrix. In the Hartree-Fock approximation E_{xc} is the exchange energy, ρ_{xc} represents the Fermi hole due to the exclusion principle and depends only on the first-order density matrix. In the X_α method, we make a simpler assumption about ρ_{xc}. If we assume that the exchange-correlation hole is centered on the electron and is spherically symmetric, it can be shown that the exchange-correlation potential

$$u_{xc} = \int \frac{\rho_{xc}(1,2)}{r_{12}}\, d\vec{r}_2 \tag{4}$$

is inversely proportional to the range of the hole, r_s, where r_2 is defined by

$$\frac{4\pi}{3}\, r_s^3\, \rho(1) = 1 \tag{5}$$

Therefore, in the X_α model, the potential U_{xc} is proportional to $\rho^{1/3}(\vec{r})$ A scaling parameter α is defined such that

$$U_{x\alpha}(1) = -\frac{9\alpha}{2} \left(3\rho(1)/8\pi\right)^{1/3} \tag{6}$$

The expression in equation (6) is defined so that $\alpha = 2/3$ for the case of a free-electron gas in the Hartree-Fock model (ref. 30) and $\alpha = 1$ for the potential originally suggested by Slater (ref. 31). A convenient way to choose this parameter for molecular and solid state applications is to optimize the solutions to the X_α equations in the atomic limit. Schwarz (ref. 32) has done this for atoms from $Z = 1$ to $Z = 41$ and found values between 2/3 and 1.

Computational Aspects of the X_α Method

To implement the X_α approximation in molecular calculations, it is usually convenient to break up the volume integrals indicated in equations (3) or (4) by defining spherical regions surrounding each atomic center. The molecular potential is then spherically averaged within these regions and assumed constant in the region between spheres. The potential falls to zero in the usual way in the region outside of an overall sphere located to encompass those spheres surrounding the individual atoms.

There are two other practical aspects of the calculations which must be considered in application of the X_α model to finite molecular systems. The first concerns the choice of the integration framework for describing the molecular-orbital wavefunctions, and the second deals with the choice of the exchange parameter, α, in different regions of space. A third consideration, convergence of the spherical harmonic expansion, was also tested. The total energy was converged when all terms up to $l = 3$ were included.

In computations with heteronuclear molecules, there are several free parameters that must be chosen: the ratio of sphere radii for the atomic spheres of integration at a given internuclear separation, the degree of sphere overlap, and the value of the exchange parameter in the atomic spheres and the intersphere region.

It has been found that changing the ratio of the sphere radii for the two atoms in a heternuclear diatomic molecule introduces changes in the total energy that can be large on a chemical scale, ($\sim$1 eV) (ref. 27). A choice for sphere radii based on covalent bonding radii does not necessarily provide a good estimate for these calculations. the value of the exchange parameter, α, and the sphere radii and/or sphere overlap is normally fixed in X_α calculations for crystals, where the geometry is fixed. However, to develop a potential curve, the molecular description needs to change substantially as the internuclear separation varies and the changing sphere radii include varying fractions of the total molecular charge (ref. 27). Our studies have shown that at any given separation, the total energy calculated from the X_α model is a minimum at the radii ratio where the spherically averaged potentials from the two atomic centers is equal at the sphere radius,

$$V_1(r_{s_1}) = V_2(r_{s_2}) \tag{7}$$

This relationship between the potential match at the sphere boundary and the minimum in the total energy appears to hold exactly for "neutral" atoms and holds well for ionic molecular constituents. In the case of two ionic species,

the long-range tail of the potential must go like +2/R from one ion and -2/R (in Rydbergs) for the other ion and so at large internuclear separations, the tails of the potential cannot match well. However, at intermediate separations, the 1/R character of the potential does not invalidate the potential match criterion for radii selection. This match for the atomic potentials is applied to the self-consistent potentials.

A double iteration is now required for each chosen internuclear geometry. Computationally, an initial choice for the sphere radii is made, and the calculation is iterated to self-consistency in the charge. A comparison of the values of the potential at the sphere radii is then made, and an adjustment in their ratios is carried out until equation (7) is satisfied to within a few percent.

In molecules with significant charge sharing in the bonds, the radii of the atomic spheres is frequently increased in X_α calculations so that an overlap region appears in the vicinity of the bond (ref. 33). Our studies have shown that the contribution to the total molecular energy from the exchange-correlation term shows a minimum at the optimum sphere radius or sphere overlap. This provides a sensitive criterion for selecting these parameters.

The values of the exchange parameters in the spherical integration region around each atomic center are frequently set at the atomic values both for neutral and for ionic molecular constituents. However, for light atoms, the value of α which best reproduces Hartree Fock results varies substantially with ionicity. In Ar and Ar^+, the following table compares the HF energy and the X_α energy calculated for several values of α.

	α	X_α Energy (a.u.)	HF Energy (a.u.)
Ar^0	.72177	-526.8176	-526.8173
$Ar^{+1/2}$	.72177	-526.5857	-
	.72213	-526.6007	-
Ar^{+1}	.72177	-526.2447	-
	.72213	-526.2596	-
	.72249	-526.2745	-526.2743

The optimum value of α changes even more rapidly in the fluorine atom, going from 0.73732 for F^0 to 0.72991 for F^{-1}. Since the total energy depends linearly on α, this parameter must be chosen carefully.

The intersphere exchange coefficient is chosen to be a weighted average of the atomic exchange parameters from the two constituents. At small internuclear separations, the optimum radius for an atomic sphere frequently places significant amounts of charge outside that atomic sphere - charge that is still strongly associated with its original center rather than being transferred to the other center or associated with the molecular binding region. To best account for these cases, the weighting coefficients are chosen to reflect the origin of the charge in the intersphere (or outersphere region).

$$\alpha_{\text{intersphere}} = \frac{\alpha_{s_1}(Q_{s_1} - Q_1^0) + \alpha_{s_2}(Q_{s_2} - Q_2^0)}{(Q_{s_1} - Q_1^0) + (Q_{s_2} - Q_2^0)} \qquad (8)$$

where $(Q_{s_i} - Q_i^0)$ is the charge lost from sphere i relative to its atomic value (or ionic value Q_i^0 and α_{si} is the atomic exchange parameter for sphere i. This value for $\alpha_{\text{intersphere}}$ is calculated dynamically - it is updated after each iteration in the self-consistent calculation.

While for heavy atoms, these changes in the exchange parameter would be small, the α's for small atoms vary rapidly with z (and with ionicity). The correct choice of the exchange parameters influences not only the total energy calculated for the molecule but also affects the distribution of charge between the atomic spheres and the intersphere region.

Ab Initio Approach - Valence CI Method

The ab initio calculation procedure chosen for these studies is the valence-configuration-interaction (VCI) method (refs. 34, 35). A spin-free nonrelativistic electrostatic Hamiltonian is employed within the Born-Oppenheimer approximation. For a diatomic molecule, this approximation leads to an electronic Hamiltonian depending parametrically on the internuclear separation R. Electronic wave functions $\psi(R)$ are made to be optimum approximations to solutions of the Schrödinger equation

$$H(R)\psi(R)=E(R)\psi(R) \tag{9}$$

by invoking the variational principle. The specific form for $\psi(R)$ may be written as

$$\psi(R)=\sum_{\mu} c_{\mu}\psi_{\mu}(R) \tag{10}$$

where each $\psi(R)$ is referred to as a configuration and has the general structure

$$\psi_{\mu}(R)=\mathcal{A}\mathcal{O}\prod_{i=1}^{n}\phi_{\mu i}(\vec{r}_i, R)\theta_M \tag{11}$$

where ψ_{ui} is a spatial orbital, $\mathcal{A}$ is the antisymmetrizing operator, η_s is the spin-projection operator for spin quantum number S, and θ_{M_s} is a product of α and β one-electron spin functions of magnetic quantum number, M_s. The spatial orbitals, ψ_i, have the general form

$$\phi_i = \exp\{-\delta_i\xi - \zeta_i\eta + i\nu_i\phi\}\xi^p\eta^q r^{n_i-1} P_l^{|\nu_i|}(\cos\theta) \qquad (12)$$

where for $\zeta_i = \pm\delta_i$, the standard STO form is required. If no restriction is imposed as to the double occupancy of the spatial orbitals, equations (10) and (11) can describe a completely general wave function.

The basis functions chosen for describing the molecular system ArF were opimized elliptic orbitals. A minimum basis was chosen for the K and L inner shells, and both minimum and elliptic basis were used to describe the valence electrons. A typical basis for R = 3.5 a.u. is given in Table I. Configuration interaction was taken only over the valence-shell electrons. Such a wave function gives an accurate representation of the interatomic potentials at large internuclear separations but must become poorer at short separations where L-shell polarization effects are important. Both σ- and π- coupled valence configurations were included as well as ionic configurations. The configuration interaction constituted a complete CI over the valence shell electrons.

RESULTS AND DISCUSSION

We have carried out both detailed ab initio and density functional X_α calculations for the ArF and Ar_2F systems to assess problems, both conceptual and computational, in defining the electronic structure of the noble gas halides.

A general correlation diagram for the diatomic systems is shown in Fig. 2. Here we have indicated the detailed coupling of atomic states to form the ground (mainly repulsive) molecular levels, the coupling of the ionic states R^+ and X^- to form the upper ionic molecular levels and the very complicated excited Rydberg state structure for these systems. Only the lower-lying Rydberg states that arise from excitation in the noble gas or excitation in the corresponding halide have been included in this correlation diagram. The left-hand side corresponds to pure (Λ,S) coupling which is mainly applicable to light systems such as ArF. The right-hand side corresponds to pure (J,J) coupling which probably is never quite realized, even for a system as heavy as XeI. Unfortunately, intermediate coupling is indicated for the majority of these noble gas halide systems and some studies of molecular spin-orbit coupling parameters are clearly indicated. The correlation diagram for the triatomic system Ar_2F is shown in Table I for C_{2v} symmetry. This symmetry dissociates to $R_2^+ + F^-$ in a symmetrical configuration. Studies of the potential energy surfaces for a lesser symmetry may be needed to examine the dissociation channel $R^+X^- + R$.

For all of the noble gas halide systems there is an outer crossing of the upper ionic states arising from $R^+ + X^-$ (or R_2^+) (R = noble gas, x = halide)

such that these upper molecular states, at their equilibrium internuclear separations, actually lie lower than any of the Rydberg molecular states. For example, the lowest Rydberg level for ArF arises from Ar $^3P(4s)$ + F ^2P at 11.55 eV. The ionic states of $Ar^+ + F^-$ at 12.31 eV thus cross these Rydberg states at R = 36 bohr radii.

The possible diatomic electronic transitions which correspond to laser activity in these systems therefore reduce to the following set:

$$\begin{array}{ll} B\ ^2\Sigma^+ \rightarrow X\ ^2\Sigma^+ & B\ ^2\Sigma^+ \rightarrow A\ ^2\Pi \\ C\ ^2\Pi \rightarrow X\ ^2\Sigma^+ & C\ ^2\Pi \rightarrow A\ ^2\Pi \end{array} \qquad (13)$$

Further the C $^2\Pi$ state is split into $^2\Pi_{3/2}$ and $^2\Pi_{1/2}$ states owing to spin-orbit coupling effects in the noble gas positive ion. This splitting is small (782 cm^{-1}) for Ne but is appreciable for Xe (10537 cm^{-1}).

As a result of these several possibilities, a definite assignment of the laser transitions becomes difficult. Brau and Ewing (refs. 7, 8) have assigned the strong laser transitions in XeBr, XeCl, XeF and KrF to $B\ ^2\Sigma^+_{1/2} \rightarrow X\ ^2\Sigma^+_{1/2}$ in accord with a simple ionic model for the potential curves. Ab initio calculations by Dunning and Hay (ref. 25) for KrF also suggest the $B\ ^2\Sigma^+_{1/2} \rightarrow X\ ^2\Sigma^+_{1/2}$ transition corresponds to the observed emission in KrF at 2480Å. Their potential curves, however, also indicate a $C\ ^2\Pi_{3/2} \rightarrow X^2\Sigma^+_{1/2}$ transition at nearly the same calculated wavelength. Further, their calculations indicate a near degeneracy of the upper ionic $B\ ^2\Sigma^+_{1/2}$ and $C^2\Pi_{3/2}$ states which is difficult to understand in terms of simple charge density models for these excited states.

Clugston and Gordon (ref 24) suggest that the dominant laser transition is C $^2\Pi_{3/2} \rightarrow X\ ^2\Sigma^+_{1/2}$, based on free-electron gas model calculations. Recent studies, however, question the reliability of non-SCF model calculations for these systems (ref. 27). In addition, this assignment of a perpendicular transition to the laser emission goes against the experimental observation that such transitions should be weak compared to allowed parallel transitions.

In order to shed some light on the above questions, both ab initio and density functional calculations were carried out for the lower and excited levels of ArF and Ar_2F. The ab initio calculations were carried out in a manner similar to that described previously (ref.34). All nonlinear parameters of the molecular orbital basis functions were individually optimized for each separate electronic state. The resultant ab initio potential curves are shown in Fig. 3 and Table III where we see that, unlike the previously reported ab initio studies of KrF (ref. 25), the B $^2\Sigma^+_{1/2}$ and C $^2\Pi_{3/2}$ systems are non-degenerate. The upper C $^2\Pi_{3/2}$ state is less strongly polarized than the B $^2\Sigma^+_{1/2}$ state and exhibits a somewhat flatter potential curve giving rise to an inner crossing of B $^2\Sigma^+_{1/2}$ and C $^2\Pi_{3/2}$ at about 1.8 Å.

These ab initio calculations indicate the following long-range behavior for the excited state potential curves:

$$B\ ^2\Sigma^+: V(R)\,(\text{a.u.}) = -\frac{1}{R} - \frac{1.16}{R^3}$$
$$C\ ^2\Pi: V(R)\,(\text{a.u.}) = -\frac{1}{R} + \frac{0.58}{R^3} \qquad (14)$$

The R^{-3} term arises, for these molecules, mainly from the quadrupole contribution to the interaction potential at long range. This term vanishes for the alkali halide diatomic molecules M^+X^- since both positive and negative ions are in the ^1S state with a non-vanishing quadrupole moment. Therefore, simple models of the ionic excited states of the noble gas halides, based on analogies with alkali halide systems, need to be modified to properly account for this long range behavior. The calculated value for the coefficient, β, of the R^{-3} term has the correct theoretical form such that

$$\beta(^2\Sigma^+) = -2\beta(^2\Pi) \tag{15}$$

Calculated spontaneous emission spectra, without inclusion of spin-orbit Σ-Π mixing, are shown in Fig. 4. They are in good agreement with previously reported emission spectra (ref. 10) when the state mixing effects are properly accounted for and suggest a mild repulsion in the ground state at the minimum of the excited potential curve since the half-width of the strong transition is about 80 Å.

Although several system assignments are possible within the calculated error of the potential curves, Fig. 4 clearly indicates that only the $B\ ^2\Sigma^+ \rightarrow X\ ^2\Sigma^+$ transition exhibits a large transition moment and hence a short (~ 5 nsec) radiative lifetime. Thus the original assignment of Ewing and Brau of the $B\ ^2\Sigma^+ \rightarrow X^2\Sigma^+$ transition to the strong laser line in these noble gas halide systems appears to be confirmed by these detailed calculations.

As a comparision, potential energy curves for ArF were also constructed using a density functional method. As described above, our program has been

extensively developed beyond the standard techniques described in the literature. Modifications to minimize the muffin-tin potential error and to insure continuity in the molecular potential function have been incorporated into our code which results in more reliable total energies. The results for ArF are shown in Fig. 5 and Table IV which indicate good agreement with our ab initio results. Again we see that the C $^2\Pi$ excited state is nondegenerate with the upper B $^2\Sigma^+$ state and that it is somewhat flatter in curvature. The origin of the somewhat steeper repulsion exhibited by all the calculated potentials using this density functional model is now understood as a manifestation of the exchange scaling parameter variation with the effective nuclear charge. Thus α in Eq. (6) should be modified at each internuclear separation to account for internal changes from Ar-F to $Ar^{+\delta}$ - $F^{-\delta}$. By introducing a concept which we call "dynamic scaling" into the density functional calculations, our most recent data for ArF are now almost in complete agreement with the ab initio results. The procedure is somewhat akin to uniform scaling of a wavefunction in an ab initio calculation. The significant point here is that this density functional method can be applied to a system such as Kr_2F with only about 2-3 times the effort that is required for KrF. In contrast, ab initio calculations for Kr_2F would constitute an enormous (> 100) increase in effort over that required for a study of KrF of comparable accuracy. The density functional method thus offers promise of giving a uniform description of the electronic structure of all the viable candidates for noble gas halide laser systems.

Recently, regions of the potential energy surfaces for Ar_2F have been studied to examine the possible stability of this triatomic molecule in an excited electronic configuration. It has been suggested (ref. 36) that the long wavelength radiation seen at 2900 Å in the e-beam excited argon-fluorine mixtures (4100 Å for krypton-fluorine mixtures) may be due to a triatomic molecule formed in an excited ionic state from $Ar_2^+ + F^-$, similar to the excited ionic state formed from $Ar^+ + F^-$. Such a molecule would radiate at longer wavelength since Ar_2^+ is stable relative to $Ar^+ + Ar$.

The molecular correlation diagram for Ar_2F, given in Table I for C_{2v} symmetry, should represent the most stable geometry for both the excited ionic and ground state surfaces. The corresponding orbital designations are also given for the linear molecule Ar-F-Ar. We have carried out preliminary calculations for the ground state in $^2A_1$ and $^2B_2$ symmetries and for excited electronic states in $^2B_2$ and $^2A_1$ symmetry. Our calculated results are shown in Fig. 6.

We find a flat potential surface for Ar_2F in the lowest $^2A_1$ state for $R_2 > 2.8$ Å as shown in Fig. 6. This results from forward charge transfer from Ar to the F atom, thereby introducing some ionic character of the type $Ar_2^{+x} - F^{-x}$ which will tend to cancel out neutral atom exchange and overlap effects. For heavier systems such as Xe_2F, some small binding may be found for this lowest $^2A_1$ configuration. The lowest $^2B_2$ state exhibits a somewhat steeper repulsion.

These initial studies indicate a stable Ar_2F molecule in the excited $^2B_2$ configuration as shown in Fig. 6. Such a molecule could dissociate

symmetrically to Ar^+_2 ($^2\Sigma_u^+$) + F^-(^1S_o) or unsymmetrically to Ar^+F^- ($^2\Sigma^+$) + Ar (^1S_o)The proper dissociation (or formation path) can be ascertained by more detailed calculations at larger internuclear separations. The excited $^2A_1$ configuration exhibits stability relative to Ar^+F^- + Ar, as shown in Fig. 6, but not to Ar_2^+ + F^-. A symmetric dissociation leads to the unbound $^2\Sigma_g$ state of Ar_2^+ + F^- (^1S_o).

These limited calculations suggest that the upper radiating state of Ar_2F (and Kr_2F) is of $^2B_2$ symmetry with equilibrium bond lengths of $R_{Ar-Ar} < 2.6$ Å and $R_{Ar-F} < 2.5$ Å. Using a dissociation energy of 1.25 eV for $X^2\Sigma_u^+$ of Ar_2^+ and our calculated ground state $^2B_2$ repulsion energy, we predict an emission wavelength of ~ 280 nm. The observed emission for Ar_2F is very broad ($\Delta \sim 50$ nm) and peaks at about 290 nm.

This $^2B_2^* \rightarrow {}^2B_2$ transition corresponds more closely to the C $^2\Pi \rightarrow$ A $^2\Pi$ transition in ArF than to the intense $^2\Sigma^+ \rightarrow {}^2\Sigma^+$ transition. Scaling our calculated transition intensities for C $^2\Pi \rightarrow$ A $^2\Pi$, we predict a radiative lifetime for the ionic $^2B_2^*$ state of ~ 200 nsec. Further detailed studies are in progress to classify the state assignments and predict the radiation characteristics of the triatomic noble gas halide excimer molecules.

TABLE I

OPTIMIZED ELLIPTIC ORBITALS FOR ArF AT R = 3.5 a.u.

Ar	$^2\Sigma^+$(I)		$^2\Sigma^+$(II)		$^2\Pi$(I)		$^2\Pi$(II)	
	δ	ζ	δ	ζ	δ	ζ	δ	ζ
3s*	2.5635	2.6390	2.5795	2.7532	2.5519	2.6489	2.5853	2.7706
$3p_1$	2.2528	2.2619	2.3049	2.3731	2.2500	2.2372	2.3114	2.4049
$3p_o$	2.2728	2.3074	2.2763	2.5828	2.2520	2.3632	2.3014	2.5164
2s	2.5507	2.5807	2.5034	2.4979	2.5544	2.5783	2.4933	2.4963
$2p_1$	2.5053	2.5498	2.3697	2.3624	2.5277	2.5713	2.3379	2.3275
$2p_0$	2.5996	2.6163	2.4338	2.4254	2.5562	2.5957	2.4198	2.3920

* The approximate STO form is used here to label these elliptic functions.

TABLE II

MOLECULAR ORBITAL CORRELATION DIAGRAM FOR Ar_2F

Symmetry	Orbitals (Valence Shell Electrons)											
	Ar	Ar	F	Ar	Ar	Ar	Ar	Ar	Ar	F	F	F
Atomic	3s	3s	2s	$3p_z$	$3p_y$	$3p_x$	$3p_y$	$3p_x$	$3p_z$	$2p_x$	$2p_z$	$2p_y$
$D_{\infty h}$	$1\sigma_g$	$1\sigma_u$	$2\sigma_g$	$3\sigma_g$	$1\pi_u$	$1\pi_u$	$1\pi_g$	$1\pi_g$	$2\sigma_u$	$2\pi_u$	$3\sigma_u$	$2\pi_u$
C_{2v}	$1a_1$	$1b_2$	$2a_1$	$3a_1$	$4a_1$	$1b_1$	$2b_2$	$1a_2$	$3b_2$	$2b_1$	$4b_2$	$5a_1$

TABLE III

Ab INITIO POTENTIAL CURVES FOR ArF (INCLUDING SPIN-ORBIT CORRECTION)

Energy (eV)

R(a.u.)	$X^2\Sigma^+$	$A^2\Pi_{3/2}$	$A'^2\Pi_{1/2}$	$B^2\Sigma^+_{1/2}$	$C^2\Pi_{3/2}$	$D^2\Pi_{1/2}$
3.50	1.8635	3.1808	3.2309	7.4317	7.5699	7.7474
3.75	1.0104	1.8191	1.8692	6.4926	6.7506	6.9281
4.00	0.5236	1.0125	1.0626	6.0937	6.4284	6.6059
4.25	0.2474	0.5393	0.5894	6.0194	6.3805	6.5580
4.50	0.0980	0.2718	0.3219	6.1318	6.4899	6.6674
4.75	0.0201	0.1238	0.1739	6.3381	6.6771	6.8546
5.00	0.0185	0.0449	0.0950	6.5854	6.8970	7.0745
6.00	0.0022	0.0049	0.0550	7.6301	7.8469	8.0244
7.00	0.0	0.0003	0.0504	8.3294	8.4655	8.6430
8.00	0.0	0.0	0.0501	8.8472	8.9373	9.1148
9.00	-0.0003	-0.0003	0.0498	9.2440	9.3068	9.4843
10.00	-0.0008	-0.0008	0.0493	9.5580	9.6035	9.7810
∞	0.0	0.0	0.0501	12.311	12.311	12.488

TABLE IV

DENSITY FUNCTIONAL POTENTIAL ENERGY CURVES FOR ArF

R(a.u.)	Energy (eV)			
	$X^2\Sigma^+(I)$	$A^2\Pi(I)$	$B^2\Sigma^+(II)$	$C^2\Pi(II)$
3.75	4.136	--	11.477	--
4.00	2.095	3.932	8.076	--
4.25	1.075	2.299	7.123	7.395
4.50	0.599	1.415	6.715	7.082
4.75	0.326	0.844	6.647	6.974
5.00	0.259	0.571	6.715	6.987
5.25	0.191	0.422	6.851	7.083
5.50	0.163	0.299	7.055	7.232
5.75	--	0.272	7.259	7.422
6.00	0.136	0.163	7.504	7.572
6.50	--	--	7.912	8.076
7.00	0.122	0.122	8.348	8.484
8.00	0.122	0.122	8.960	9.042
9.00	0.122	0.122	9.463	9.504
∞	0.0	0.0	12.375	12.375

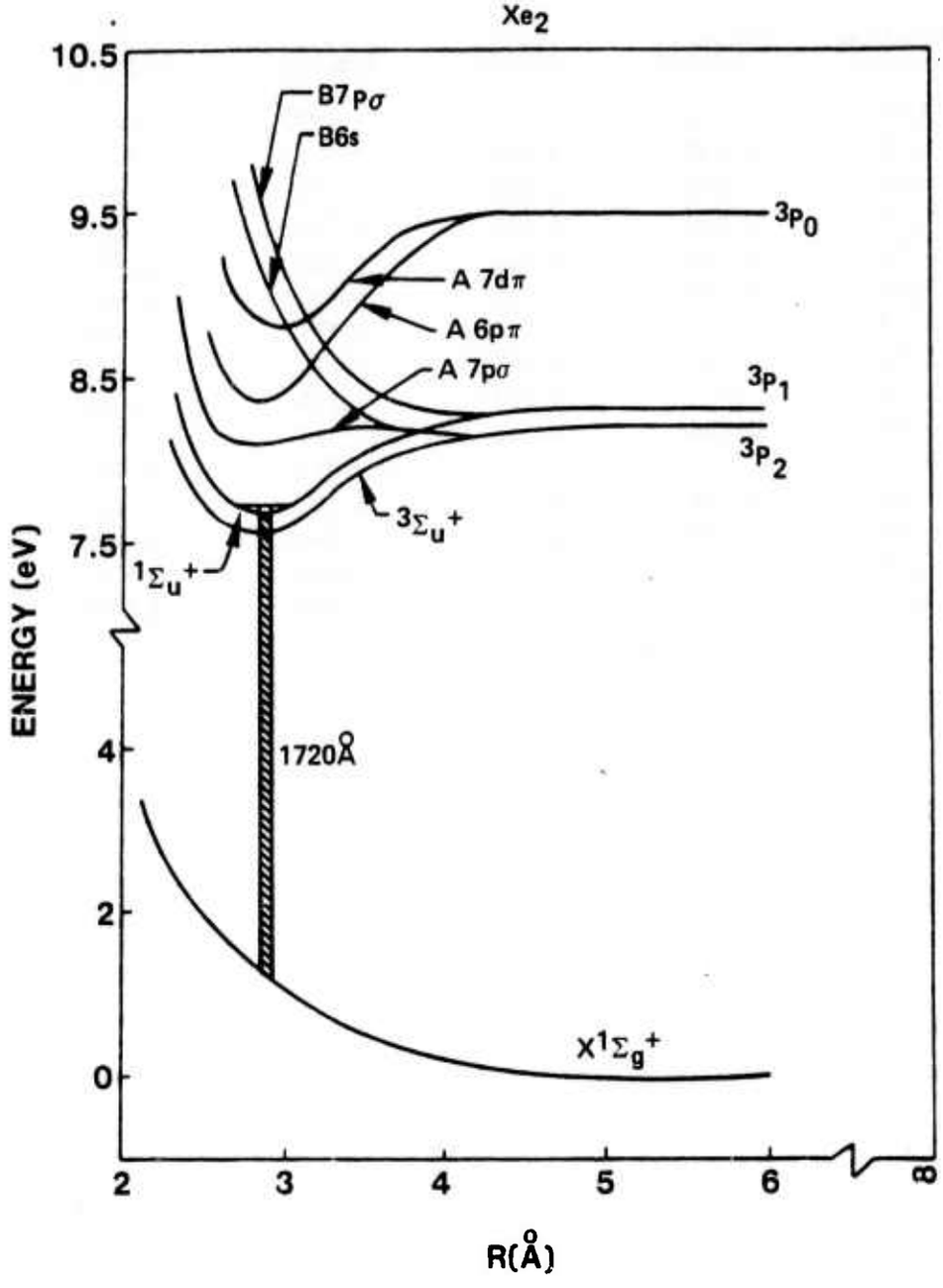

Figure 1 - Electronic Transition Laser - Xe_2

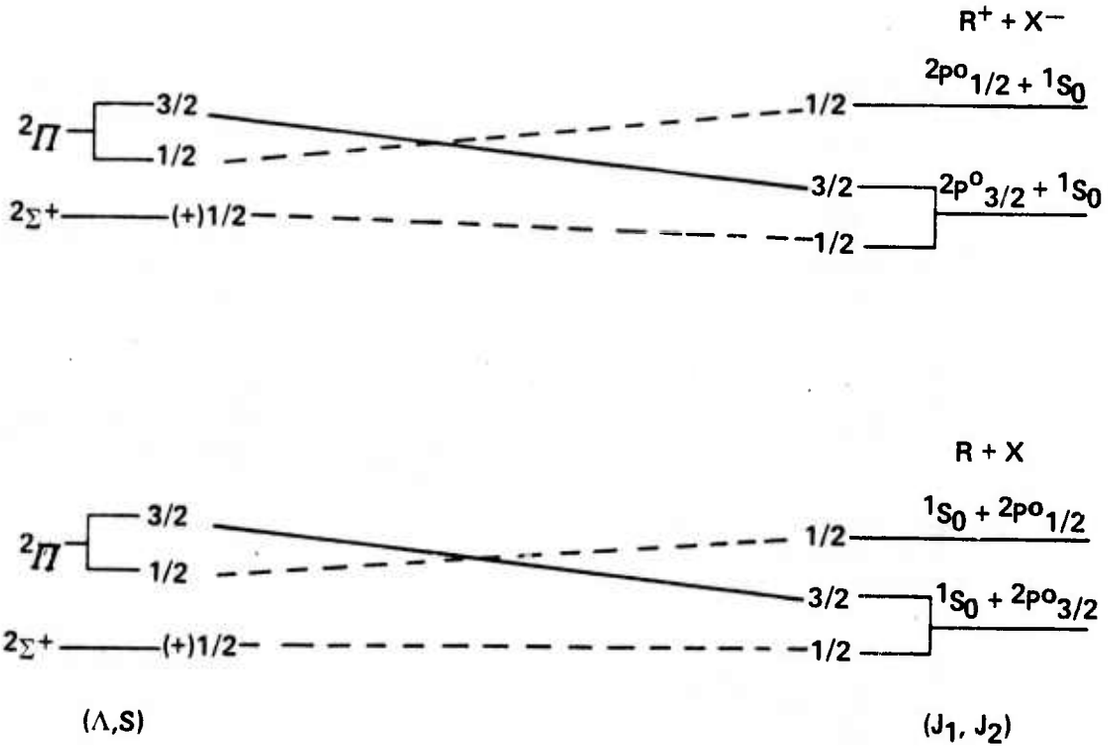

UNIQUE ASSIGNMENTS FROM (J_1, J_2) TO (Λ, S) COUPLING ARE INDICATED BY SOLID LINES

Figure 2 - General Correlation Diagram for Intermediate Coupling of Noble-gas Halide Diatomic Molecules Including Low-Lying Rydberg States

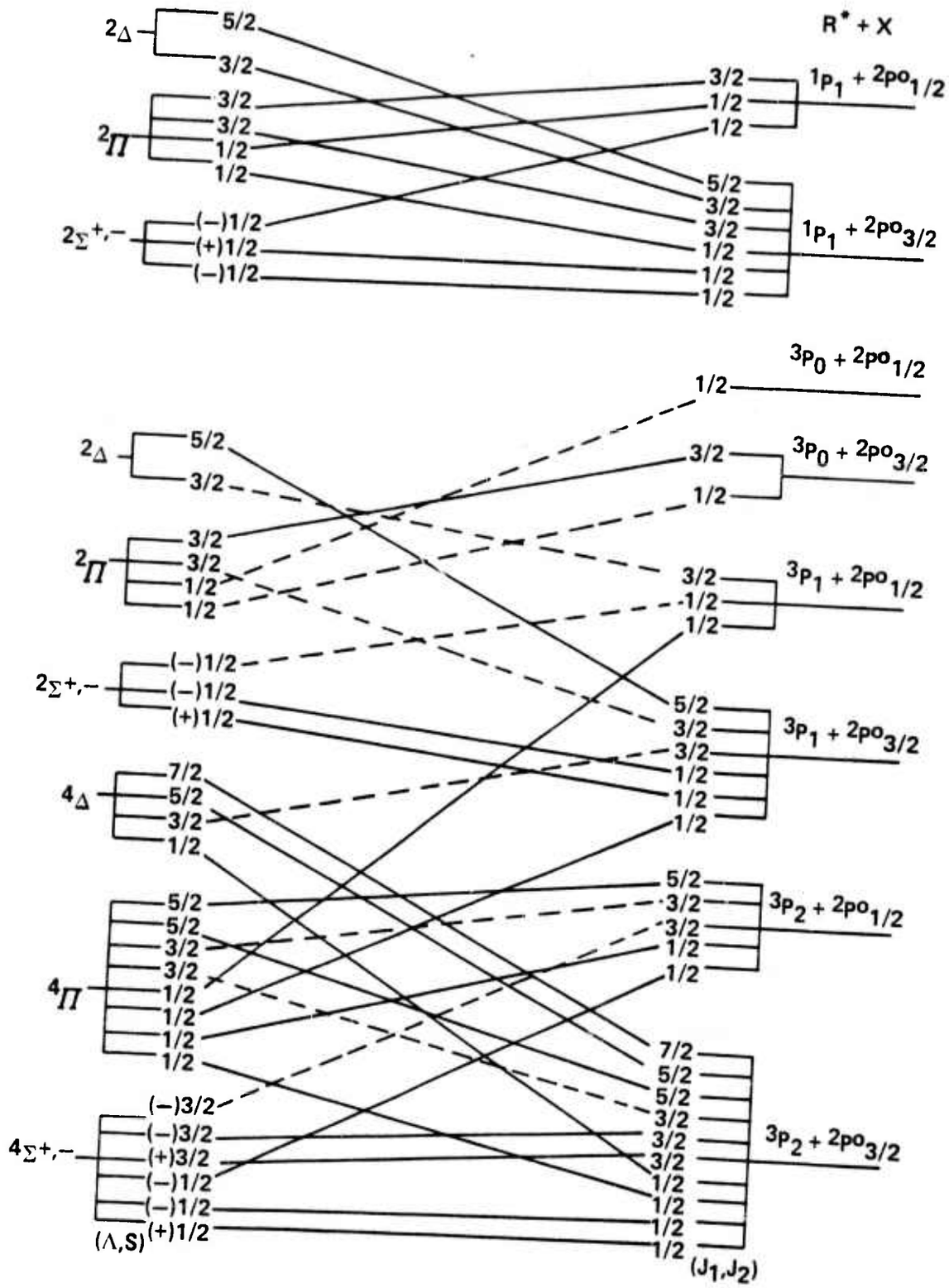

UNIQUE ASSIGNMENTS FROM (J_1,J_2) TO (Λ,S) COUPLING ARE INDICATED BY SOLID LINES

Figure 2 (Continued)

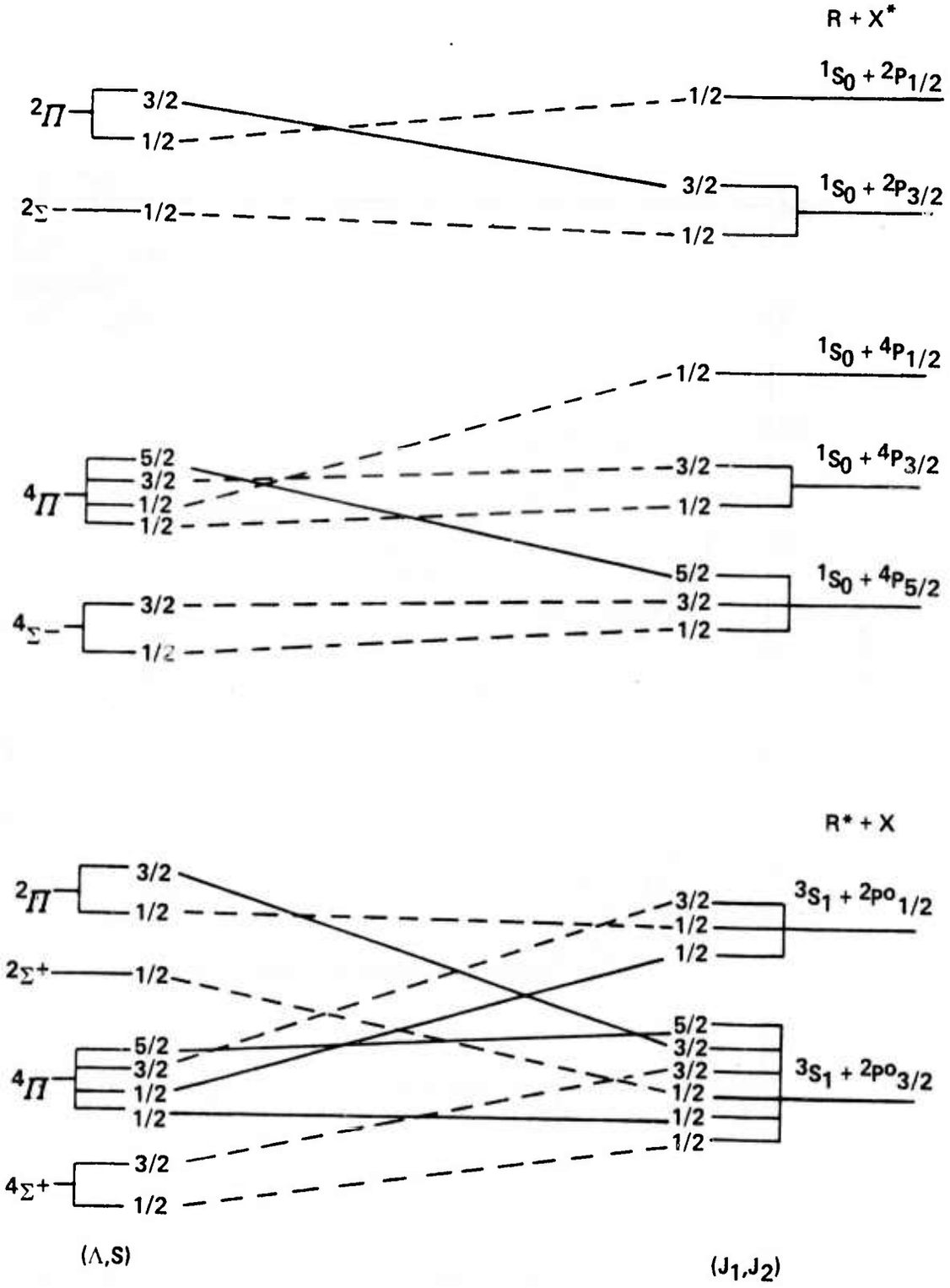

UNIQUE ASSIGNMENTS FROM (J_1,J_2) TO (Λ,S) COUPLING ARE INDICATED BY SOLID LINES

Figure 2 (Continued)

77-02-92-6

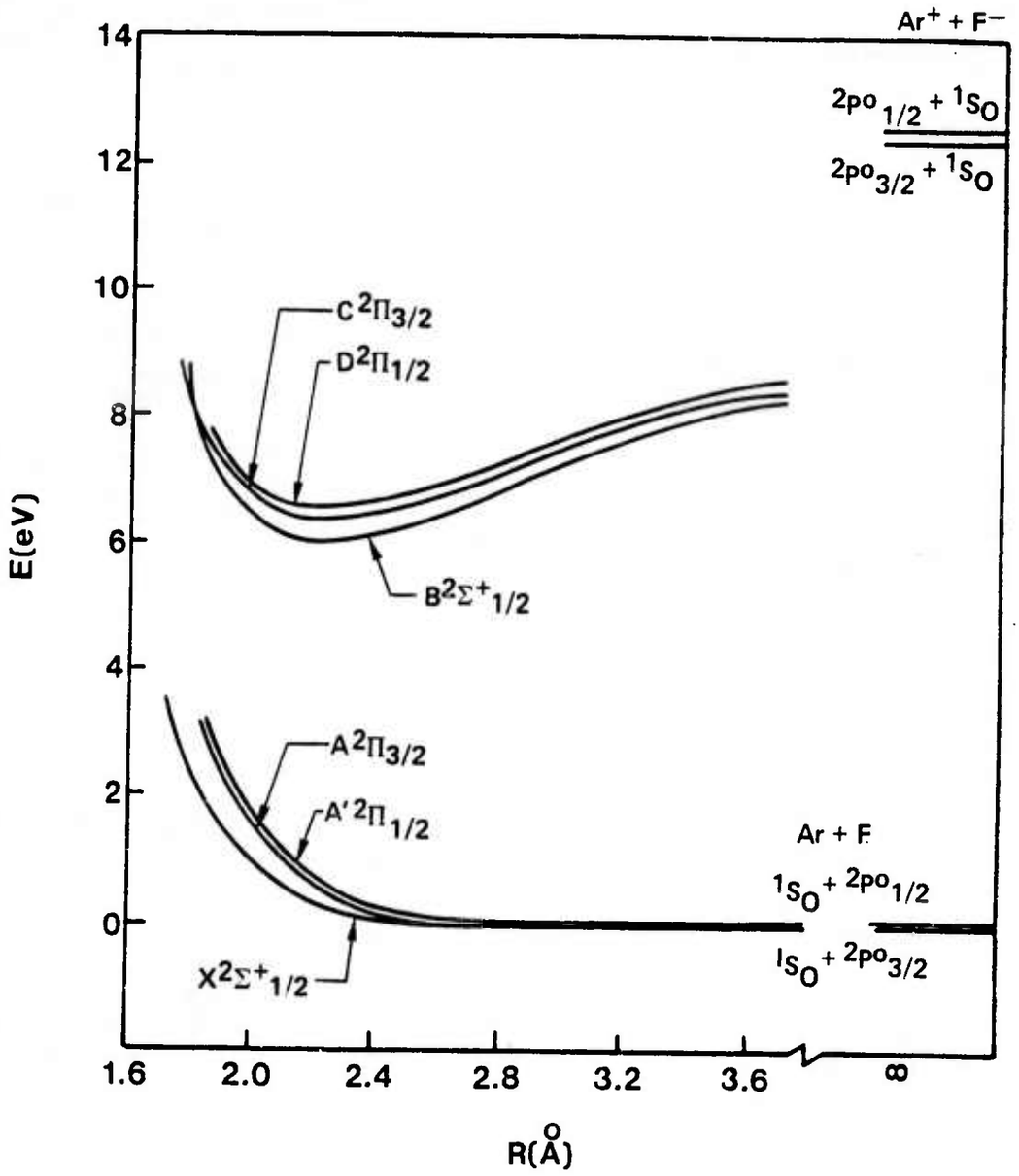

Figure 3 - Potential Energy Curves for ArF (Ab Initio Method)

77-02-92-5

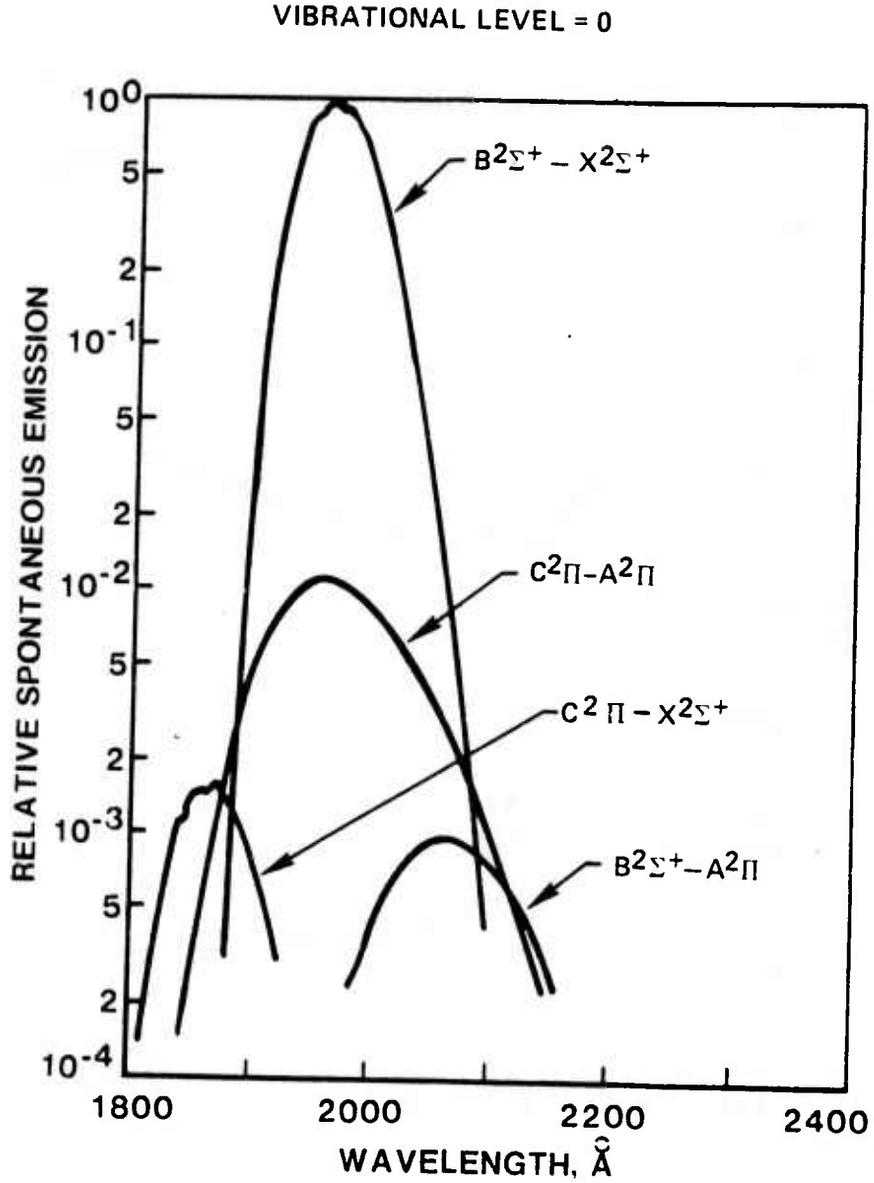

Figure 4 - Calculated Relative Emission Spectra Versus Wavelength for ArF

77-02 92 9

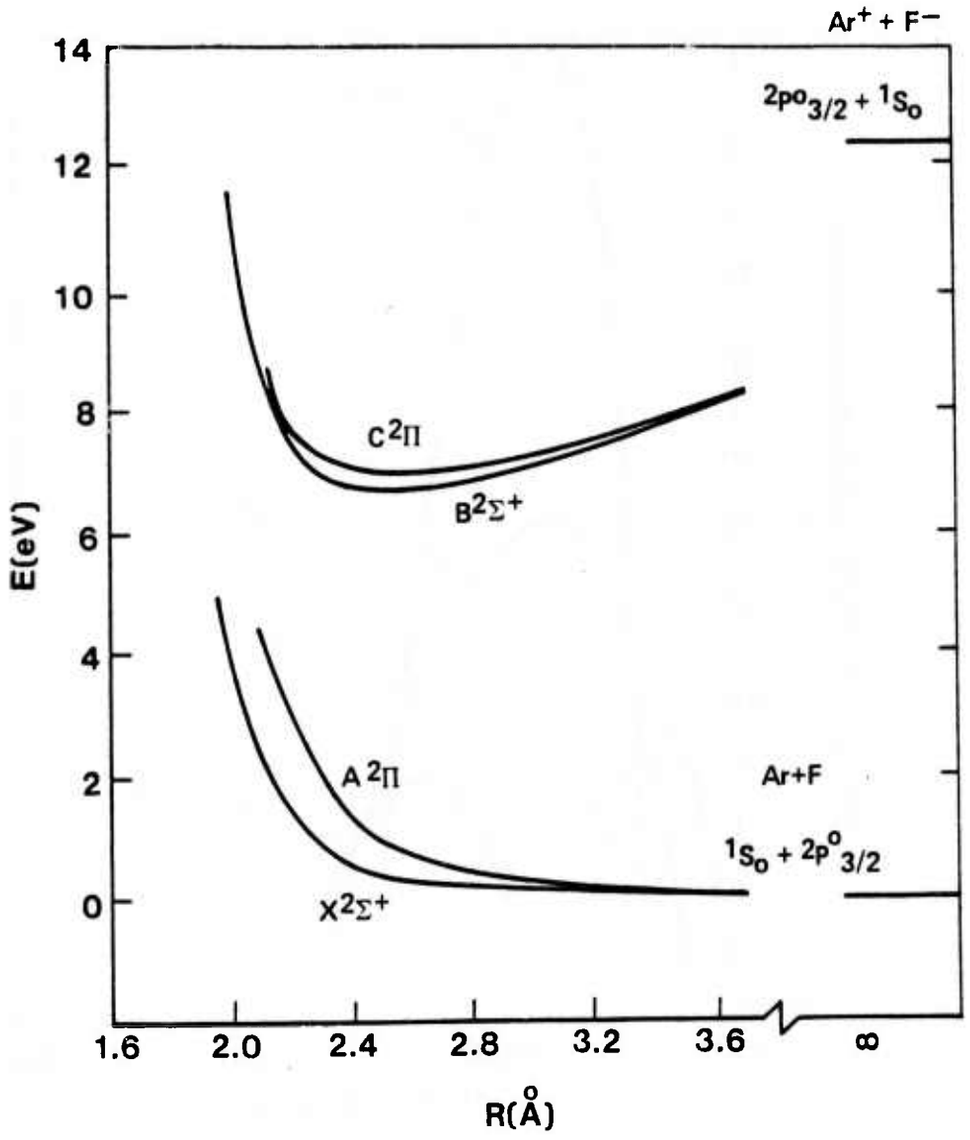

Figure 5 - Potential Energy Curves for ArF (Density Functional Method)

77-02-92-1

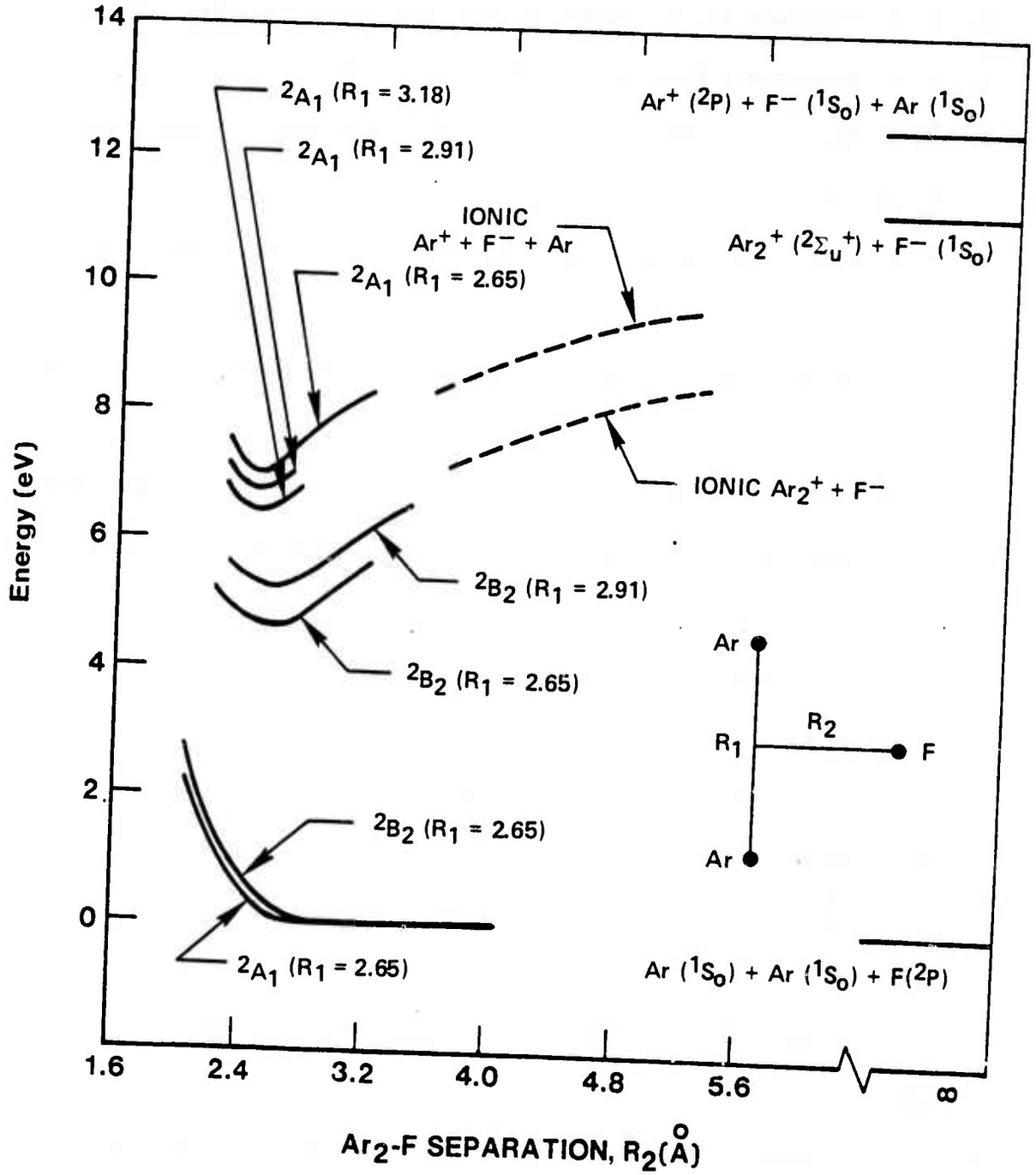

Figure 6 - Potential Energy Curves for Ar_2F (Density Functional Method)

77-04-40-1

REFERENCES

1. P. G. Wilkinson and Y. Tanaka, J. Opt. Soc. Amer., 45, 344 (1955).
2. F. G. Houtermans, Helv. Phys. Acta 33, 933 (1960).
3. N. G. Basov, V. A. Danilychev and Yu. M. Popov, Sov. J. Quant. Electron., 1, 18 (1971).
4. P. W. Hoff, J. C. Swingle and C. K. Rhodes, Appl. Phys. Lett., 23, 245 (1973).
5. J. E. Velazco and D. W. Setser, Journal of Chemical Physics, 62, 1990 (1975).
6. M. F. Golde and B. A. Thrush, Chemical Physics Letters, 29, 486 (1974).
7. C. A. Brau and J. J. Ewing, Journal of Chemical Physics, 63, 4640 (1975).
8. J. J. Ewing and C. A. Brau, Physical Review, 12, 129 (1975).
9. S. K. Searles and G. A. Hart, Appl. Phys. Lett., 27, 243 (1975).
10. J. J. Ewing and C. A. Brau, Appl. Phys. Lett., 27, 350 (1975).
11. C. A. Brau and J. J. Ewing, Appl. Phys. Lett., 27, 435 (1975).
12. E. R. Ault, R. S. Bradford, Jr. and M. L. Bhaumik, Appl. Phys. Lett., 27, 413 (1975).
13. M. L. Bhaumik, R. S. Bradford, Jr., and E. R. Ault, Appl. Phys. Lett., 28, 23 (1975).
14. G. C. Tisone, A. K. Hayes and J. M. Hoffman, Optical Communications, 15, 188 (1975).

REFERENCES (Cont'd)

15. J. Tellinghuisen, J. M. Hoffman, G. C. Tisone and A. K. Hays, Journal of Chemical Physics, 65, 4473 (1976).

16. R. A. Gerber and E. L. Patterson, IEEE J. Quantum Electron. QE-11, 642 (1975).

17. M. F. Golde, Journal of Molecular Spectroscopy, 58, 261 (1975).

18. J. M. Hoffman, A. K. Hayes and G. C. Tisone, Appl. Phys. Lett., 28, 538 (1976).

19. M. W. McGeoch, G. R. Fournier and P. Ewart, Journal of Physics B, 9, L121 (1976).

20. M. G. Stupavsky, W. F. Drake and L. Krause, Physics Letters, 39A, 349 (1972).

21. R. S. Carbone and M. M. Litvak, J. Applied Physics, 39, 2413 (1968).

22. R. S. Mulliken, Journal of Chemical Physics, 52, 5170 (1970).

23. F. R. Gilmore, T. L. Barr and D. Dee, Journal of Quantitative Spectroscopy and Radiative Transfer, 15, 625 (1975).

24. M. J. Clugston and R. G. Gordon, Journal of Applied Physics (to be published).

25. T. H. Dunning, Jr. and P. J. Hay, Applied Physics Letters, 28, 649 (1976).

26. P. J. Hay and T. H. Dunning, Third Colloquium on Electronic Transition Lasers, Aspen, Colorado, September 7-10, 1976.

27. H. H. Michels, R. H. Hobbs and J. C. Connolly, Optimized SCF-X_a Procedures for Heterpolar Molecules, Journal of Chemical Physics (to be published).

28. J. C. Slater, Advances in Quantum Chemistry, 6, 1 (1972).

29. P. O. Löwdin, Physical Review, 97, 1474 (1955).

30. W. Kohn and L. Sham, Physical Review, 140A, 1133 (1965).

31. J. C. Slater, Physical Review, 81, 385 (1951).

32. K. Schwarz, Physical Review, B5, 2466, (1972).

33. Rösch, N. and K. H. Johnson, Chem. Phys. Lett., 23, 149 (1973).

34. F. E. Harris and H. H. Michels, Intern. J. Quant. Chem. IS, 329 (1967).

35. A. C. Wahl, P. J. Bertoncini, G. Das, and T. L. Gilbert, Intern. J. Quantum Chem. IS, 123 (1967).

36. M. Krauss, private communication.

APPENDIX C

Electronic Structure of the Noble Gas Dimer Ions*

L. A. Wright
Kirtland Air Force Base, New Mexico 87117

ABSTRACT

A systematic study of the electronic structure and chemical binding in the dimer ion sequence, Ne_2^+, Ar_2^+, Kr_2^+ and Xe_2^+, has been carried out using both density functional and ab initio configuration interaction computational approaches. This study includes detailed calculations of the pertinent potential energy curves and an analysis of the calculated spectroscopic properties of the bound $A\ ^2\Sigma_u^+$ ($1/2_uI$) state of these ions.

* Supported in part by DARPA under ARPA Order No. 3432 under AFWL Contract F29601-78-C-0031 and AFOSR under Contract F49620-77-C-0064.

INTRODUCTION

The diatomic molecules formed from the noble gases, from the partially closed shell Group IIA and IIB elements or from the noble gas-halogen combinations constitute an interesting and important class of molecules for laser applications. These molecules are characterized by a repulsive or weakly bound ground state potential curve and by bound, electronically excited states. These excited diatomic molecules, known as excimers, radiate in a narrow visible or uv continuum band by making a transition to a repulsive lower state that dissociates into ground state neutral atoms. The resulting laser's operating characteristics are controlled by kinetic processes competing for the formation and destruction of the excited molecular levels and by absorption losses arising from noble gas dimer ions and high-lying Rydberg states of the excimer molecules. This last observation suggested the need for the present study of the electronic structure and absorption characteristics of the noble gas dimers which rate studies show to be present in large concentrations in the candidate noble gas excimer laser systems.[1-4]

Recent experimental studies[1-4] have drawn attention to photodissociation of the noble gas dimer ions as an important loss mechanism in excimer lasers. Hunter[1] has measured the absorption cross-section profiles for the strong $1/2_u I \rightarrow 1/2_g$ II ($A\ ^2\Sigma_u^+ \rightarrow D\ ^2\Sigma_g^+$) transition in both Ar_2^+ and Kr_2^+. He finds very strong, broad band absorption peaking at 292 nm for Ar_2^+ and at 325 nm for Kr_2^+. These wavelengths are near the operating region of several excimer lasers: XeBr (282 nm), XeCl (308 nm), XeF (353 nm); thus providing some concern for possible inherent low efficiency operating characteristics for these systems.

Theoretical treatments of the noble gas dimer ions have consisted mainly of *ab initio* SCF studies of the ground $A\ ^2\Sigma_u^+$ state and, by far, most of these studies have been devoted to He_2^+. We shall consider here only the systems, Ne_2^+, Ar_2^+, Kr_2^+ and Xe_2^+, which are chemically similar, with binding arising from the outer shell p-electrons.

The Ne_2^+ and Ar_2^+ ions were first studied by Gilbert and Wahl[5] using SCF wavefunctions constructed from STO basis functions. These authors have also reported limited SCF studies of the B $^2\Pi_g$, C $^2\Pi_u$ and D $^2\Sigma_g^+$ excited states of Ne_2^+ and Ar_2^+. CI studies of the ground state of the Ne_2^+ ion were reported by Cohen and Schneider[7,8] as part of a study of the Rydberg states of this system. SCF calculations for Ar_2^+ at short internuclear separations have been reported by Sidis, et al[9] and more recently by Stevens, et al[10], using an extensive STO basis. Finally, a uniform study of the systems Ar_2^+, Kr_2^+ and Xe_2^+ has been reported by Wadt[11] who employed a POL CI[12] using gaussian basis functions.

The theoretical principles underlying the electronic structure of the homonuclear noble gas molecular ions have been discussed by Mulliken[13] using Xe_2^+ as a prototype and, more recently, by Gilmore, Barr and Dee[14] for the case of Kr_2^+. For these dimer ions, four electronic states ($A^2\Sigma_u^+$, $B^2\Pi_g$, $C^2\Pi_u$ and $D^2\Sigma_g^+$) arise from a ground state atom (^1S_o) and a ground state ion ($^2P_{1/2,3/2}$). The lowest state, usually labeled A $^2\Sigma_u^+$, is bound for the four systems Ne_2^+, Ar_2^+, Kr_2^+ and Xe_2^+ and has been partially characterized experimentally through scattering experiments, although there has been much controversy concerning the dissociation energies of these ions. For the heavier ions, Λ - S coupling is no longer strictly valid and the B $^2\Pi_g$ and C $^2\Pi_u$ states split into J-J coupled components with a resultant mixing of Σ and Π symmetries. This splitting is small for Ne_2^+, but six distinct J-J coupled molecular ion states arise for Xe_2^+.

With the exception of the recent calculations by Wadt,[11] no attempts at systematic studies of these ions have been reported. Accurate ab initio methods would appear to be practical only for the lighter ions with diminished accuracy for heavier systems such as Xe_2^+. Wadt reports such a trend in his calculations[11] which indicate that his gaussian basis is less flexible in the case of Xe_2^+ than for the corresponding study of Ar_2^+. Recent density function calculations of noble gas halide molecules[15,16] have yielded reliable predictions of geometry and chemical binding, provided certain optimization criteria are followed. Such calculations, which

should be of more uniform quality than ab initio studies, constitute the principle effort in the present study. A limited number of ab initio calculations were carried out for Ar_2^+ for comparison purposes. The overall agreement between the two methods is excellent.

Method of Approach

Density Functional Approach - X_α Model

The X_α model[17] for the electronic structure of atoms, molecules, clusters and solids is a local potential model obtained by making a simple approximation to the exchange-correlation energy. If we assume a non-relativistic Hamiltonian with only electrostatic interactions, it can be shown that the total energy E of a system can be written exactly[18] (in atomic units) as

$$E = \sum_i n_i \langle u_i \left| -\tfrac{1}{2}\nabla_i^2 + \sum_\mu \frac{z_\mu}{r_{1\mu}} \right| u_i \rangle + \tfrac{1}{2} \sum_{\mu \neq \nu} \frac{z_\mu z_\nu}{r_{\mu\nu}}$$

$$+ \tfrac{1}{2} \sum_{ij} n_i n_j \langle u_i u_j \left| \frac{1}{r_{12}} \right| u_i u_j \rangle + E_{xc} \qquad (1)$$

This expression is exact provided the u_i are natural orbitals and n_i are their occupation numbers (i.e., eigenfunctions and eigenvalues of the first order density matrix). The first term in Eq. (1) represents the kinetic and electron-nuclear energies. The second term is the nuclear repulsion energy. The sums (μ,ν) are over all the nuclear charges in the system. The third term is the electron-electron repulsion term, which represents the classical electrostatic energy of the charge density ρ interacting with itself, where

$$\rho(1) = \sum_i n_i u_i^*(1)\, u_i(1) \qquad (2)$$

The last term E_{xc} represents the exchange-correlation energy and can be expressed formally as

$$E_{xc} = \frac{1}{2} \int \rho(1)\, d\vec{r}_1 \int \frac{\rho_{xc}(1,2)}{r_{12}}\, d\vec{r}_2 \,, \tag{3}$$

where $\rho_{xc}(1,2)$ represents the exchange-correlation hole around an electron at position 1. In the exact expression, ρ_{xc} is dependent on the second-order density matrix. In the Hartree-Fock approximation E_{xc} is the exchange energy. ρ_{xc} represents the Fermi hole due to the exclusion principle and depends only on the first-order density matrix. In the X_α method, a simpler assumption about ρ_{xc} is made. If we assume that the exchange-correlation hole is centered on the electron and is spherically symmetric, it can be shown that the exchange-correlation potential

$$u_{xc} = \int \frac{\rho_{xc}(1,2)}{r_{12}}\, d\vec{r}_2 \tag{4}$$

is inversely proportional to the range of the hole, r_s, where r_s is defined by

$$\frac{4\pi}{3}\, r_s^3\, \rho(1) = 1 \tag{5}$$

Therefore, in the X_α model, the potential U_{xc} is proportional to $\rho^{1/3}(r)$. A scaling parameter α is defined such that

$$U_{x_\alpha}(1) = -\frac{9\alpha}{2} \left(3\rho(1)/8\pi\right)^{1/3} \tag{6}$$

The expression in Eq. 6 is defined so that $\alpha = 2/3$ for the case of a free electron gas in the Hartree-Fock model[19] and $\alpha = 1$ for the potential originally suggested by Slater[20]. A convenient way to choose this parameter for molecular and solid state applications is to optimize the solutions to the X_α equations in the atomic limit. Schwarz[21] has done this for atoms from Z = 1 to Z = 41 and found values between 2/3 and 1.

Computational Aspects of the X_α Method

To implement the X_α approximation in molecular calculations it is usually convenient to break up the volume integrals indicated in Eqs. (3) or (4) by defining spherical regions surrounding each atomic center. The molecular potential is than spherically averaged within these regions and assumed constant in the region between spheres. The potential falls to zero in the usual way in the region outside of an overall sphere located to encompass those spheres surrounding the individual atoms.

There are two other practical aspects of the calculations which must be considered in application of the X_α model to finite molecular systems. The first concerns the choice of the integration framework for describing the molecular-orbital wavefunctions and the second deals with the choice of the exchange parameter, α, in different regions of space. A third consideration, convergence of the spherical harmonic expansion, was also tested. The total energy was converged when all terms up to $\ell = 3$ were included. In molecules with significant charge sharing in the bonds, the radii of the atomic spheres is frequently increased in X_α calculations so that an overlap region appears in the vicinity of the bond.[22] Our studies[16] have shown that the contribution to the total molecular energy from the exchange-correlation term shows a minimum at an optimum sphere radius or sphere overlap. This result can be deduced from the X_α model by comparing the exchange energy of the electron density at the edge of the spherical integration region with that across this boundary in the intersphere region. This provides a

sensitive criterion for selecting these parameters.

The values of the exchange parameters in the spherical integration region around each atomic center are frequently set at the atomic values both for neutral and for ionic molecular constituents. It is known, however, that the value of α which best reproduces Hartree Fock results varies with ionicity.[21] While for heavy atoms, these changes in the exchange parameter would be small, the α's for small atoms vary rapidly with z (and with ionicity). The correct choice of the exchange parameters influences not only the total energy calculated for the molecule but also affects the distribution of charge between the atomic spheres and the intersphere region.

Ab Initio Approach - Valence CI Method

The ab initio calculation procedure chosen for these studies is the valence-configuration-interaction (VCI) method.[23,24] The specific form for $\psi(R)$ may be written as

$$\psi^{g,u}(R) = \sum_{\mu} c_{\mu} \psi_{\mu}^{g,u}(R) \tag{7}$$

where each $\psi_{\mu}(R)$ is referred to as a configuration and has the general structure

$$\psi_{\mu}^{g,u}(R) = \mathcal{A}\mathcal{O}_s \Pi \left[\phi_{\mu 1}(A)\phi_{\mu 2}(A)\cdots\phi_{\mu n}(A)\right]\left[\phi'_{\mu 1}(B)\phi'_{\mu 2}(B)\cdots\phi'_{\mu n-1}(B)\right] \tag{8}$$

$$\pm \left[\phi_{\mu 1}(B)\phi_{\mu 2}(B)\cdots\phi_{\mu n}(B)\right]\left[\phi'_{\mu 1}(A)\phi'_{\mu 2}(A)\cdots\phi'_{\mu n-1}(A)\right]\theta_{M_s}$$

and where $\phi_{\mu i}$ is a spatial orbital, $\mathcal{A}$ is the antisymmetrizing operator, $\mathcal{O}_s$ is the spin-projection operator for spin quantum number S, and θ_{M_s} is a product of α and β one-electron spin functions of magnetic quantum number, M_s. The spatial orbitals, $\phi_{\mu i}$ have the general form

$$\phi_i = e^{-\delta_i \xi - \zeta_i \eta \pm \nu_i \phi} \xi^p \eta^q r^{n_i - 1} P_{\ell_i}^{|\nu_i|}(\cos\theta) \tag{9}$$

where for $\zeta_i = \pm\delta_i$, the standard STO form is recovered.

The wavefunctions represented by Eq. (8) correctly dissociate to an atom and ion valence bond product wavefunction at large internuclear separations with an optimized description of the charge density about the separate atom and ion nuclei. This situation is to be contrasted with that arising from the construction of a Hartree-Fock wavefunction for the molecular ion. Within the HF framework we write

$$\psi^{g,u} = A\Pi\left[U_1^{g,u}(\alpha)U_1^{g,u}(\beta)\ldots U_{2n-1}^{g,u}(\alpha)\right] \qquad (10)$$

where

$$U_i^{g,u} = \phi_i(A) \pm \phi_i(B); \qquad \phi_i = \text{av.}(\phi_i + \phi_i') \qquad (11)$$

This symmetry adaptation of the orbital basis, represented by Eq. (11), introduces a severe, non-physical correlation error into the calculations which manifests itself at large internuclear spearations. The wavefunction represented by Eq. (10) dissociates into an atom and ion pair with charge density of the hypothetical species $R^{+1/2}$. This situation has been noted by previous authors[5], who suggested, however, that this correlation error arising from symmetry adaptation did not vary significantly with changing internuclear separations. We find different results, especially for Ne_2^+, which separates into an atom and ion pair with significantly different spatial charge distributions. This symmetry dilemma arising from the restricted Hartree-Fock model has been discussed previously by Löwdin[25] who suggested alternate computational routes.

There are several complications introduced by the choice of Eq. (8) for the molecular ion configuration. For heavy nuclei systems such as Xe_2^+, the atomic and ionic basis functions will be similar and Eq. (11) may be a satisfactory approximation. For light nuclei systems such as Ne_2^+, the distinction between

the atomic and ionic basis functions must be retained which introduces a non-orthogonality problem into Eq. (8). One solution is to remain within a non-orthogonal framework. This leads to a secular equation of the form

$$\left(\underset{\sim}{\mathcal{H}} - \lambda \underset{\sim}{\mathcal{S}} \right) \psi = 0 \qquad (12)$$

where $\underset{\sim}{\mathcal{S}}$ is the non-orthogonality matrix. Calculations of this type have been reported by Harris and co-workers.[26,27] An alternate approach is to expand the atomic and ionic functions as linear combinations of symmetry adapted MO's such as

$$\phi_{A,B} = \left(U_g \pm U_u \right); \qquad \phi'_{A,B} = \left(U'_g \pm U'_u \right) \qquad (13)$$

This leads to a restricted CI among symmetry adapted functions which can be cast in an orthogonal framework. Both approaches were examined for the calculations reported herein.

Spin-Orbit Effects

The ground state of a noble gas ion is split by spin-orbit coupling into two components, a $^2P_{3/2}$ state, which lies lowest, and a $^2P_{1/2}$ state. This splitting is small in the case of Ne^+ (781 cm^{-1}) but is of the same magnitude as the chemical binding energy in the case of Xe^+ (10537 cm^{-1}). Rigorous inclusion of spin-orbit effects in molecular calculations is still computationally prohibitive,[28] but for these noble gas ions, which exhibit small changes from separated atom-ion pair electron densities, an asymptotic atomic approximation is valid.[7,8] In this approximation, the hamiltonian is written as

$$\mathcal{H}(R) = \mathcal{H}^{\Lambda,S}(R) + V^{S-O} \qquad (14)$$

where V^{S-O} is taken in the atom-ion limit of infinite internuclear separation and is considered to be R-independent. For the $\Omega = 1/2$ components, Eq. (14) leads to a secular equation of the form

$$\begin{vmatrix} E^{\Sigma}(R) - \lambda_{1/2} & -\sqrt{2}\,\alpha \\ -\sqrt{2}\,\alpha & [E^{\Pi}(R) + \alpha] - \lambda_{1/2} \end{vmatrix} = 0 \qquad (15)$$

where $E^{\Sigma}(R)$ and $E^{\Pi}(R)$ are the pure Λ-S coupled eigenvalues and α is the spin-orbit splitting parameter ($3\alpha = \Delta E_{^2P_{3/2} - {}^2P_{1/2}}$) which can be obtained from atomic data. For the $\Omega = 3/2$ components, there is no mixing of the Σ and Π states and Eq. (14) leads simply to

$$\left| [E^{\Pi}(R) - \alpha] - \lambda_{3/2} \right| = 0 \qquad (16)$$

For illustration, the spin-orbit components for $\Omega = 1/2$ take the form

$$\begin{aligned} {}^1/_2{}_{g,u}\ \mathrm{I} &= C^{\Sigma}_{g,u}\,\psi^{\Sigma}_{g,u} + C^{\Pi}_{g,u}\,\psi^{\Pi}_{g,u} \\ {}^1/_2{}_{g,u}\ \mathrm{II} &= -C^{\Pi}_{g,u}\,\psi^{\Sigma}_{g,u} + C^{\Sigma}_{g,u}\,\psi^{\Pi}_{g,u} \end{aligned} \qquad (17)$$

where $C^{\Sigma}_{g,u} \to \sqrt{2/3}$ and $C^{\Pi}_{g,u} \to \sqrt{1/3}$ for large internuclear separations. For the lighter systems such as Ne_2^+, $C^{\Sigma}_{g,u} \to 1$ and $C^{\Pi}_{g,u} \to 0$ for internuclear separations near R_e. Inclusion of these spin-orbit effects was carried out for all of the ions studied herein. We find that this effect fully accounts for the systematic decrease of the dissociation energy of the ground state of these molecular ions in the progression from Ne_2^+ to Xe_2^+.

RESULTS AND DISCUSSION

We have carried out uniform quality density functional X_α calculations for the molecular ions Ne_2^+, Ar_2^+, Kr_2^+ and Xe_2^+ to define the gound $A\ ^2\Sigma_u^+$ state, and its spectroscopic properties, and the nature of the repulsive $B\ ^2\Pi_g$, $C\ ^2\Pi_u$ and $D\ ^2\Sigma_g^+$ states which arise from a ground state noble gas atom-ion pair. As a check on the accuracy of these calculations, ab initio wavefunctions were constructed for Ar_2^+ in both orthogonal and non-orthogonal frameworks. The ab-initio calculations were carried out using computational programs which have been previously described.[23,27] The density functional calculations were carried out with both overlap and α parameters optimized for each internuclear separation.[16] There is a small variation in the optimum parameters arising from molecular ion symmetry considerations. These changes were found to be negligible for Kr_2^+ and Xe_2^+ but were important in the case of Ne_2^+. Although we constructed separate optimum functions for each molecular ion symmetry, we observe that transition state calculations of energy differences between these ion states would suffice for Kr_2^+ and Xe_2^+ but would definitely be in error for Ne_2^+.

The general nature of the potential energy curves arising from a ground state atom-ion pair is illustrated in Fig. 1 for Ar_2^+. These curves were constructed from a CI expansion, as described above, using a minimum STO basis augmented by the inclusion of optimized 4s and 4p functions to allow more flexibility in the valence shell charge distribution. Spin-orbit effects are not included and the asymptotic limit is the center of gravity of the $^2P_{3/2,1/2}$ argon ion components. The ground $A\ ^2\Sigma_u^+$ state is seen to be bound by 1.38 eV with an equilibrium separation of 2.4Å. This is in excellent agreement with the latest experimental study of this ion by Mosely, et al[30] who conclude that the dissociation energy of Ar_2^+ is 1.33 ±.02 eV. There is a small binding (.1-.2 eV) of the $B\ ^2\Pi_g$ state at R~3Å but this

state is clearly repulsive in the Franck-Condon region of the ground state. The higher C $^2\Pi_u$ and D $^2\Sigma_g^+$ states indicate no binding at the internuclear separations (≤ 4.0Å) that we examined, although a weak polarization ($-\alpha/R^4$) term must be found at larger separations.

Systematic studies of these ions were carried out using the density functional X_α method, as described above. Separate calculations were performed for each molecular ion symmetry and for a wide range of internuclear separations. A double iteration computation scheme was employed since each separate calculation was optimized for both the charge distribution and the radii of the spheres of integration. The results are illustrated in Figs. 2-5 for the ion sequence Ne_2^+, Ar_2^+, Kr_2^+ and Xe_2^+. In these figures we have included the spin-orbit splitting of the $^2\Pi_{g,u}$ Λ-S coupled states and the resultant mixing of the $1/2_{g,u}$ components with the corresponding $^2\Sigma_g$ and $^2\Sigma_u$ states. As previously mentioned, this splitting is small for Ne_2^+ but is very significant for Xe_2^+.

Comparing the results of our calculations in the sequence $Ne_2^+ \rightarrow Xe_2^+$, we find a regular progression in the calculated dissociation energy and the equilibrium internuclear separation for the ground $1/2_u$I [A $^2\Sigma_u^+$] state. The calculated binding energy decreases from 1.3 eV for Ne_2^+ to 1.0 eV for Xe_2^+ while the equilibrium separation increases smoothly from 3.2 to 5.9 bohrs. A summary of our calculated spectroscopic constants for these dimer ions is given in Table I. These data were obtained by fitting our calculated J-J coupled potential curves to the Hulbert-Hirschfelder modification of the Morse function[31] using a least-squares fit to the calculated values near R_e.

An examination of the calculated constants reported in Table I indicates some remarkable regularities. We observe that, in the absence of spin-orbit coupling effects, the dissociation energy of all four dimer ions is identical, within the error of our calculations. This suggests that the binding arising from Λ - S

coupling in these systems is independent of the principal quantum number of the valence shell and that the experimentally observed decrease in the binding energies in the sequence $Ne_2^+ \rightarrow Xe_2^+$ has its origin in the increased degree of mixing of the repulsive $^2\Pi_u(\frac{1}{2})$ component into the ground electronic state. A second remarkable simplicity in the structure of these ions can be found by examining the progression in the calculated equilibrium separations. In Table I we list a column of the average expectation of $\langle \bar{r} \rangle$ for these ions, taken from accurate Hartree-Fock calculations,[32] and compare this with our computed values for R_e. We find the condition of additivity of radii is an excellent approximation for these dimer ions with $R_e(a.u.) = 2.0 \langle \bar{r} \rangle +$ constant. Thus, in the absence of spin-orbit effects, these molecular ions exhibit textbook simplicity for our understanding of their binding and geometry.

Further confirmation of the results reported here can be obtained by comparison of the calculated data given in Table I with experimental determinations of dissociation energies of these ions from photoionization or rainbow scattering collision studies.[30,33-36] For all of the ions studied here, differences between theory and experiment lie within the reported experimental uncertainties.

In addition to studies of the stable ground state of these ions, we show in Figs. 2-5 the calculated J-J coupled excited molecular ion states which correlate with a ground state atom-ion pair. There are some experimental data available to verify the location of these excited states, from rainbow scattering experiments[35] and, more recently, from photoabsorption studies in Ar_2^+ and Kr_2^+.[1,30,36] We find peak absorption for the strong $1/2_uI \rightarrow 1/2_gII$ transition at 298 nm for Ar_2^+ and at 323 nm for Kr_2^+. These calculated data can be compared with the recent experimental profiles obtained by Hunter[1] who obtained peaks at 292 nm and 325 nm for Ar_2^+ and Kr_2^+, respectively. The long wavelength transitions for photoabsorption ($1/2_uI \rightarrow 1/2_gI$ and $1/2_uI \rightarrow 3/2_gI$) have been studied by Miller, et al[36]

who report an overlapped absorption profile with a peak at 720 nm. This can be compared with our estimate of 720-770 nm.

Further studies of the photoabsorption characteristics of these noble gas ions are in progress.

ACKNOWLEDGEMENTS

The authors wish to thank Judith B. Addison for her valuable assistance in carrying out these computations. We also wish to express our thanks to R. Hunter for communicating his experimental results prior to publication and to J. Mann for performing various Hartree-Fock calculations for several of the noble gas atomic ions. Use of the computer facilities at the Kirtland Air Force Base in Albuquerque is also acknowledged.

TABLE I SUMMARY OF SPECTROSCOPIC CONSTANTS FOR THE $1/2_u$ I ($A^2\Sigma_u^+$) STATE OF THE NOBLE GAS DIMER IONS

Ion	ω_e[cm^{-1}]	D_e[eV]	[-SO] D_e[eV]	$\langle\bar{r}\rangle$[a.u.]	R_e[a.u.]
Ne_2^+	606.56	1.32	1.37	0.965	3.19
Ar_2^+	300.07	1.35	1.40	1.663	4.59
Kr_2^+	184.04	1.21	1.39	1.952	5.17
Xe_2^+	127.90	1.03	1.38	2.338	5.94

[-SO]: without spin-orbit effects

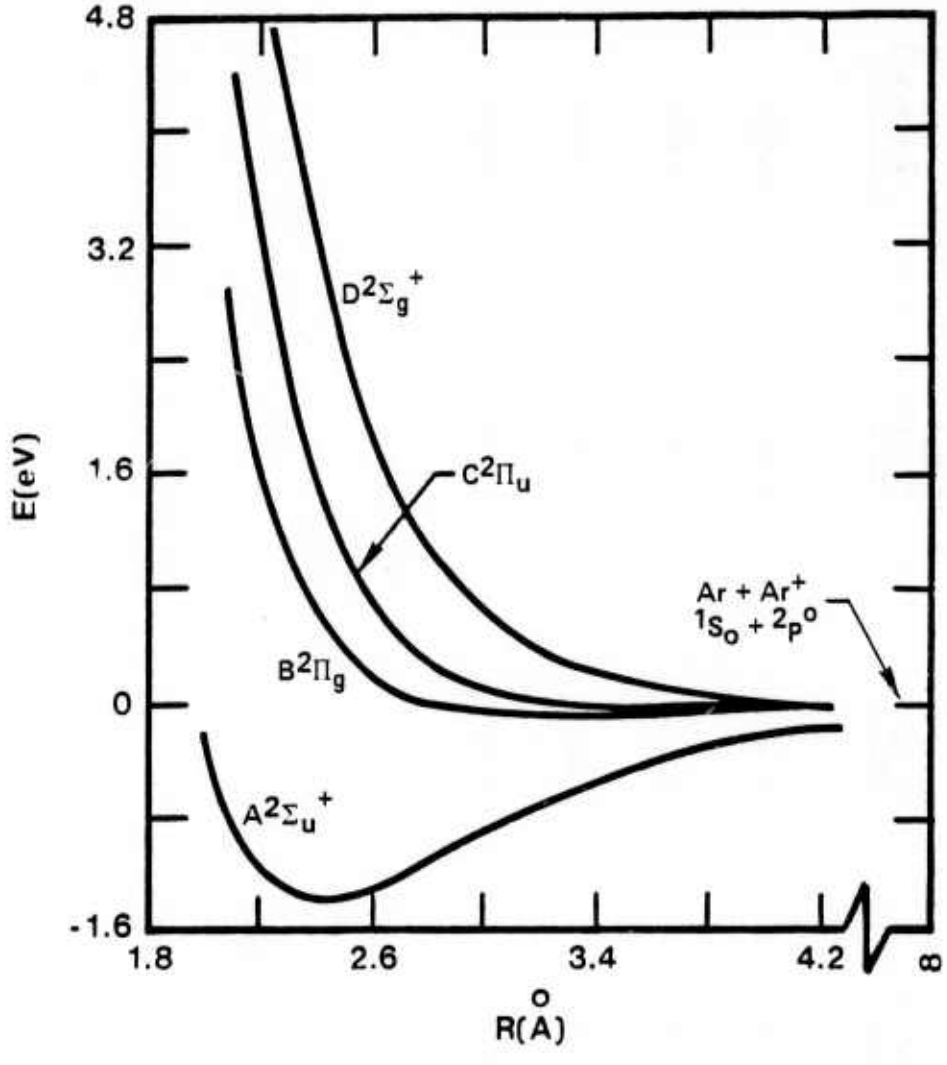

Figure 1. Ab initio potential energy curves for Ar_2^+ without inclusion of spin-orbit coupling

78-03-98-1

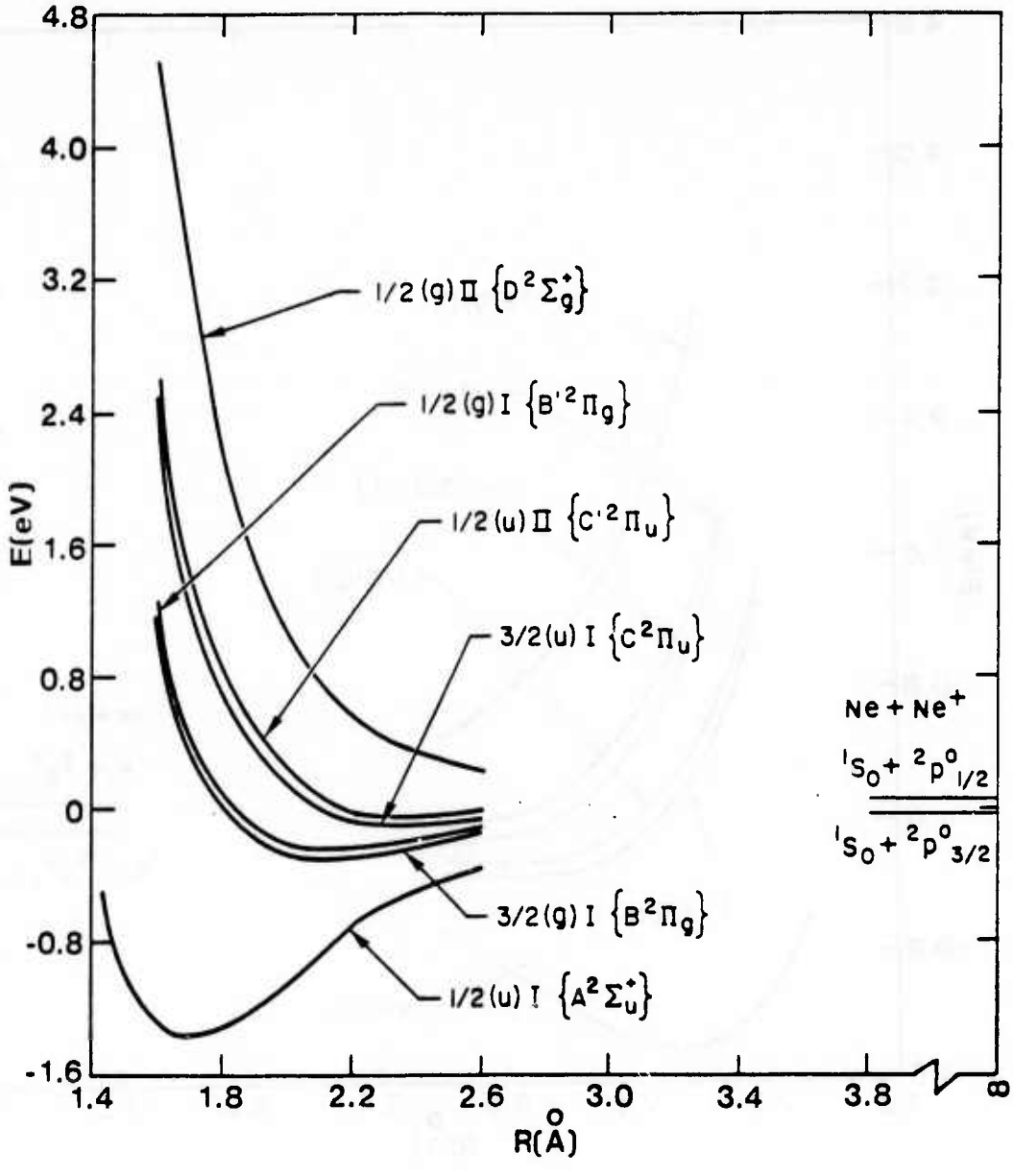

Figure 2. Density functional potential energy curves for Ne_2^+ (spin-orbit effects included)

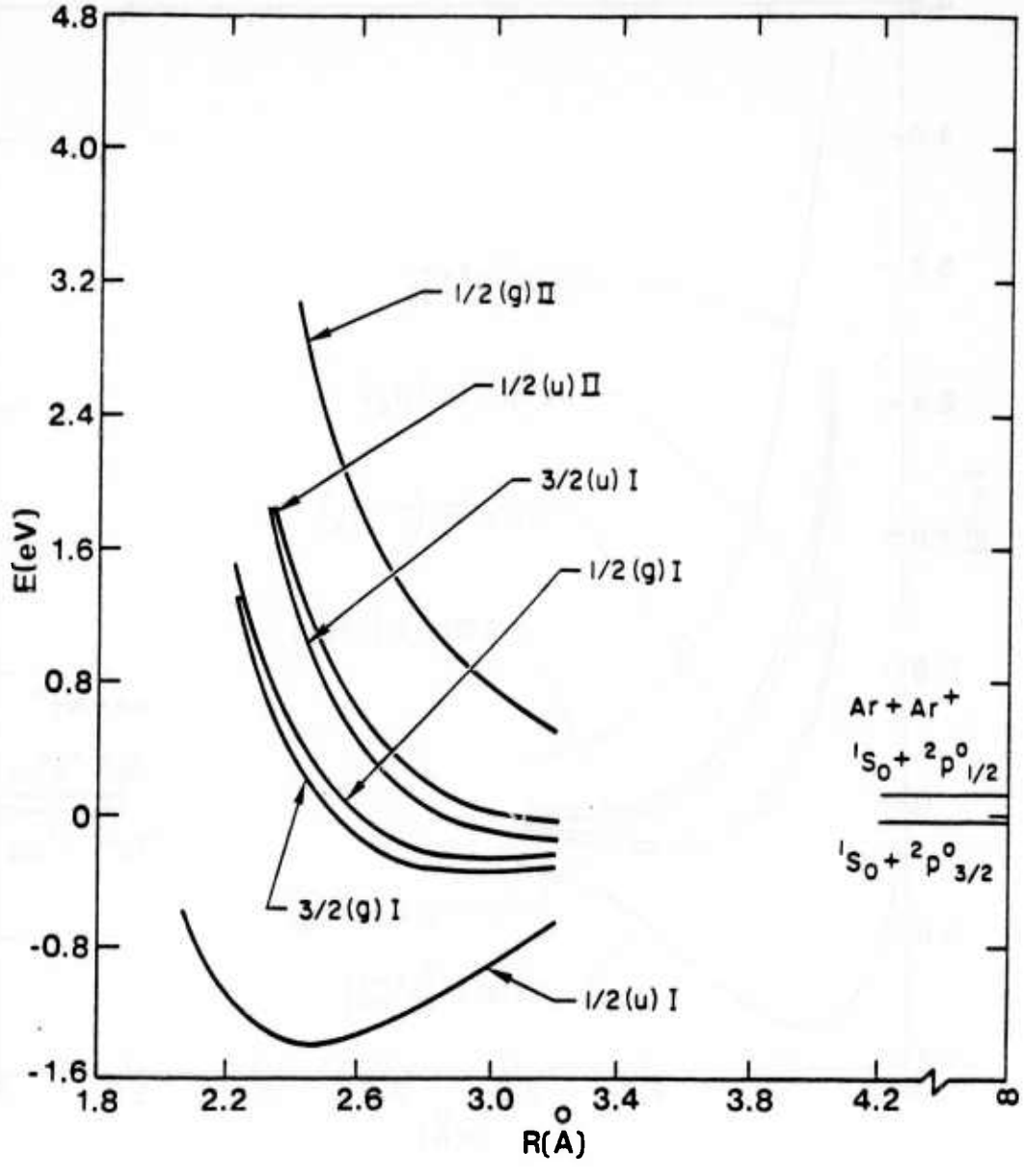

Figure 3. Density functional potential energy curves for Ar_2^+ (spin-orbit effects included)

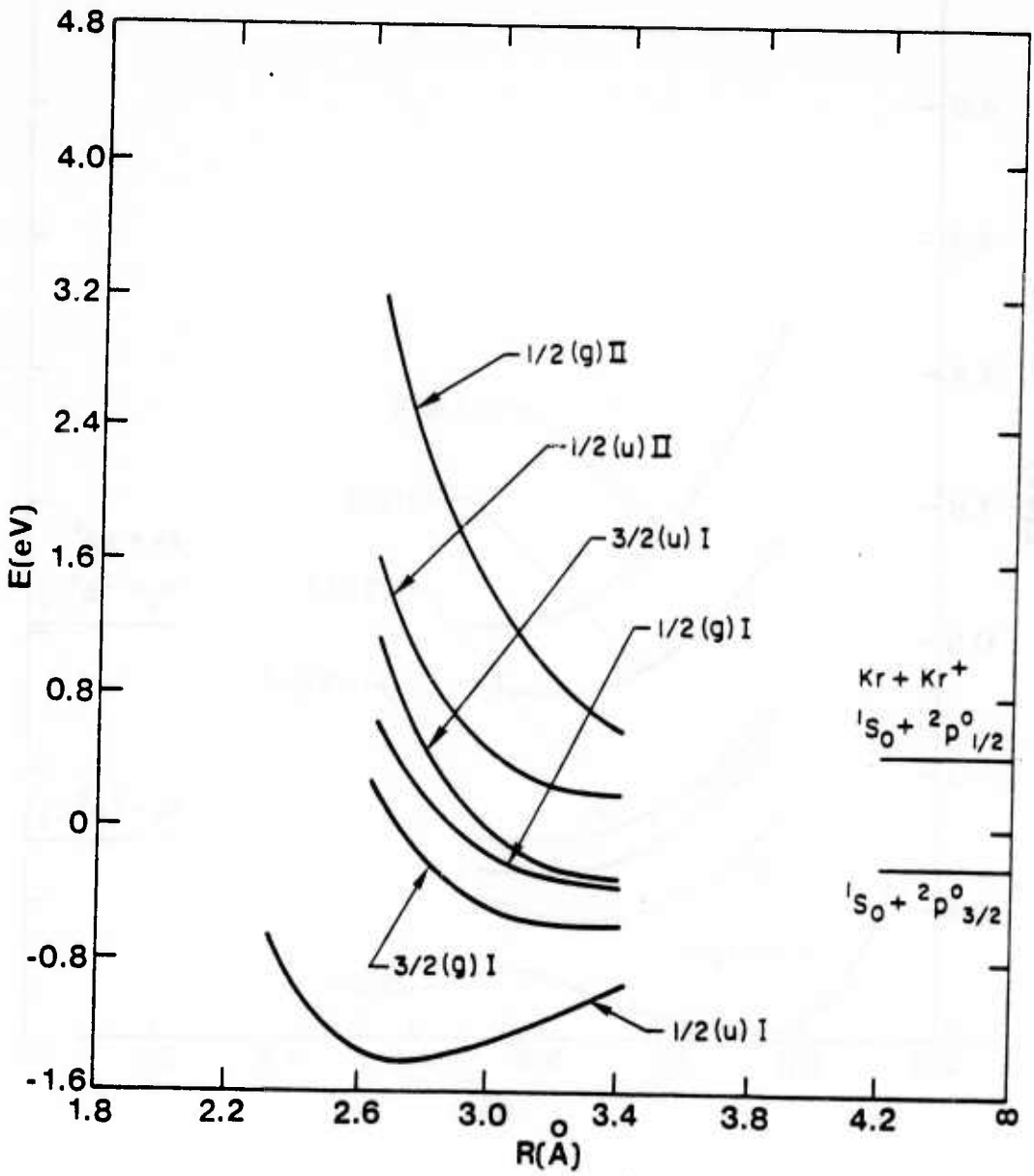

Figure 4. Density functional potential energy curves for Kr_2^+ (spin-orbit effects included)

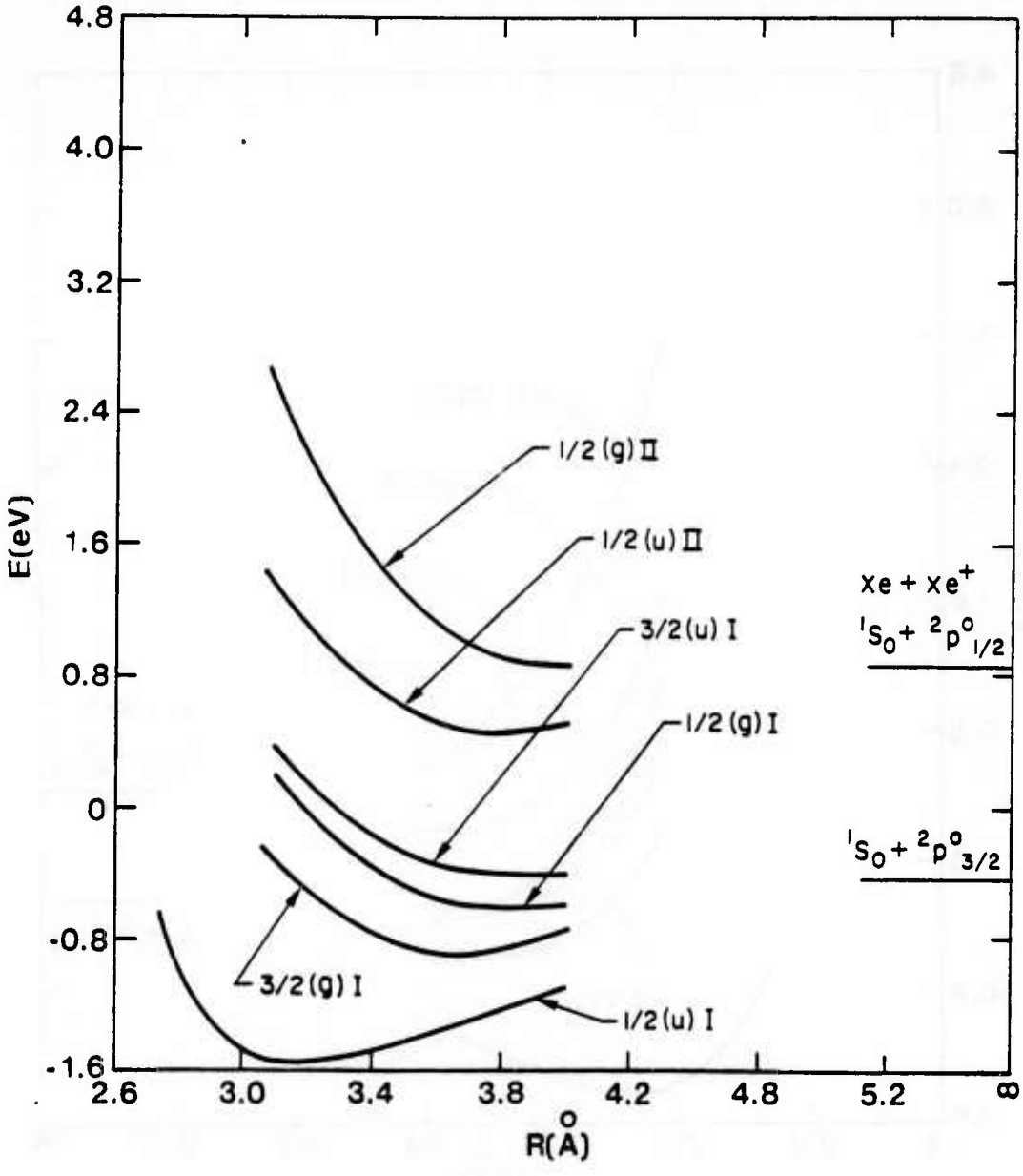

Figure 5. Density functional potential energy curves for Xe_2^+ (spin-orbit effects included)

References

1. R. O. Hunter, J. Oldenettel, C. Howton & M. V. McCusker, submitted to J. Chem. Phys.
2. D. L. Huestis and E. Zamer, preprint.
3. A. M. Hawryluk, J. A. Mangano and J. H. Jacob, preprint.
4. J. Fenn, private communication.
5. T. L. Gilbert and A. C. Wahl, J. Chem. Phys. 55, 5247 (1971).
6. T. L. Gilbert and A. C. Wahl, "Compendium of Ab Initio Calculations of Molecular Energies and Properties" edited by M. Krauss, NBS Technical Note 438 (1967).
7. J. S. Cohen and B. I. Schneider, J. Chem. Phys. 61, 3230 (1974).
8. B. I. Schneider and J. S. Cohen, J. Chem. Phys. 61, 3240 (1974).
9. V. Sidis, M. Barat and D. Dhuicq, J. Phys. B 8, 474 (1975).
10. W. J. Stevens, M. Gardner and A. Karo, preprint.
11. Willard R. Wadt, submitted to J. Chem. Phys.
12. P. J. Hay and T. H. Dunning, Jr., J. Chem. Phys. 64, 5077 (1976).
13. R. S. Mulliken, J. Chem. Phys. 52, 5170 (1970).
14. F. R. Gilmore, T. L. Barr and D. Dee, J. Quant. Spect. Rad. Trans. 15, 625 (1975).
15. H. H. Michels, R. H. Hobbs and L. A. Wright, Chem. Phys. Lett. 48, 158 (1977).
16. H. H. Michels, R. H. Hobbs, L. A. Wright and J.W.D. Connolly, Int. J. Quant. Chem., in press.
17. J. C. Slater, Adv. Quant. Chem. 6, 1 (1972).
18. P. O. Löwdin, Phys. Rev. 97, 1474 (1955).
19. W. Kohn and L. Sham, Phys. Rev. 140A, 1133 (1965).
20. J. C. Slater, Phys. Rev. 81, 385 (1951).
21. K. Schwarz, Phys. Rev. B5, 2466 (1972).
22. N. Rösch and K. H. Johnson, Chem. Phys. Lett. 23, 149 (1973).

23. F. E. Harris and H. H. Michels, Int. J. Quant. Chem. IS, 329 (1967).

24. A. C. Wahl, P. J. Bertoncini, G. Das and T. L. Gilbert, Int. J. Quant. Chem. IS, 123 (1967).

25. P. O. Löwdin, Molecular Orbitals in Chemistry, Physics and Biology, Academic Press, N.Y., (1964).

26. F. E. Harris, J. Chem. Phys. 32, 3 (1960).

27. H. H. Michels and F. E. Harris, J. Chem. Phys. 39, 1464 (1963).

28. S. R. Langhoff and C. W. Karn, Modern Theoretical Chemistry, Vol. II, Plenum Press, N.Y., (1977).

29. C. E. Moore, Atomic Energy Levels, NBS Circular 467, (1949).

30. J. T. Mosely, R. P. Saxon, B. A. Huber, P. C. Cosby, R. Abouaf and M. Tadjeddine, J. Chem. Phys. 67, 1659 (1977).

31. H. M. Hulburt and J. O. Hirschfelder, J. Chem. Phys. 9, 61 (1940).

32. J. B. Mann, Atomic Structure Calculations, Los Alamos Scientific Laboratory Report LA-3690, (1967).

33. C.Y. Ng, D. J. Trevor, B. H. Mahan and Y. T. Lee, J. Chem. Phys. 66, 446 (1977).

34. M. S. Munson, J. L. Franklin and F. H. Field, J. Chem. Phys. 67, 1542 (1963).

35. H. V. Mittmann and H. P. Weise, Z. Naturforsch, 29a, 400 (1974).

36. T. M. Miller, J. H. Ling, R. P. Saxon and J. T. Mosely, Phys. Rev. A 13, 2171 (1976).

APPENDIX D

Electronic Structure of the Noble Gas Dimer Ions. I. Potential Energy Curves and Spectroscopic Constants*

L. A. Wright
Kirtland Air Force Base, New Mexico 87117

ABSTRACT

A systematic study of the electronic structure and chemical binding in the dimer ion sequence, Ne_2^+, Ar_2^+, Kr_2^+ and Xe_2^+, has been carried out using both density functional and ab initio configuration-interaction computational techniques. This study includes detailed calculations of the pertinent potential energy curves and an analysis of the calculated spectroscopic properties of the bound states of these ions. A regular progression is found in the spectroscopic properties for the ground $A\ ^2\Sigma^+_{1/2u}$ state which leads to some remarkably simple conclusions concerning the nature of the binding and the size of these dimer ions. For the heavier systems, Kr_2^+ and Xe_2^+, spin-orbit coupling becomes important, resulting in a strong mixture of the Λ-S coupled Σ and Π states. This mixing affects the strength of the binding in the ground state. A comparison with other ab initio studies and an analysis of the asymptotic behavior at large internuclear separations is given. These dimer ion species illustrate the classic Hartree-Fock symmetry dilemma arising from improper dissociation character. The nature of this problem for ionized homopolar species is discussed.

*Supported in part by AFWL under Contract F29601-78-C-0031 and by AFOSR under Contract F49620-77-C-0064.

I. INTRODUCTION

The diatomic molecules formed from the noble gases, from the partially closed shell Group IIA and IIB elements or from the noble gas-halogen combinations constitute an interesting and important class of molecules for laser applications. These molecules are characterized by a repulsive or weakly bound ground state potential curve and by bound, electronically excited states. These excited diatomic molecules, known as excimers, radiate in a narrow visible or uv continuum band by making a transition to a repulsive lower state that dissociates into ground state neutral atoms. The resulting laser's operating characteristics are controlled by kinetic processes competing for the formation and destruction of the excited molecular levels and by absorption losses arising from noble gas dimer ions and high-lying Rydberg states of the excimer molecules. This last observation suggested the need for the present studies of the electronic structure and absorption characteristics of the noble gas dimer ions which rate studies show to be present in large concentrations in the candidate excimer systems.[1-4]

In this paper, we present the results of electronic structure calculations for the dimer ion sequence Ne_2^+, Ar_2^+, Kr_2^+ and Xe_2^+. These results include the pertinent potential energy curves and calculated spectroscopic constants. Further papers in this series deal with photodissociation and absorption processes of the noble gas dimer ions. These include the predicted absorption spectrums for the strong $A\ ^2\Sigma_u^+ \rightarrow D\ ^2\Sigma_g^+$ system and the weaker $A\ ^2\Sigma_u^+ \rightarrow B\ ^2\Pi_g$ system.

Theoretical treatments of the noble gas dimer ions have consisted mainly of *ab initio* SCF studies of the ground $A\ ^2\Sigma_u^+$ state and, by far, most of these studies have been devoted to He_2^+. We consider here only the systems, Ne_2^+, Ar_2^+, Kr_2^+ and Xe_2^+, which are chemically similar, with binding arising from the outer shell p-electrons.

The Ne_2^+ and Ar_2^+ ions were first studied by Gilbert and Wahl[5] using SCF wavefunctions constructed from STO basis functions. These authors have also reported[6] limited SCF studies of the B $^2\Pi_g$, C $^2\Pi_u$ and D $^2\Sigma_g^+$ excited states of Ne_2^+ and Ar_2^+. CI studies of the ground state of the Ne_2^+ ion were reported by Cohen and Schneider[7,8] as part of a study of the Rydberg states of this system. SCF calculations for Ar_2^+ at short internuclear separations have been reported by Sidis, et al[9] and more recently by Stevens, et al[10], using an extensive STO basis. A uniform study of the systems Ar_2^+, Kr_2^+ and Xe_2^+ has also recently been reported by Wadt[11] who employed a POL CI[12] calculation using gaussian basis functions. This study, like the present, was directed toward the prediction of the absorption properties of these dimer ions. Calculations for Xe_2^+ using an effective core potential have been reported by Ermler, et al.[13] These calculations were part of a more extensive study of Xe_2 which included the Rydberg states of this system.

Finally, a semi-empirical analysis of the potential energy curves for Xe_2^+ has been reported by Dehmer and Dehmer.[14] These authors constructed potential energy curves based, in part, on their photoelectron spectrum of the Xe_2 molecule, on the elastic scattering measurements of difference potentials reported by Jones, et al,[15] and on the ab initio calculations of Wadt,[11] which were used in reduced potential form.

The theoretical principles underlying the electronic structure of the homonuclear noble gas molecular ions have been discussed by Mulliken[16] using Xe_2^+ as a prototype and, more recently, by Gilmore, Barr and Dee[17] for the case of Kr_2^+. For these dimer ions, four electronic states ($A^2\Sigma_u^+$, $B^2\Pi_g$, $C^2\Pi_u$ and $D^2\Sigma_g^+$) arise from a ground state atom (^1S_o) and a ground state ion ($^2P_{1/2,3/2}$). The lowest state, usually labeled A $^2\Sigma_u^+$, is bound for the four systems Ne_2^+, Ar_2^+, Kr_2^+ and Xe_2^+ and has been partially characterized experimentally through scattering experiments, although there has been much controversy concerning the dissociation

energies of these ions.[16] For the heavier ions, Λ-S coupling is no longer strictly valid and the B $^2\Pi_g$ and C $^2\Pi_u$ states split into J-J coupled components with a resultant mixing of Σ and Π symmetries. This splitting is small for Ne_2^+ but six distinct J-J coupled molecular ion states arise for Xe_2^+.

With the exception of the recent calculations by Wadt,[11] no attempts at systematic studies of these ions have been reported. Accurate ab initio methods would appear to be practical only for the lighter ions with diminished accuracy for heavier systems such as Xe_2^+. Wadt reports such a trend in his calculations[11] which indicate that his gaussian basis is less flexible or less complete in the case of Xe_2^+ than for the corresponding study of Ar_2^+. Recent density functional calculations of noble gas halide molecules[18,19] have yielded reliable predictions of geometry and chemical binding, provided certain optimization criteria are followed. Such calculations, which should be of more uniform quality than ab initio studies, since numerical molecular orbitals are employed, constitute the principle effort in the present study. A limited number of ab initio calculations were carried out for Ar_2^+ for comparison purposes.

II. Method of Approach

A. Density Functional Approach - X_α Model

The X_α model[20] for the electronic structure of atoms, molecules, clusters and solids is a local potential model obtained by making a simple approximation to the exchange-correlation energy. If we assume a non-relativistic Hamiltonian with only electrostatic interactions, it can be shown[21] that the total energy E of a system can be written (in atomic units) as

$$E = \sum_i n_i \langle u_i \left| -\tfrac{1}{2}\nabla_i^2 + \sum_\mu \frac{z_\mu}{r_{i\mu}} \right| u_i \rangle + \tfrac{1}{2} \sum_{\mu \neq \nu} \frac{z_\mu z_\nu}{r_{\mu\nu}} + \tfrac{1}{2} \sum_{ij} n_i n_j \langle u_i u_j \left| \frac{1}{r_{12}} \right| u_i u_j \rangle + E_{xc} \qquad (1)$$

This expression is exact provided the u_i are natural orbitals and n_i are their occupation numbers (i.e., eigenfunctions and eigenvalues of the first order density matrix). The first term in Eq. (1) represents the kinetic and electron-nuclear energies. The second term is the nuclear repulsion energy. The sums (μ,ν) are over all the nuclear charges in the system. The third term is the electron-electron repulsion term, which represents the classical electrostatic energy of the charge density ρ interacting with itself, where

$$,(1) = \sum_i n_i u_i^*(1)\, u_i(1) \qquad (2)$$

The last term E_{xc} represents the exchange-correlation energy and can be expressed formally as

$$E_{xc} = \frac{1}{2} \int \rho(1)\, d\vec{r}_1 \int \frac{\rho_{xc}(1,2)}{r_{12}}\, d\vec{r}_2 \,, \qquad (3)$$

where $\rho_{xc}(1,2)$ represents the exchange-correlation hole around an electron at position 1. In the exact expression, ρ_{xc} is dependent on the second-order density matrix. In the Hartree-Fock approximation E_{xc} is simply the exchange energy and ρ_{xc} represents the Fermi hole due to the exclusion principle and depends only on the first-order density matrix. In the X_α method, a simpler assumption about ρ_{xc} is made. If we assume that the exchange-correlation hole is centered on the electron and is spherically symmetric, it can be shown that the exchange-correlation potential

$$u_{xc} = \int \frac{\rho_{xc}(1,2)}{r_{12}}\, d\vec{r}_2 \qquad (4)$$

is inversely proportional to the range of the hole, r_s, where r_s is defined by

$$\frac{4\pi}{3} r_s^3 \rho(1) = 1 \qquad (5)$$

Therefore, in the X_α model, the potential U_{xc} is proportional to $\rho^{1/3}(r)$. A scaling parameter α is defined such that

$$U_{x_\alpha}(1) = -\frac{9\alpha}{2} (3\rho(1)/8\pi)^{1/3} \qquad (6)$$

The expression in Eq. 6 is defined so that $\alpha=2/3$ for the case of a free electron gas in the Hartree-Fock model[22] and $\alpha=1$ for the potential originally suggested by Slater[23]. A convenient way to choose this parameter for molecular and solid state applications is to optimize the solutions to the X_α equations in the atomic limit. Schwarz[24] has done this for atoms from Z = 1 to Z = 41 and found values between 2/3 and 1. However, the optimum value for α is dependent on the ionicity of the system. For accurate total energies, this variation must be properly described as is discussed below.

B. Computational Aspects of the X_α Method

To implement the X_α approximation in molecular calculations it is usually convenient to break up the volume integrals indicated in Eqs. (3) or (4) by defining spherical regions surrounding each atomic center. The molecular potential is then spherically averaged within these regions and assumed constant in the region between spheres. The potential falls to zero in the usual way in the region outside of an overall sphere located to encompass those spheres surrounding the individual atoms.

There are two other practical aspects of the calculations which must be considered in application of the X_α model to finite molecular systems. The first concerns the choice of the integration framework for describing the molecular-

orbital wavefunctions and the second deals with the choice of the exchange parameter, α, in different regions of space. A third consideration, convergence of the spherical harmonic expansion, was also tested. For the systems studied here, the total energy was converged when all terms up to $\ell=3$ were included.

In molecules with significant charge sharing in the bonds, the radii of the atomic spheres is frequently increased in X_α calculations so that an overlap region appears in the vicinity of the bond.[25] Our studies[19] have shown that the contribution to the total molecular energy from the exchange-correlation term shows a minimum at an optimum sphere radius or sphere overlap. This result can be deduced from the X_α model by comparing the exchange energy of the electron density at the edge of the spherical integration region with that across this boundary in the intersphere region. This provides a sensitive criterion for selecting these parameters.

The values of the exchange parameters in the spherical integration region around each atomic center are frequently set at the atomic values both for neutral and for ionic molecular constituents. It is known, however, that the value of α which best reproduces Hartree Fock results varies with ionicity.[24] While for heavy atoms, these changes in the exchange parameter would be small, the α's for small atoms vary rapidly with z (and with ionicity). In Table I we show the optimum exchange parameters for the ion pairs included in this study. It is obvious that the exchange parameters, and the corresponding electron densities, must be optimized for correct ion-atom pair separation. The correct choice of the exchange parameters influences not only the total energy calculated for the molecule but also affects the distribution of charge between the atomic spheres and the intersphere region.

C. Ab Initio Approach - Valence CI Method

The ab initio calculation procedure chosen for these studies is the valence-configuration-interaction (VCI) method.[27,28] The specific form for $\psi(R)$ may be

written as

$$\psi^{g,u}(R) = \sum_{\mu} c_{\mu} \psi_{\mu}^{g,u}(R) \tag{7}$$

where each $\psi_{\mu}^{g,u}(R)$ is referred to as a configuration and has the general structure

$$\psi_{\mu}^{g,u}(R) = \mathcal{A}\mathcal{O}_s \Pi \left[\phi_{\mu 1}(A)\phi_{\mu 2}(A)\cdots\phi_{\mu n}(A)\right]\left[\phi'_{\mu 1}(B)\phi'_{\mu 2}(B)\cdots\phi'_{\mu n-1}(B)\right] \tag{8}$$

$$\pm \left[\phi_{\mu 1}(B)\phi_{\mu 2}(B)\cdots\phi_{\mu n}(B)\right]\left[\phi'_{\mu 1}(A)\phi'_{\mu 2}(A)\cdots\phi'_{\mu n-1}(A)\right]\theta_{M_s}$$

and where $\phi_{\mu i}$ is a spatial orbital, $\mathcal{A}$ is the antisymmetrizing operator, $\mathcal{O}_s$ is the spin-projection operator for spin quantum number S, and θ_{M_s} is a product of α and β one-electron spin functions of magnetic quantum number, M_s. The spatial orbitals, $\phi_{\mu i}$ have the general form

$$\phi_i = e^{-\delta_i \xi - \zeta_i \eta + i\nu_i \phi} \xi^p \eta^q r^{n_i - 1} P_{\ell_i}^{|\nu_i|}(\cos\theta) \tag{9}$$

where for $\zeta_i = \pm\delta_i$, the standard STO form is recovered.

The wavefunctions represented by Eq. (8) correctly dissociate to an atom and ion valence bond product wavefunction at large internuclear separations with an optimized description of the charge density about the separate atom and ion nuclei. This situation is to be contrasted with that arising from the construction of a Hartree-Fock wavefunction for the molecular ion. Within the HF framework we write

$$\psi^{g,u} = \mathcal{A}\Pi\left[U_1^{g,u}(\alpha)U_1^{g,u}(\beta)\cdots U_{2n-1}^{g,u}(\alpha)\right] \tag{10}$$

where

$$U_i^{g,u} = \phi_i(A) \pm \phi_i(B); \qquad \phi_i = \text{av.}(\phi_i + \phi_i') \tag{11}$$

This symmetry adaptation of the orbital basis, represented by Eq. (11), introduces a severe, non-physical correlation error into the calculations which manifests itself at large internuclear spearations. The wavefunction represented by Eq. (10) dissociates into an averaged atom-ion pair with charge density of the hypothetical species $R^{+\,1/2}$. This situation has been noted by previous authors[5], who suggested, however, that this correlation error arising from symmetry adaptation did not vary significantly with changing internuclear separations. We find different results, especially for Ne_2^+, which separates into an atom and ion pair with significantly different spatial charge distributions. This symmetry dilemma arising from the restricted Hartree-Fock model has been discussed previously by Lowdin[29] who suggested alternate computational routes.

There are several complications introduced by the choice of Eq. (8) for the molecular ion configuration. For heavy nuclei systems such as Xe_2^+, the atomic and ionic basis functions will be similar and Eq. (11) may be a satisfactory approximation. For light nuclei systems such as Ne_2^+, the distinction between the atomic and ionic basis functions must be retained which introduces a non-orthogonality problem into Eq. (8). One solution is to remain within a non-orthogonal framework. This leads to a secular equation of the form

$$\left(\underset{\sim}{\mathcal{H}} - \lambda \underset{\sim}{\mathcal{S}}\right)\psi = 0 \tag{12}$$

where $\underset{\sim}{S}$ is the non-orthogonality matrix. Calculations of this type have been reported by Harris and co-workers.[30,31] An alternate approach is to expand the atomic and ionic functions as linear combinations of symmetry adapted MO's such as

$$\phi_{A,B} = \left(U_g \pm U_u\right); \qquad \phi'_{A,B} = \left(U'_g \pm U'_u\right) \tag{13}$$

This leads to a restricted CI among symmetry adapted functions which can be cast in an orthogonal framework.

D. Spin-Orbit Effects

The ground state of a noble gas ion is split by spin-orbit coupling into two components, a $^2P_{3/2}$ state, which lies lowest, and a $^2P_{1/2}$ state. This splitting is small in the case of Ne^+ (781 cm^{-1}) but is of the same magnitude as the chemical binding energy in the case of Xe^+ (10537 cm^{-1}). Rigorous inclusion of spin-orbit effects in molecular calculations is still computationally prohibitive,[32] but for these noble gas ions, which exhibit small changes from separated atom-ion pair electron densities, an asymptotic atomic approximation is valid.[7,8] In this approximation, the hamiltonian is written as

$$\mathcal{H}(R) = \mathcal{H}^{\Lambda,S}(R) + V^{S-O} \tag{14}$$

where V^{S-O} is taken in the atom-ion limit of infinite internuclear separation and is considered to be R-independent. For the $\Omega = 1/2$ components, Eq. (14) leads to a secular equation of the form

$$\begin{vmatrix} E^{\Sigma}(R) - \lambda_{1/2} & -\sqrt{2}\,\alpha \\ -\sqrt{2}\,\alpha & [E^{\Pi}(R) + \alpha] - \lambda_{1/2} \end{vmatrix} = 0 \tag{15}$$

where $E^{\Sigma}(R)$ and $E^{\Pi}(R)$ are the pure Λ-S coupled eigenvalues and α is the spin-orbit splitting parameter ($3\alpha = \Delta E_{^2P_{3/2} - {}^2P_{1/2}}$) which can be obtained from atomic data. For the Ω = 3/2 components, there is no mixing of the Σ and Π states and Eq. (14) leads simply to

$$\left| [E^{\Pi}(R) - \alpha] - \lambda_{3/2} \right| = 0 \qquad (16)$$

For illustration, the spin-orbit components for Ω = 1/2 take the form

$$\begin{aligned} {}^{1}/_{2}\, {}_{g,u}\ \mathrm{I} &= C^{\Sigma}_{g,u}\, \psi^{\Sigma}_{g,u} + C^{\Pi}_{g,u}\, \psi^{\Pi}_{g,u} \\ {}^{1}/_{2}\, {}_{g,u}\ \mathrm{II} &= -C^{\Pi}_{g,u}\, \psi^{\Sigma}_{g,u} + C^{\Sigma}_{g,u}\, \psi^{\Pi}_{g,u} \end{aligned} \qquad (17)$$

where $C^{\Sigma}_{g,u} \to \sqrt{2/3}$ and $C^{\Pi}_{g,u} \to \sqrt{1/3}$ for large internuclear separations. For the lighter systems such as Ne_2^+, $C^{\Sigma}_{g,u} \to 1$ and $C^{\Pi}_{g,u} \to 0$ for internuclear separations near R_e. Inclusion of these spin-orbit effects was carried out for all of the ions studied herein. We shall see that this effect fully accounts for the systematic decrease of the dissociation energy of the ground state of these molecular ions in the progression from Ne_2^+ to Xe_2^+.

E. Long-Range Interactions

The long-range energy of interaction between a noble gas atom and a singly charged ion (with the exception of He-He^+) can be written as[33,34]

$$V(R\to\infty) \simeq -\frac{\alpha_o}{2R^4} - \frac{3\alpha_o\alpha_+}{2[I_o^{-1} + I_+^{-1}]R^6} - \frac{3\alpha_o Q_+^2}{2R^8} \qquad (18)$$

The first and third terms represent the main components of energy of induction between the charge and the induced dipole. The second term is the London dispersion energy based on the approximate Drude formula. A small contribution arising from the quadrupole polarizability of the noble gas atom has been neglected in this term. The term in R^{-8} is unimportant for these dimer ions owing to the smallness of the permanent moments for these systems.

In Table II we give values for the parameters appearing in Eq. (18). Since dipole polarizabilities for the noble gas ions are unavailable, they are estimated from those for the neutral atoms using expectation values, $\langle r^2 \rangle$, calculated from corresponding neutral and ionic Hartree-Fock atomic wavefunctions. This approximation appears to be reliable for the corresponding halogen-halogen ion pairs, where there are known experimental data for comparison. The long-range form of the interaction potentials can be represented(in a.u.) as

$$Ne\text{-}Ne^+: \quad U(R\to\infty) \simeq -\frac{1.331}{R^4} - \frac{2.749}{R^6} \tag{19}$$

$$Ar\text{-}Ar^+: \quad U(R\to\infty) \simeq -\frac{5.540}{R^4} - \frac{39.945}{R^6} \tag{20}$$

$$Kr\text{-}Kr^+: \quad U(R\to\infty) \simeq -\frac{8.368}{R^4} - \frac{88.697}{R^6} \tag{21}$$

$$Xe\text{-}Xe^+: \quad U(R\to\infty) \simeq -\frac{13.645}{R^4} - \frac{219.327}{R^6} \tag{22}$$

Values of the long-range interaction calculated from Eq. (19)-(22) are presented in Table III. These data are compared below with the results obtained from the density functional calculations.

III. RESULTS AND DISCUSSION

We have carried out density functional X_α calculations for the molecular ions Ne_2^+, Ar_2^+, Kr_2^+ and Xe_2^+ to define the ground $A\ ^2\Sigma_u^+$ state, and its spectroscopic properties, and the nature of the mainly repulsive $B\ ^2\Pi_g$, $C\ ^2\Pi_u$ and $D\ ^2\Sigma_g^+$ states which arise from a ground state noble gas atom-ion pair. As a check on the accuracy of these calculations, ab initio wave functions were constructed for Ar_2^+ in both orthogonal and non-orthogonal frameworks. The ab initio calculations were carried out using computational programs which have been previously described.[27,31] The density functional calculations were carried out with both overlap and α parameters optimized for each ion symmetry.[19] There is a small variation in the optimum parameters arising from molecular ion symmetry considerations. These changes were found to be negligible for Kr_2^+ and Xe_2^+ but were important in the case of Ne_2^+. Although we constructed separate optimum functions for each molecular ion symmetry, we observed that transition state calculations of energy differences between these ion states would suffice for Kr_2^+ and Xe_2^+ but would definitely be in error for Ne_2^+.

A. Ab Initio Results

The general nature of the potential energy curves arising from a ground state noble gas atom-ion pair can be illustrated using Ar_2^+ as a prototype. Since our main emphasis was on density functional methods, which appeared to offer more promise of uniform quality, Ar_2^+ represented a typical system with relative ease of ab initio computations.

A CI expansion was constructed as described above using a minimum elliptic basis optimized at each internuclear separation studied, and augmented by the inclusion of optimized 4s and 4p functions to allow more flexibility in the valence shell charge distribution. In the computational framework described by Eq. (8), a partial orthogonalization of the basis set is possible. This involves orthogonalization of the core functions among themselves, followed by separate orthogonalization of the valence shell functions to the core functions. The antisymmetrizing

operator then spans only the valence shell electrons and the inner (Ne-core) electrons are taken to be pairwise singlet-coupled. An alternate approach, within a totally orthogonal framework, is to construct a double set of symmetry orbitals based separately on the optimized neutral atom and ion basis functions. This new orbital basis (essentially equivalent to a double-zeta basis for the valence electrons) can then be projected into a restricted CI equivalent to Eq. (8), by expansion of the separate atomic and ionic orbitals in terms of their symmetrized representation as given in Eq. (11). Except for some small higher excitation contributions in the orthogonalized CI framework, the calculated results (and computational effort), using either approach, were virtually identical. The trade-off is between a large CI in an orthogonal framework and more complicated matrix elements with the non-orthogonal basis.

The resultant ab initio potential curves for Ar_2^+ are given in Table IV and illustrated in Fig. 1. Spin-orbit effects are not included and the asymptotic limit is the center of gravity of the $^2P_{3/2,1/2}$ argon ion components.[35] The ground $A\ ^2\Sigma_u^+$ state is seen to be bound by 1.26 eV with an equilibrium separation of 2.42Å. This is in reasonable agreement with the latest experimental study of this ion by Moseley, et al[36] who conclude that the dissociation energy of Ar_2^+ is 1.33 ±.02 eV. Inclusion of spin-orbit effects would tend to reduce the calculated dissociation energy of Ar_2^+ and somewhat worsen the agreement. There is a small binding ($\sim$ .1 eV) of the $B\ ^2\Pi_g$ state at R$\sim$3 Å but this state is clearly repulsive in the Franck-Condon region of the ground state. The $C\ ^2\Pi_u$ state potential curve suggests little or no binding, at least for separations < 3 Å. The $D\ ^2\Sigma_g$ state is repulsive over the entire range of internuclear separations that were studied. We shall see that very similar results are found for Ar_2^+ using the density functional method.

B. Density Functional X_α Results

Systematic studies of these dimer noble gas ions were carried out using the density functional X_α method, as described above. Previous studies[19] had indicated that these, nearly closed-shell, interacting atom-ion systems should be favorable candidates for application of density functional methods. This is based on the observation that the binding in these systems is dominated by simple exchange forces and that no drastic charge redistribution occurs during molecular ion formation. Separate calculations were performed for each molecular ion symmetry and for a wide range of internuclear separations. A double iteration computation scheme was employed since each separate calculation was optimized for both the charge distribution and the radii of the spheres of integration. The optimum overlap radii vary slightly with the symmetry of the species but are close to the values, 24.5, 21.0, 20.5 and 20.0%, respectively, for the sequence $Ne_2^+ \rightarrow Xe_2^+$. This optimization is very important if accurate total energies are required. The one-electron excitation spectra are much less sensitive to overlap optimization.

The resultant density functional potential energy curves, assuming Λ-S coupling, are given in Tables V-VIII for the ion sequence Ne_2^+, Ar_2^+, Kr_2^+ and Xe_2^+. A comparison can be made between these calculated potential curves and the long-range ion-atom potentials, as given in Table III, at large internuclear separations. Considering only g-u symmetry effects, the $B\ ^2\Pi_g$ and $C\ ^2\Pi_u$ states have asymptotic behavior of the form

$$U_{g(u)}(R \rightarrow \infty) = U(R \rightarrow \infty)_{(+)}^{(-)} < \chi_A^\circ \chi_B^+ | \mathcal{H} | \chi_B^\circ \chi_A^+ > \qquad (23)$$

where $U(R\rightarrow\infty)$ is given by Eqs. 19-22 and χ_A° and χ_B^+ refer to separated atom and ion wavefunctions located on centers A and B, respectively. A similar argument can be made for states of Σ symmetry which is valid at somewhat larger internuclear

separations. We see that Eq. (23) closely corresponds to our density functional results; the g-u states split the long-range polarization potential. The ab initio potential energy curves reported by Wadt[11] do not exhibit this behavior. In his studies, the B $^2\Pi_g$ state for $Ar_2^+ \rightarrow Xe_2^+$ closely follows Eqs. 20-22 indicating too much long-range repulsion in the calculated potential energy curves.

In Tables IX-XII we have included the spin-orbit splitting of the Λ-S coupled states and the resultant mixing of the Ω = 1/2 component of the corresponding $^2\Sigma$ and $^2\Pi$ states. As previously mentioned, this splitting is small for Ne_2^+ but is very significant for Xe_2^+. Figures 2-5 illustrate our calculated potential energy curves including these spin-orbit coupling effects.

Summaries of our calculated spectroscopic constants are given in Tables XIII-XVI for the dimer ion sequence $Ne_2^+ \rightarrow Xe_2^+$. These spectroscopic data were obtained by fitting our calculated J-J coupled potential curves to the Hulbert-Hirschfelder modification of the Morse function[37] using a least-squares fit to the calculated values near R_e. Comparing the results of our calculations in the sequence $Ne_2^+ \rightarrow Xe_2^+$ we find a regular progression in the calculated dissociation energy and the equilibrium internuclear separation for the ground A $^2\Sigma^+_{1/2u}$ state. The calculated binding energy decreases from 1.31 eV for Ne_2^+ to 1.06 eV for Xe_2^+ while the equilibrium separation increases uniformly from 1.7 to 3.2 Å.

A comparison of our calculated data for the A $^2\Sigma^+_{1/2u}$ state of these ions is given in Table XVII. An examination of these calculated data reveals some remarkable regularities. We observe that, in the absence of spin-orbit coupling effects, the dissociation energy of all four dimer ions is identical, within the error of our calculations (1.38 ± .02 eV). This suggests that the binding arising from Λ-S coupling in these systems is independent of the principal quantum number of the valence shell and that the experimentally observed decrease in the binding energies in the sequence $Ne_2^+ \rightarrow Xe_2^+$ has its origin in the increased degree of mixing of

the repulsive $^2\Pi_{1/2u}$ component into the ground electronic state. A second remarkable simplicity in the structure of these ions can be found by examining the progression in the calculated equilibrium separations. In Table XVII we list a column of the average expectation of $\langle\bar{r}\rangle$ for these atom-ion pairs, taken from accurate Hartree-Fock calculations,[26,38] and compare this with our computed values for R_e. We find the condition of additivity of radii is an excellent approximation for these dimer ions with R_e(a.u.) = 2.0 $\langle\bar{r}\rangle$ + constant. Thus, in the absence of spin-orbit effects, these molecular ions exhibit text-book simplicity for our understanding of their binding and geometry.

A comparison of the density functional potential energy curves given in Tables V-VIII can be made with the recent ab initio calculations reported by Wadt[11] for the ions Ar_2^+, Kr_2^+ and Xe_2^+ and the ab initio with effective core potential calculations recently reported by Ermler, et. al[13] for Xe_2^+. The ab initio potential curves of Wadt[11] all tend to exhibit more repulsive energy than the corresponding density functional curves. These differences increase as the internuclear separation decreases, with the result that the ab initio potential curves for the ground $A\ ^2\Sigma_{1/2u}$ states underestimate the true dissociation energies. The differences are correspondingly greater for Xe_2^+ than for Ar_2^+ which suggests a deficiency in the analytic basis functions chosen for the ab initio studies. The studies by Ermler, et. al[13] point out the significant savings in the use of core potentials but suffer from a common deficiency in the basis functions chosen for the valence shell electrons.

At short internuclear separations ($< R_e$), the differences between the ab initio curves and our density functional curves appear to diminish. This suggests an accumulating error in the density functional results at shorter separations, probably arising from core overlap effects which are not fully represented in our calculations. Qualitatively, the ab initio and density functional results are remarkably similar.

A further comparison of our calculated dissociation energies can be made with the recent data reported by Dehmer and Dehmer[14,45] for the excited states of Ar_2^+, Kr_2^+ and Xe_2^+ and previous experimental studies of the ground state. This comparison is shown in Table XVIII which indicates good agreement for all of these dimer ions. Dehmer and Dehmer[14] also report semi-empirical potential energy curves for Xe_2^+ based, in part, on their photoelectron spectrum of the Xe_2 molecule, on the elastic scattering measurements of difference potentials reported by Jones, et. al[15], and on the ab initio calculations of Wadt,[11] which were used in reduced potential form. These semi-empirical curves all qualitatively disagree both with our results for Xe_2^+ and with the ab initio results reported by Wadt. The curves reported by Dehmer and Dehmer exhibit much flatter shapes with softer repulsive branches for all symmetries of Xe_2^+. Part of the difference arises from their assumption of a constant scaling error in using Wadt's potential curves in reduced (U(R)/De) form. Ab initio potential curves, in general, cannot be characterized by an error term of their functional form.

Partial confirmation of the results reported here can also be obtained by comparison of the calculated data given in Tables XIII-XVI with experimental determinations of dissociation energies of these ions from photoionization or rainbow scattering collision studies.[36,39-43] For all of the ions studied here, differences between theory and the most recent experimental values for the dissociation energies lie within the reported experimental uncertainties. There are also some experimental data available to verify the location of the excited states of these dimer ions. These data are from rainbow scattering experiments[41] and, more recently, from photoabsorption studies in Ar_2^+ and Kr_2^+.[1,36,42-44] We find a peak calculated absorption for the strong $A\ ^2\Sigma_{1/2u} \rightarrow D\ ^2\Sigma_{1/2g}$ transition at 298 nm for Ar_2^+ and at 323 nm for Kr_2^+. These calculated data can be compared with the recent

experimental profiles obtained by Hunter[1] who obtained peaks at 292 nm and 325 nm for Ar_2^+ and Kr_2^+, respectively. The long wavelength transitions for photoabsorption ($A\ ^2\Sigma_{1/2u} \rightarrow B\ ^2\Pi_{1/2g}$ and $A\ ^2\Sigma_{1/2u} \rightarrow B\ ^2\Pi_{3/2g}$) have been studied in detail by Moseley et al[36,42-43] for Ar_2^+, Kr_2^+ and Xe_2^+. Further papers in this series will report more detailed comparisons of these photoabsorption spectra with our calculated profiles.

The apparent success of the density functional method in describing the electronic structure of these noble gas dimer ions should not be interpreted as suggesting that this method, in general, is to be preferred over ab initio methods. As has been pointed out above, closed shell system interactions, where there are no drastic charge rearrangements and no degeneracy complications, are ideal candidates for the density functional method. This method, when properly applied, is capable of yielding results of uniform accuracy for both light and heavy atom systems owing to numerical representation of the valence shell orbitals. The well-known analytic expansion problems of ab initio basis functions are, in a sense, circumvented. In addition, there is a large body of accumulating evidence that density functional methods, in general, can yield reliable one-electron excitation spectra.

However, the density functional method, at least in any of its present simplified forms, is not particularly useful for total energy calculations of systems which exhibit a large charge rearrangement with a change in internuclear separation. In addition, the method is not useful at all for systems with electronic degeneracies or complicated spin representation. In these regards, it suffers the same limitations as conventional Hartree-Fock methods. When such considerations are present, and unfortunately they are in the general case and not as exceptions, ab initio techniques must be relied upon for quantitative results.

Our conclusion is, when properly used and applied to systems involving simple charge descriptions, density functional methods are a valuable addition to our

list of techniques for electronic structure calculations.

ACKNOWLEDGEMENTS

The authors wish to thank Judith B. Addison for her valuable assistance in carrying out these computations. We also wish to express our thanks to J. B. Mann for performing various Hartree-Fock calculations for several of the noble gas atomic ions, and to W. R. Wadt, N. W. Winter and P. M. Dehmer for preprints of their work prior to publication. Use of the computer facilities at the Kirtland Air Force Base in Albuquerque is also acknowledged.

Table I. Optimum Atomic and Ionic Density Functional Exchange Parameters and Energies.

Species	Exchange Parameter, α	X_α energy (a.u.)	HF energy* (a.u.)
Ne	0.73081	-128.5470	-128.5474
Ne^+	0.73684	-127.8176	-127.8178
Ar	0.72177	-526.8176	-526.8173
Ar^+	0.72249	-526.2745	-526.2745
Kr	0.70574	-2752.0560	-2752.0569
Kr^+	0.70583	-2751.5679	-2751.5674
Xe	0.69986	-7232.1501	-7232.1500
Xe^+	0.69986	-7231.7114	7231.7118

*Ref. 26

Table II. Long-Range Force Interaction Parameters for the Noble Gas Dimer Ions.

Species	α_o (bohr^3)	$\sum_i \langle r_i^2 \rangle$ (bohr^2)	I (eV)
Ne	2.66 [a,b]	9.699 [d]	21.564 [e,f]
Ne^+	(1.32) [c]	6.842	40.962
Ar	11.08	26.145	15.759
Ar^+	(6.52)	20.054	27.629
Kr	16.74	39.674	13.999
Kr^+	(10.78)	31.847	24.359
Xe	27.29	62.511	12.127
Xe^+	(18.90)	52.022	21.2

[a] R. R. Teachout and R. T. Pack, Atomic Data 3, 195 (1971).

[b] A. Dalgarno, Adv. Physics 11, 281 (1962).

[c] The ion polarizabilities are scaled from the atomic α_o using the hydrogenic form, $\alpha_o \sim \sum_i \langle r_i^2 \rangle^2$

[d] Non-relativistic Hartree-Fock calculation.

[e] R. L. Kelly and D. E. Harrison, Jr., Atomic Data 3, 177 (1971).

[f] C. E. Moore, Nat. Bur. Std. (U.S.) Circ. 467 (1958).

Table III. Long Range Interaction Potentials for the Noble Gas Dimer Ions

R (a.u.)	U(R) (a.u.)	R (a.u.)	U(R) (a.u.)
$Ne-Ne^+$		$Kr-Kr^+$	
8.0	-.00034	10.0	-.00093
7.0	-.00058	9.0	-.00144
6.0	-.00109	8.0	-.00238
5.0	-.00326	7.5	-.00314
4.6	-.00393	7.2	-.00375
4.4	-.00478	7.0	-.00424
4.2	-.00587	6.8	-.00481
		6.4	-.00628
$Ar-Ar^+$		$Xe-Xe^+$	
9.0	-.00092	11.0	-.00106
8.0	-.00151	10.0	-.00158
7.0	-.00265	9.0	-.00249
6.5	-.00363	8.2	-.00374
6.2	-.00445	8.0	-.00417
6.0	-.00513	7.6	-.00523
5.8	-.00595	7.4	-.00589
5.4	-.00813	7.0	-.00755

Table IV. Ab Initio Potential Energy Curves for Ar_2^+ assuming Λ-S coupling. Energies in a. u.

R (a.u.)	$A\ ^2\Sigma_u^+$	$B\ ^2\Pi_g$	$C\ ^2\Pi_u$	$D\ ^2\Sigma_g^+$
3.5	.0869	.2727	.3923	.4707
3.75	.0145	-	-	.3440
4.0	-.0238	-	-	.2388
4.25	-.0409	-	-	.1674
4.5	-.0459	.0264	.0593	.1185
4.75	-.0454	-	-	.0847
5.0	-.0397	-	-	.0596
5.5	-.0278	-.0013	.0069	.0299
6.0	-.0177	-.0032	-.0006	.0143
∞	0.	0.	0.	0.

Table V. Density Functional Potential Energy Curves for Ne_2^+ assuming Λ-S coupling. Energies in a.u. relative to $E(\infty) = -256.3646$ a.u.

R (a.u.)	$A\,^2\Sigma_u^+$	$B\,^2\Pi_g$	$C\,^2\Pi_u$	$D\,^2\Sigma_g^+$
3.0	-.04737	.04756	.09573	.16557
3.2	-.05068	.01916	.05401	.11261
3.4	-.04840	.00404	.02933	.07765
3.6	-.04340	-.00355	.01487	.05417
3.8	-.03729	-.00686	.00659	.03820
4.0	-.03101	-.00785	.00200	.02720
4.2	-.02515	-.00767	-.00044	.01951
4.4	-.01998	-.00693	-.00161	.01410
4.6	-.01563	-.00599	-.00207	.01024
∞	0.	0.	0.	0.

Table VI. Density Functional Potential Energy Curves for Ar_2^+ assuming Λ-S coupling. Energies in a.u. relative to $E(\infty)^2 = -1053.0921$.

R (a.u.)	$A\,^2\Sigma_u^+$	$B\,^2\Pi_g$	$C\,^2\Pi_u$	$D\,^2\Sigma_g^+$
4.2	-.04353	.06295	.10399	.18203
4.6	-.05070	.01862	.04412	.10336
4.8	-.04945	.00756	.02765	.07887
5.0	-.04659	.00081	.01663	.06072
5.2	-.04279	-.00316	.00931	.04707
5.4	-.03855	-.00504	.00478	.03706
5.8	-.02991	-.00608	.00001	.02330
6.0	-.02589	-.00566	-.00086	.01890
6.2	-.02221	-.00515	-.00137	.01532
∞	0.	0.	0.	0.

Table VII. Density Functional Potential Energy Curves for Kr_2^+ assuming Λ-S coupling. Energies in a.u. relative to E(∞) = -5503.6239

R (a.u.)	$A\,^2\Sigma_u^+$	$B\,^2\Pi_g$	$C\,^2\Pi_u$	$D\,^2\Sigma_g^+$
5.0	-.04987	.03373	.06103	.11527
5.2	-.05068	.01831	.04035	.08833
5.4	-.04949	.00843	.02613	.06817
5.6	-.04701	.00210	.01635	.05288
5.8	-.04373	-.00243	.00920	.04059
6.0	-.03999	-.00420	.00505	.03206
6.4	-.03211	-.00620	-.00021	.01933
6.8	-.02468	-.00616	-.00229	.01159
7.0	-.02136	-.00577	-.00266	.00897
7.2	-.01835	-.00532	-.00282	.00690
∞	0.	0.	0.	0.

Table VIII. Density Functional Potential Energy Curves for Xe_2^+ assuming Λ-S coupling. Energies in a.u. relative to $E(\infty) = -14463.8615$

R(a.u.)	$A\,^2\Sigma_u^+$	$B\,^2\Pi_g$	$C\,^2\Pi_u$	$D\,^2\Sigma_g^+$
5.8	-.05028	.02817	.05042	.09204
6.0	-.05064	.01683	.03519	.07264
6.2	-.04955	.00992	.02505	.05813
6.4	-.04748	.00359	.01606	.04531
6.6	-.04475	-.00037	.00989	.03544
6.8	-.04161	-.00311	.00533	.02750
7.0	-.03825	-.00455	.00239	.02142
7.4	-.03139	-.00548	-.00080	.01292
7.6	-.02808	-.00537	-.00153	.01000
7.8	-.02494	-.00510	-.00166	.00768
8.0	-.02202	-.00469	-.00211	.00580
8.2	-.01932	-.00418	-.00205	.00451
∞	0.	0.	0.	0.

Table IX. Potential Energy Curves for Ne_2^+ including spin-orbit coupling. Energies in eV relative to c.g. of Ne_2^+ at R=∞.

R (a.u.)	$A\ ^2\Sigma^+_{1/2u}$	$B\ ^2\Pi_{3/2g}$	$B\ ^2\Pi_{1/2g}$	$C\ ^2\Pi_{3/2u}$	$C\ ^2\Pi_{1/2u}$	$D\ ^2\Sigma^+_{1/2u}$
2.8	-0.89497	-	-	-	-	-
3.0	-1.28953	1.26194	1.32586	2.57256	2.63768	4.50598
3.2	-1.37990	0.48908	0.55283	1.43735	1.50265	3.06507
3.4	-1.31808	0.07755	0.14109	0.76574	0.83129	2.11391
3.6	-1.18232	-0.12882	-0.06558	0.37242	0.43830	1.47550
3.8	-1.01630	-0.21895	-0.15609	0.14705	0.21334	1.04125
4.0	-0.84617	-0.24597	-0.18362	0.02207	0.08890	0.74236
4.2	-0.68726	-0.24091	-0.17924	-0.04416	0.02338	0.53395
4.4	-0.54766	-0.22074	-0.15998	-0.07598	-0.00748	0.38739
4.6	-0.43046	-0.19535	-0.13579	-0.08868	-0.01897	0.28363
∞	-0.03230	-0.03230	-0.03230	-0.03230	0.06460	0.06460

Table X. Potential Energy Curves for Ar_2^+ including spin-orbit coupling. Energies in eV relative to c.g. of Ar_2^+ at R=∞.

R (a.u.)	$A\ ^2\Sigma^+_{1/2}$	$B\ ^2\Pi_{3/2g}$	$B\ ^2\Pi_{1/2g}$	$C\ ^2\Pi_{3/2u}$	$C\ ^2\Pi_{1/2u}$	$D\ ^2\Sigma^+_{1/2u}$
4.2	-1.18618	1.65365	1.76982	2.77055	2.89064	4.95560
4.4	-1.34226	-	-	-	-	-
4.6	-1.38227	0.44736	0.56260	1.14139	1.26240	2.81570
4.8	-1.34896	0.14654	0.26118	0.69322	0.81483	2.14999
5.0	-1.27160	-0.03714	0.07676	0.39334	0.51563	1.65681
5.2	-1.16918	-0.14504	-0.03200	0.19416	0.31726	1.28605
5.4	-1.05453	-0.19620	-0.08425	0.07089	0.19489	1.01491
5.8	-0.82182	-0.22463	-0.11562	-0.05891	0.06740	0.64328
6.0	-0.71382	-0.21307	-0.10599	-0.08259	0.04512	0.52554
6.2	-0.61523	-0.19933	-0.09464	-0.09647	0.03290	0.43043
∞	-0.05919	-0.05919	-0.05919	-0.05919	0.11837	0.11837

Table XI. Potential energy curves for Kr_2^+ including spin-orbit coupling. Energies in eV relative to c.g. of Kr_2^+ at R=∞ .

R (a.u.)	$A\ ^2\Sigma^+_{1/2u}$	$B\ ^2\Pi_{3/2g}$	$B\ ^2\Pi_{1/2g}$	$C\ ^2\Pi_{3/2u}$	$C\ ^2\Pi_{1/2u}$	$D\ ^2\Sigma^+_{1/2u}$
4.8	-1.28087	-	-	-	-	-
5.0	-1.38709	0.69575	1.09151	1.43876	1.91284	3.18488
5.2	-1.41503	0.27623	0.66358	0.87603	1.35598	2.46023
5.4	-1.38910	0.00729	0.38423	0.48908	0.97546	1.92201
5.6	-1.32866	-0.16482	0.19960	0.22295	0.71627	1.51846
5.8	-1.24730	-0.28795	0.06150	0.02825	0.52948	1.19889
6.0	-1.15345	-0.33612	-0.00457	-0.08468	0.42439	0.98465
6.4	-0.95763	-0.39054	-0.10324	-0.22768	0.30020	0.68250
6.8	-0.77681	-0.38945	-0.15500	-0.28414	0.26501	0.52489
7.0	-0.69752	-0.37898	-0.17192	-0.27435	0.26591	0.48097
7.2	-0.62696	-0.36673	-0.18626	-0.29870	0.27285	0.45125
∞	-0.22197	-0.22197	-0.22197	-0.22197	0.44393	0.44393

Table XII. Potential Energy Curves for Xe_2^+ including spin-orbit coupling. Energies in eV relative to c.g. of Xe_2^+ at R=∞.

R (a.u.)	$A\ ^2\Sigma^+_{1/2u}$	$B\ ^2\Pi_{3/2g}$	$B\ ^2\Pi_{1/2g}$	$C\ ^2\Pi_{3/2u}$	$C\ ^2\Pi_{1/2u}$	$D\ ^2\Sigma^+_{1/2u}$
5.6	-1.40193	-	-	-	-	-
5.8	-1.48344	0.33100	0.95693	0.93646	1.92269	2.74968
6.0	-1.50867	0.02237	0.61482	0.52197	1.52369	2.25511
6.2	-1.49362	-0.16564	0.38771	0.24616	1.26243	1.89954
6.4	-1.45490	-0.33783	0.17473	0.00150	1.03543	1.59142
6.6	-1.39811	-0.44565	0.02261	-0.16640	0.88498	1.36717
6.8	-1.33076	-0.52015	-0.09755	-0.29043	0.77902	1.19677
7.0	-1.25661	-0.55939	-0.18338	-0.37035	0.71648	1.07791
7.4	-1.10398	-0.58459	-0.29772	-0.45724	0.66367	0.93575
7.6	-1.03040	-0.58149	-0.33514	-0.47699	0.66026	0.89673
7.8	-0.95973	-0.57425	-0.36461	-0.48069	0.67123	0.87026
8.0	-0.89665	-0.56304	-0.38755	-0.49278	0.67575	0.85330
8.2	-0.83747	-0.54924	-0.40162	-0.49133	0.69129	0.84609
∞	-0.43549	-0.43549	-0.43549	-0.43549	0.87098	0.87098

Table XIII. Spectroscopic Constants for Ne_2^+

State	T_e (eV)	$\omega_e(cm^{-1})$	$\omega_e X_e(cm^{-1})$	$\alpha_e(cm^{-1})$	$r_e(\AA)$	$B_e(cm^{-1})$	D_e(eV)	D_o(eV)
$D\ ^2\Sigma^+_{1/2g}$	4.445	(vertical excitation energy, repulsive curve)						
$C\ ^2\Pi_{1/2u}$	1.359	122.5	8.4	0.0166	2.50	0.2665	0.085	0.078
$C\ ^2\Pi_{3/2u}$	1.287	103.9	8.7	0.0194	2.54	0.2579	0.060	0.054
$B\ ^2\Pi_{1/2g}$	1.195	246.5	9.0	0.0125	2.15	0.3626	0.152	0.137
$B\ ^2\Pi_{3/2g}$	1.132	250.8	9.8	0.0122	2.14	0.3634	0.215	0.199
$A\ ^2\Sigma^+_{1/2u}$	0.0	597.0	6.1	0.0090	1.69	0.5840	1.347	1.310

Table XIV. Spectroscopic Constants for Ar_2^+

State	T_e(eV)	ω_e(cm^{-1})	$\omega_e X_e$(cm^{-1})	α_e(cm^{-1})	r_e(Å)	B_e(cm^{-1})	D_e(eV)	D_o(eV)
$D\ ^2\Sigma^+_{1/2g}$	4.198	(vertical excitation energy, repulsive curve)						
$C\ ^2\Pi_{1/2u}$	1.413	62.4	9.3	0.0047	3.40	0.0732	0.087	0.084
$C\ ^2\Pi_{3/2u}$	1.285	53.7	3.7	0.0043	3.40	0.0732	0.037	0.034
$B\ ^2\Pi_{1/2g}$	1.264	146.9	12.0	0.0030	3.02	0.0924	0.058	0.049
$B\ ^2\Pi_{3/2g}$	1.155	153.7	10.1	0.0024	3.02	0.0927	0.167	0.158
$A\ ^2\Sigma^+_{1/2u}$	0.0	297.9	1.7	0.0011	2.43	0.1428	1.322	1.304

Table XV. Spectroscopic Constants for Kr_2^+

State	T_e(eV)	ω_e(cm^{-1})	$\omega_e X_e$(cm^{-1})	α_e(cm^{-1})	r_e(Å)	B_e(cm^{-1})	D_e(eV)	D_o(eV)
$D\ ^2\Sigma^+_{1/2g}$	3.875	(vertical excitation energy, repulsive curve)						
$B\ ^2\Pi_{1/2g}$	2.079	(vertical excitation energy, repulsive curve)						
$C\ ^2\Pi_{1/2u}$	1.679	70.2	1.3	0.0004	3.64	0.0304	0.179	0.175
$C\ ^2\Pi_{3/2u}$	1.115	51.7	0.4	0.0001	3.85	0.0271	0.077	0.074
$B\ ^2\Pi_{3/2g}$	1.019	78.0	1.9	0.0004	3.48	0.0333	0.173	0.168
$A\ ^2\Sigma^+_{1/2u}$	0.0	176.7	0.7	0.0002	2.75	0.0533	1.192	1.181

Table XVI. Spectroscopic Constants for Xe_2^+

State	T_e(eV)	ω_e(cm^{-1})	$\omega_e X_e$(cm^{-1})	α_e(cm^{-1})	r_e(Å)	B_e(cm^{-1})	D_e(eV)	D_o(eV)
$D\ ^2\Sigma^+_{1/2g}$	3.764	(vertical excitation energy, repulsive curve)						
$C\ ^2\Pi_{1/2u}$	2.169	54.5	0.3	0.0002	3.97	0.0163	0.209	0.206
$B\ ^2\Pi_{1/2g}$	2.123	(vertical excitation energy, repulsive curve)						
$C\ ^2\Pi_{3/2u}$	1.034	58.5	0.3	0.0009	4.00	0.0160	0.042	0.038
$B\ ^2\Pi_{3/2g}$	0.923	49.7	0.3	0.0003	3.91	0.0168	0.149	0.146
$A\ ^2\Sigma^+_{1/2u}$	0.0	117.2	0.4	0.0001	3.18	0.0253	1.072	1.065

Table XVII. Summary of Spectroscopic Constants for the $A\ ^2\Sigma^+_{1/2u}$ State of the Noble Gas Dimer Ions

Ion	D_e(eV)	{-SO} D_e(eV)	$\langle \bar{r} \rangle$(a.u.)	{-SO} R_e(a.u.)
Ne_2^+	1.35	1.37	0.965	3.19
Ar_2^+	1.32	1.40	1.663	4.59
Kr_2^+	1.19	1.39	1.952	5.17
Xe_2^+	1.07	1.38	2.338	5.94

{-SO} : without spin-orbit effects

Table XVIII. Dissociation Energies for Electronic States of the Noble Gas Dimer Ions. Energies in eV.

State	Ne_2^+		Ar_2^+		Kr_2^+		Xe_2^+	
	Present Study	Other Work	Present Study	Other Work	Present Study	Other Work	Present Study	Other Work
$D\ ^2\Sigma^+_{1/2g}$	repulsive		repulsive		repulsive		repulsive	
$C\ ^2\Pi_{1/2u}$	0.08		0.08	0.10[e]	0.17	0.14[e]	0.21	0.19[e]
				0.04[f]		0.10[f]		0.12[f]
$B\ ^2\Pi_{1/2g}$	0.14	0.07[b]	0.05		repulsive		repulsive	
$C\ ^2\Pi_{3/2u}$	0.05		0.03	0.01[f]	0.07	0.02[f]	0.04	0.03[f]
$B\ ^2\Pi_{3/2g}$	0.20	0.07[b]	0.16	0.14[e]	0.16	0.16[e]	0.15	0.18[e]
				0.10[f]		0.13[f]		0.12[f]
$A\ ^2\Sigma^+_{1/2u}$	1.31	1.35[a]	1.30	1.33[g]	1.18	1.176[i]	1.06	1.03[j]
		1.20[b]		1.19[f]		1.05[f]		0.79[f]
		1.65[c]		1.25[c]				
		1.10[d]		1.20[h]				

a T. R. Connor and M. A. Biondi, Phys. Rev. 140, A778 (1965); L. Frommhold and M. A. Biondi, ibid 185, A244 (1969).

b Ref. 7 (CI calculation).

c Refs. 5, 6 (SCF calculation).

d Ref. 16*

e Ref. 14 (Photoionization studies).

f Ref. 11 (CI calculation).

g Ref. 36*

h Ref. 10 (SCF calculation)

i Ref. 43*

j Ref. 39*

* This reference contains a summary of D_o from other experimental studies.

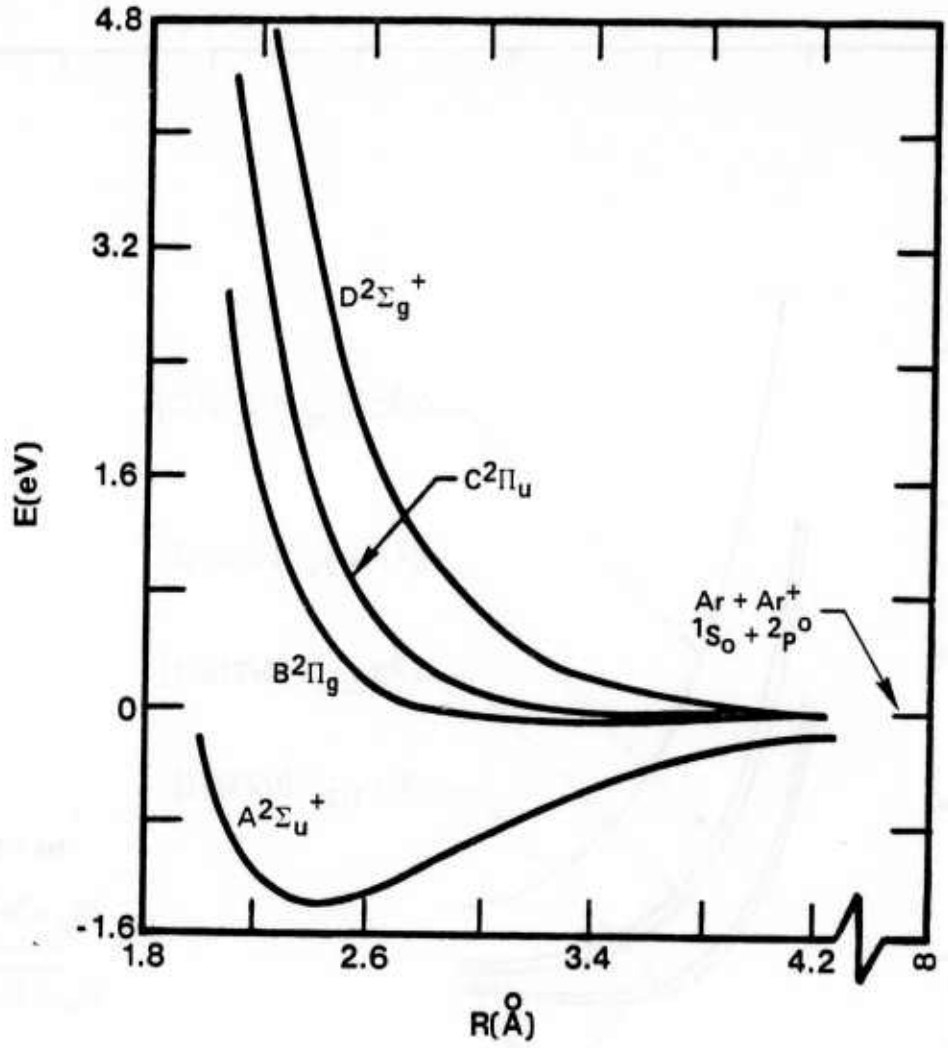

Figure 1. Ab initio potential energy curves for Ar_2^+ without inclusion of spin-orbit coupling.

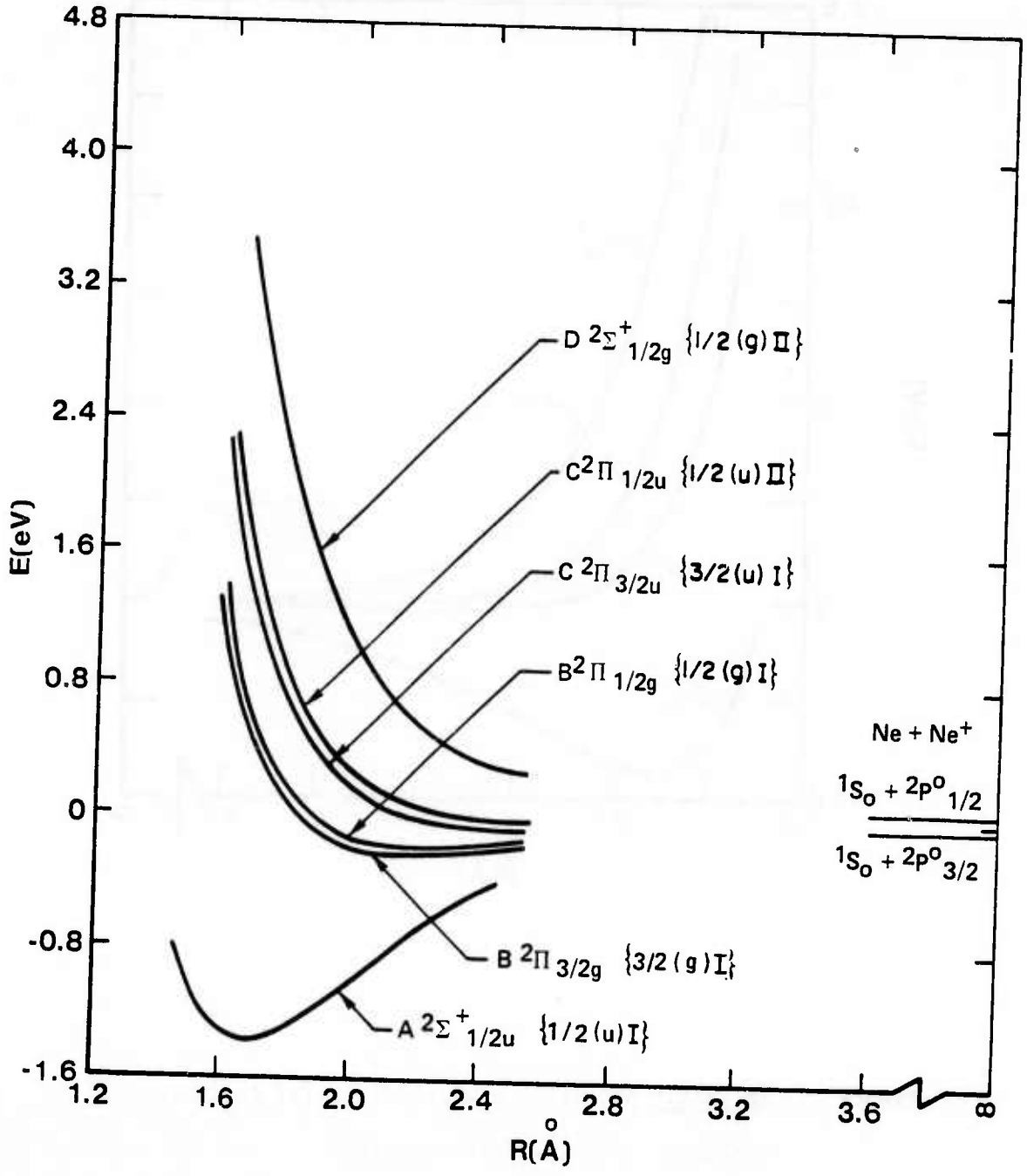

Figure 2. Density functional potential energy curves for Ne_2^+ (spin-orbit effects included)

78-05-157-1

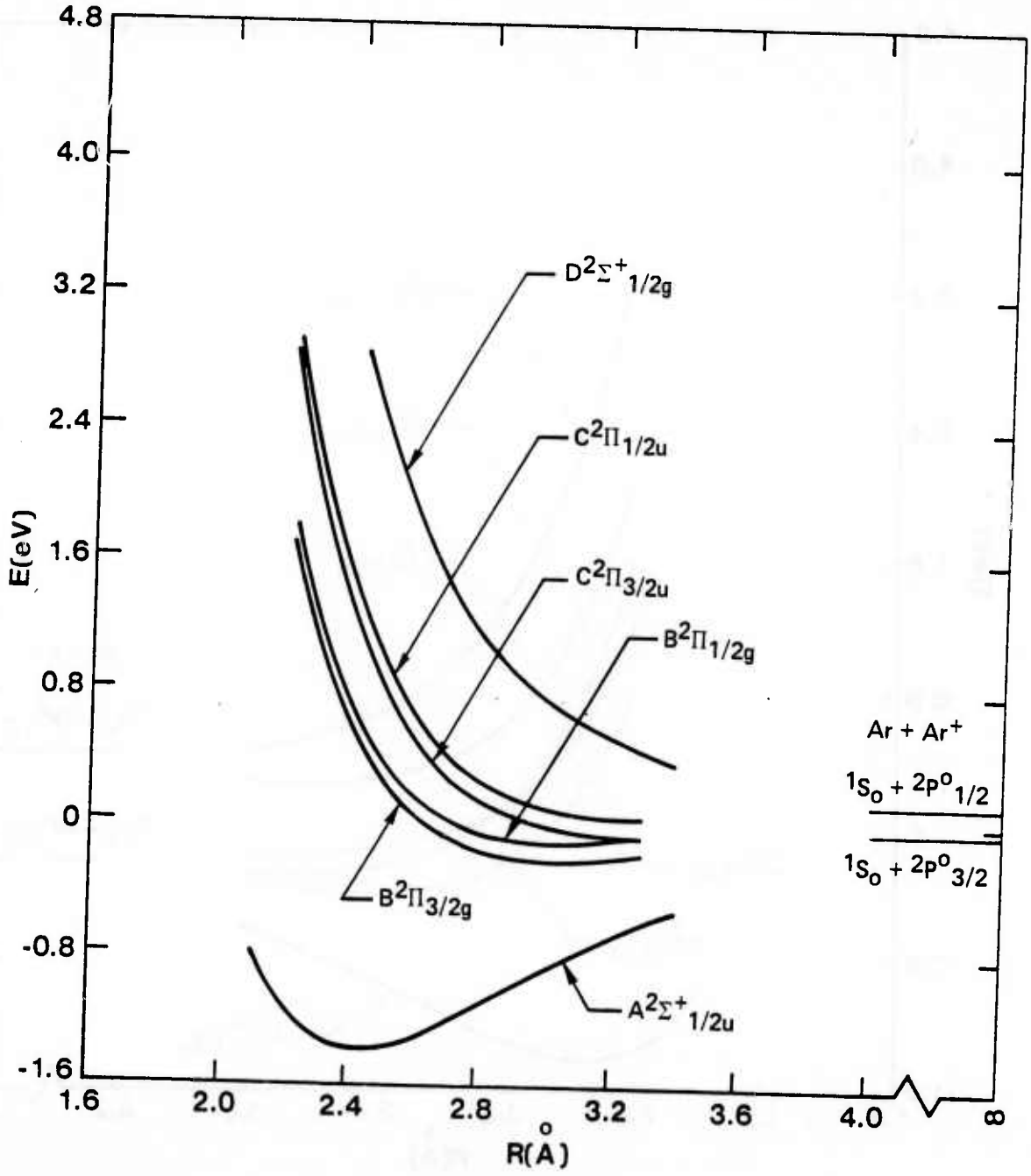

Figure 3. Density functional potential energy curves for Ar_2^+ (spin-orbit effects included)

78-05-157-3

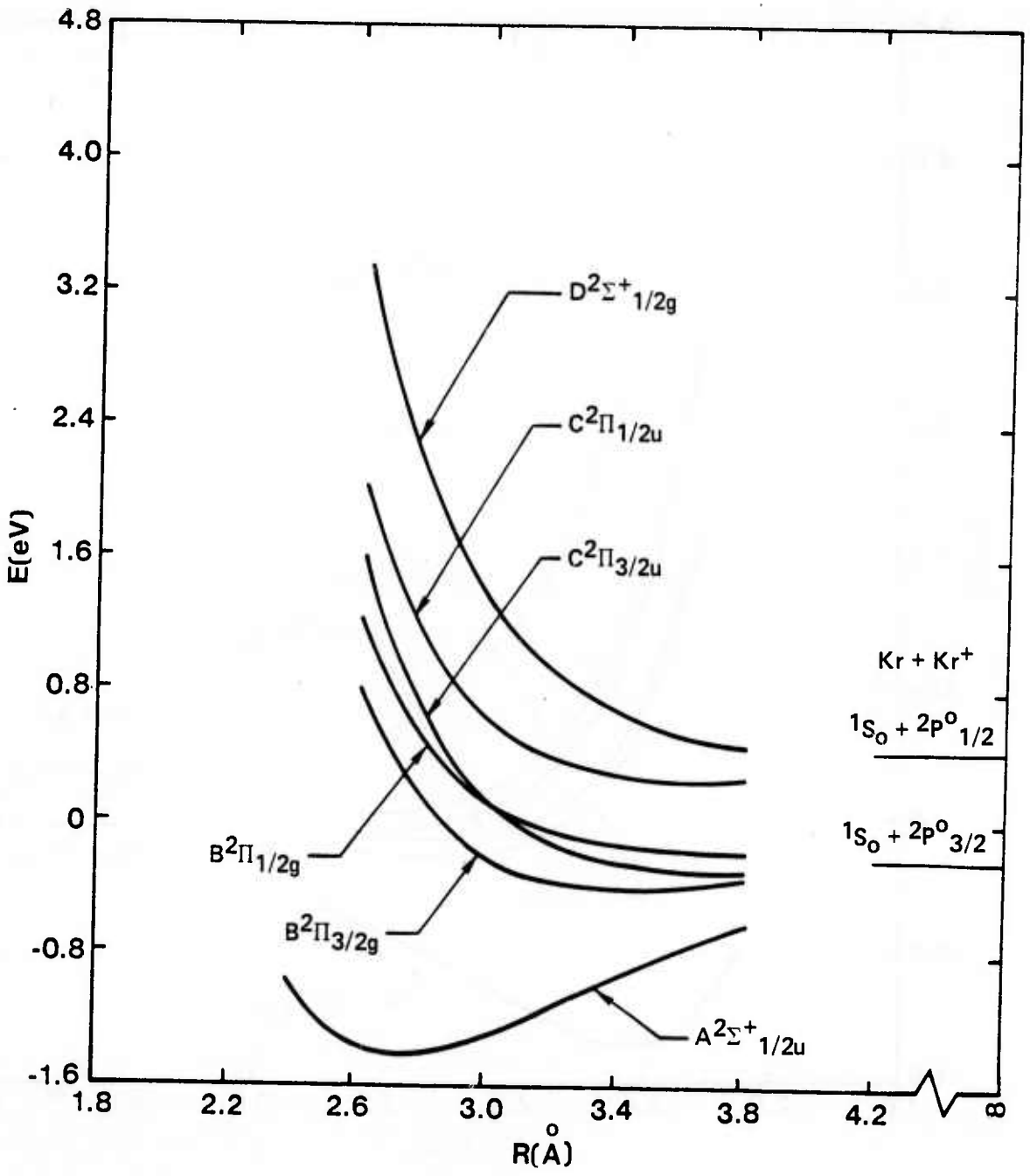

Figure 4. Density functional potential energy curves for Kr_2^+ (spin-orbit effects included)

78-05-157-2

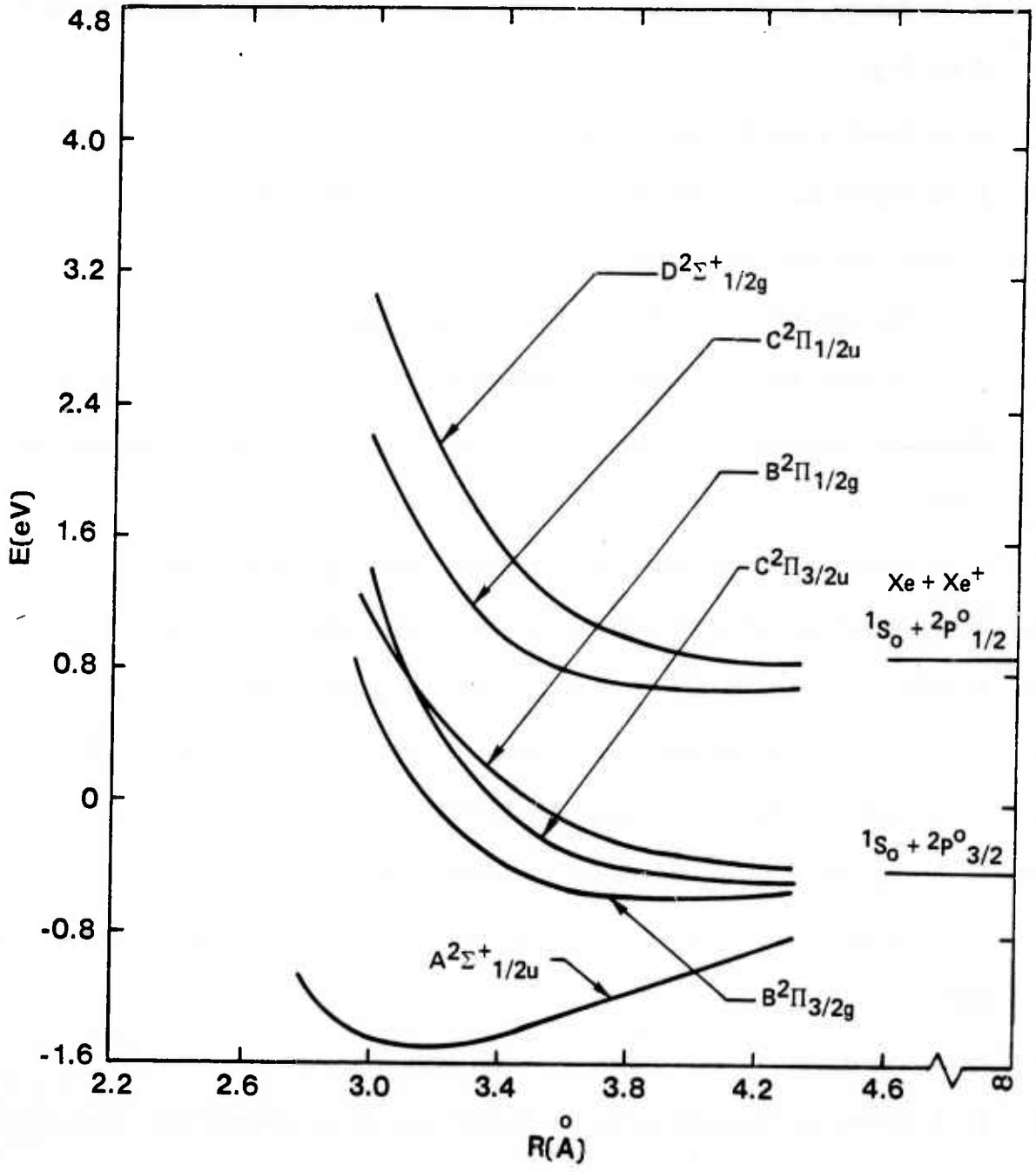

Figure 5. Density functional potential energy curves for Xe_2^+ (spin-orbit effects included)

78-05-157-4

References

1. R. O. Hunter, J. Oldenettel, C. Howton and M. V. McCusker, submitted to J. Chem. Phys.
2. D. L. Huestis and E. Zamer, preprint.
3. A. M. Hawryluk, J. A. Mangano and J. H. Jacob, preprint.
4. J. Fenn, private communication.
5. T. L. Gilbert and A. C. Wahl, J. Chem. Phys. 55, 5247 (1971).
6. T. L. Gilbert and A. C. Wahl, "Compendium of Ab Initio Calculations of Molecular Energies and Properties" edited by M. Krauss, NBS Technical Note 438 (1967).
7. J. S. Cohen and B. I. Schneider, J. Chem. Phys. 61, 3230 (1974).
8. B. I. Schneider and J. S. Cohen, J. Chem. Phys. 61, 3240 (1974).
9. V. Sidis, M. Barat and D. Dhuicq, J. Phys. B 8, 474 (1975).
10. W. J. Stevens, M. Gardner and A. Karo, J. Chem. Phys. 67, 2860 (1977).
11. W. R. Wadt, J. Chem. Phys. 68, 402 (1978).
12. P. J. Hay and T. H. Dunning, Jr., J. Chem. Phys. 64, 5077 (1976).
13. W. C. Ermler, Y. S. Lee, K. S. Pitzer and N. W. Winter, submitted to J. Chem. Phys.
14. P. M. Dehmer and J. L. Dehmer, J. Chem. Phys., in press.
15. P. R. Jones, G. M. Conklin, D. C. Lorents and R. E. Olson, Phys. Rev. A10, 102 (1974).
16. R. S. Mulliken, J. Chem. Phys. 52, 5170 (1970).
17. F. R. Gilmore, T. L. Barr and D. Dee, J. Quant. Spect. Rad. Trans. 15, 625 (1975).

References (Cont'd)

18. H. H. Michels, R. H. Hobbs and L. A. Wright, Chem. Phys. Lett. 48, 158 (1977).

19. H. H. Michels, R. H. Hobbs, L. A. Wright and J. W. D. Connolly, Int. J. Quant. Chem., 13, 169 (1978).

20. J. C. Slater, Adv. Quant. Chem. 6, 1 (1972).

21. P. O. Löwdin, Phys. Rev. 97, 1474 (1955).

22. W. Kohn and L. Sham, Phys. Rev. 140A, 1133 (1965).

23. J. C. Slater, Phys. Rev. 81, 385 (1951).

24. K. Schwarz, Phys. Rev. B5, 2466 (1972).

25. N. Rösch and K. H. Johnson, Chem. Phys. Lett. 23, 149 (1973).

26. J. B. Mann, Atomic Data 12, 1 (1973) and private communication.

27. F. E. Harris and H. H. Michels, Int. J. Quant. Chem. IS, 329 (1967).

28. A. C. Wahl, P. J. Bertoncini, G. Das and T. L. Gilbert, Int. J. Quant. Chem. IS, 123 (1967).

29. P. O. Löwdin, Molecular Orbitals in Chemistry, Physics and Biology, Academic Press, NY, (1964).

30. F. E. Harris, J. Chem. Phys. 32, 3 (1960).

31. H. H. Michels and F. E. Harris, J. Chem. Phys. 39, 1464 (1963).

32. S. R. Langhoff and C. W. Kern, Modern Theoretical Chemistry, Vol. II, Plenum Press, NY, (1977).

33. J. O. Hirschfelder, C. F. Curtiss and R. B. Bird, Molecular Theory of Gases and Liquids, John Wiley & Sons, NY, (1954).

34. Intermolecular Forces, ed. J. O. Hirschfelder, Adv. Chem. Phys. 12, Interscience, NY (1967).

35. C. E. Moore, Atomic Energy Levels, NBS Circular 467 (1949).

36. J. T. Moseley, R. P. Saxon, B. A. Huber, P. C. Cosby, R. Abouaf and M. Tadjeddine, J. Chem. Phys. 67, 1659 (1977).

37. H. M. Hulburt and J. O. Hirschfelder, J. Chem. Phys. 9, 61 (1940).

38. J. B. Mann, Atomic Structure Calculations, Los Alamos Scientific Laboratory Report LA-3690 (1967).

39. C. Y. Ng, D. J. Trevor, B. H. Mahan and Y. T. Lee, J. Chem. Phys. 65, 4372 (1976); 66, 446 (1977).

40. M. S. Munson, J. L. Franklin and F. H. Field, J. Chem. Phys. 67, 1542 (1963).

41. H. V. Mittmann, H. P. Weise and Z. Naturforsch, 29a, 400 (1974).

42. T. M. Miller, J. H. Ling, R. P. Saxon and J. T. Moseley, Phys. Rev. A 13, 2171 (1976).

43. R. Abouaf, B. A. Huber, P. C. Cosby, R. P. Saxon and J. T. Moseley, J. Chem. Phys. 68, 2406 (1978).

44. J. A. Vanderhoff, J. Chem. Phys. 68, 3311 (1978).

45. P. M. Dehmer and J. L. Dehmer, J. Chem. Phys. 67, 1774 (1977).

APPENDIX E

ELECTRONIC STRUCTURE OF THE NOBLE GAS DIMER IONS.

II. ABSORPTION SPECTRUM FOR THE A $^2\Sigma_g^+ \rightarrow$ D $^2\Sigma_g^+$ SYSTEM

ABSTRACT

A systematic study of the electronic structure and chemical binding in the dimer ion sequence, Ne_2^+, Ar_2^+, Kr_2^+ and Xe_2^+, has been carried out using both density function and ab initio configuration interaction computational approaches. From the results of this study, the absorption spectrum for the UV transitions of the A $^2\Sigma_u^+ \rightarrow$ D $^2\Sigma_g^+$ system has been calculated.

APPENDIX F

ELECTRONIC STRUCTURE OF THE NOBLE GAS DIMER IONS.

III. ABSORPTION SPECTRUM FOR THE A $^2\Sigma_u^+ \rightarrow$ B $^2\Pi g$ SYSTEM

ABSTRACT

A systematic study of the electronic structure and chemical binding of the dimer ion sequence, Ne_2^+, Ar_2^+, Kr_2^+ and Xe_2^+, has been carried out using both density functional and ab initio configuration interaction computational approaches. From the results of this study, the absorption spectrum for the visible/IR transition of the A $^2\Sigma_u^+ \rightarrow$ B $^2\Pi g$ system has been calculated.

APPENDIX G

ELECTRONIC STRUCTURE AND PHOTOABSORPTION OF THE Hg_2^+ DIMER ION

ABSTRACT

Calculations have been performed on the electronic structure, potential energy curves, spectroscopic constants and photoabsorption characteristics of the Hg_2^+ dimer ion. These studies indicate that the ground $A^1/_2u$ state of the Hg_2^+ ion is stable with a calculated dissociation energy of 0.44 eV. This ion exhibits strong absorption ($\sigma \sim 1.0$ $\mathring{A}^2$) for the $A^1/_2u \rightarrow B^1/_2g$ transition at $\lambda = 1.1$ μ. The only other predicted absorption is for wavelengths shorter than 250 nm. We conclude that photoabsorption of Hg_2^+ does not appear to represent an important loss mechanism in excimer lasers based on Hg chemistry.

APPENDIX H

ELECTRONIC STRUCTURE AND PHOTOABSORPTION PROPERTIES OF NOBLE GAS TRIMER IONS

ABSTRACT

A study of the electronic structure and absorption characteristics of the Ar_3^+ ion has been carried out to determine the relative importance of such species in the analysis of loss mechanisms in the noble gas-halide excimer systems. This study included detailed quantum mechanical calculations of the potential energy hypersurfaces for Ar_3^+ and prediction of the absorption bands. We find this ion to have trigonal symmetry with a bound $^2E'$ ground state ($^2B_2 + {}^2A_1$ in C_{2v}). The vertical excitation spectra are $^2A_2'$ (.21 eV), $^2E''$ (.63 eV), $^2A_2''$(1.06 eV) and $^2A_1'$ (2.12 eV). The short wavelength transitions (300-500 nm) are found to be weak for photoabsorption from the ground state. A strong photoabsorption band ($\lambda \sim 590$ nm) is predicted for the $^2E' \rightarrow {}^2A_1$ transition. This suggests that trimer ion absorption may be very important in the analysis of loss mechanisms in excimer lasers operating under high pressure conditions.

APPENDIX I

ELECTRONIC STRUCTURE OF NOBLE GAS DIMER AND TRIMER IONS

ABSTRACT

A systematic study of the electronic structure and chemical binding of the noble gas dimer and trimer ions has been carried out. This study includes detailed quantum mechanical calculations of the ground and low-lying excited state potential energy curves for Ne_2^+, Ar_2^+, Kr_2^+ and Xe_2^+ and the ground and low-lying excited state surfaces for Ar_3^+. Both density functional and ab initio configuration-interaction computational techniques have been employed. A regular progression is found in the calculated spectroscopic properties of the dimer ions which results in some remarkably simple conclusions regarding the nature of the binding and the geometry of these ions. For the Ar_3^+ trimer ion, studies in D_{3h}, C_{2v} and $D_{\infty h}$ point groups were carried out. The lowest surface corresponds to the degenerate $^2E'$ symmetry with an indicated bond strength of ~0.2 eV relative to $Ar_2^+(A^2\Sigma^+_u)$ + $Ar(^1S_o)$. This trimer ion exhibits a Jahn-Teller distortion arising from the degenerate vibrational modes of the ground state. Several low-lying excited state surfaces of Ar_3^+ have also been studied include $^2A_2'$, $^2E''$ and $^2A_1'$ symmetries. A strong photoabsorption band (λ~590 nm) is predicted for the $^2E' \rightarrow {}^2A_1$ transition of this trimer ion. This suggests that such species may be very important in the analysis of loss mechanisms in excimer lasers operating under high pressure conditions.

APPENDIX J

VISIBLE PHOTOABSORPTION BY NOBLE GAS TRIMER IONS

ABSTRACT

A study of the electronic structure and photoabsorption characteristics of noble gas trimer ions has been carried out using quantum mechanical methods. This study includes detailed density functional calculations of the potential energy surfaces for a prototype system, Ar_3^+, an analysis of the spectroscopic properties of the ground state of this ion and prediction of the strong absorption bands. Studies in D_{3h}, C_{2v} and $D_{\infty h}$ symmetries were carried out. The lowest state of Ar_3^+ corresponds to the degenerate $^2E'$ symmetry with an indicated dissociation energy of 0.17 eV relative to Ar_2^+ ($A^2\Sigma_u^+$) + Ar (^1S_o). This trimer ion exhibits a small Jahn-Teller distortion which does not significantly alter our conclusions concerning the ground state stability or absorption characteristics. A strong and very broad photoabsorption band (λ=496-670 nm) is predicted for the $^2E' \rightarrow {}^2A_1'$ transition of this trimer ion. This suggests that such species may be very important in the analysis of loss mechanisms in visible excimer lasers, operating under high pressure conditions, with mixtures containing the noble gases.